



Cite this: DOI: 10.1039/c5cs00781j

Layer-by-layer assembly of versatile nanoarchitectures with diverse dimensionality: a new perspective for rational construction of multilayer assemblies

Fang-Xing Xiao,^a Mario Pagliaro,^{*b} Yi-Jun Xu^{*cd} and Bin Liu^{*a}

Over the past few decades, layer-by-layer (LbL) assembly of multilayer thin films has garnered considerable interest on account of its ability to modulate nanometer control over film thickness and its extensive choice of usable materials for coating planar and particulate substrates, thus allowing for the fabrication of responsive and functional thin films for their potential applications in a myriad of fields. Herein, we provide elaborate information on the current developments of LbL assembly techniques including different properties, molecular interactions, and assembly methods associated with this promising bottom-up strategy. In particular, we highlight the principle for rational design and fabrication of a large variety of multilayer thin film systems including multi-dimensional capsules or spatially hierarchical nanostructures based on the LbL assembly technique. Moreover, we discuss how to judiciously choose the building block pairs when exerting the LbL assembly buildup which enables the engineering of multilayer thin films with tailor-made physicochemical properties. Furthermore, versatile applications of the diverse LbL-assembled nanomaterials are itemized and elucidated in light of specific technological fields. Finally, we provide a brief perspective and potential future challenges of the LbL assembly technology. It is anticipated that our current review could provide a wealth of guided information on the LbL assembly technique and furnish firm grounds for rational design of LbL assembled multilayer assemblies toward tangible applications.

Received 21st December 2015

DOI: 10.1039/c5cs00781j

www.rsc.org/chemsocrev

1. Introduction

Over the past few decades, increasing interest has been devoted to the fabrication of nanostructured functional materials with tunable composition, structure, and dimension *via* assembly techniques. The precise control over the characteristics of nanostructured materials such as size, shape, morphology and composition plays a pivotal role in creating various categories of nanosized materials and is beneficial for tuning their optical, electrical, mechanical and other physicochemical properties. In this regard, bottom-up methods, as an effective strategy for spontaneous assembly of small molecules into complex and functional multi-dimensional nanostructures including 1D, 2D,

or 3D assemblies, have been extensively explored in diverse fields. Although significant advancements have recently been made in the preparation of individual nanoscale materials, rational control over assembly at different length scales by the way of systems materials engineering still poses a great challenge. It is thus highly desirable to develop efficient, easily operable bottom-up approaches to achieve the assembly of single nanoscale building blocks into desirable functional architectures in a controlled elegant fashion.

Conventionally, bottom-up methods mainly center on the Langmuir–Blodgett (LB)^{1–5} and self-assembled monolayers (SAMs),^{6–9} which render the fabrication of intimately packed and well-defined ordered monolayers; nevertheless, intrinsic drawbacks associated with these methods hinder their widespread practical applications. In the LB method, the requirements for specific molecules to prepare the films and long processing time limit its extensive applications.^{10,11} In addition, the mechanical stability and robustness of the LB monolayer films are still far from satisfactory under certain conditions. With regard to the SAM method, the limited deposition of targeted molecules within the films owing to the unfavorable stability of the films and, moreover, the need for pre-deposition

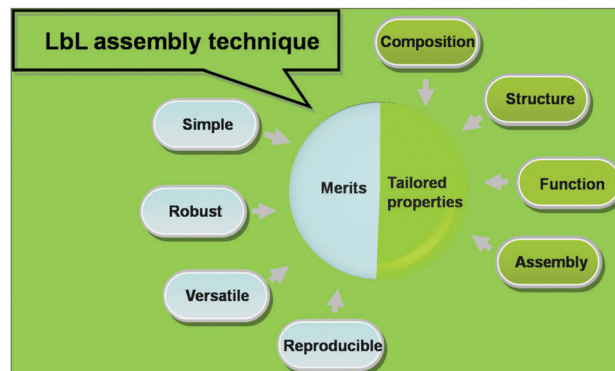
^a School of Chemical and Biomedical Engineering, Nanyang Technological University, 62, Nanyang Drive, 637459, Singapore. E-mail: liubin@ntu.edu.sg; Fax: +65-6794-7553; Tel: +65-6513-7971

^b Istituto per lo Studio dei Materiali Nanostrutturati, CNR via U. La Malfa 153, 90146 Palermo, Italy. E-mail: mario.pagliaro@cnr.it

^c State Key Laboratory of Photocatalysis on Energy and Environment, College of Chemistry, Fuzhou University, Fuzhou 350002, P. R. China

^d College of Chemistry, Fuzhou University, New Campus, Fuzhou 350108, P. R. China. E-mail: yjxu@fzu.edu.cn; Fax: +86 591 83779326; Tel: +86 591 83779326

of specific compounds (*e.g.*, thiols) on the substrate during the preparation of monolayers concurrently restrict its practical applications. Other surface assembling strategies including polymer grafting,^{12–14} pulsed laser ablation,¹⁵ and chemical vapor deposition^{16,17} have also been developed to construct various thin films; nonetheless, all of these have met with limited success in terms of their relatively tedious assembly procedure as well as confined selection of assembled materials. In contrast, the layer-by-layer (LbL) self-assembly technique represents a prominent bottom-up strategy to assemble a large number of multilayer thin films or hierarchical nanostructures, and has rapidly emerged as a versatile methodological platform for the assembly of nanomaterials with desired nanoarchitectures (Scheme 1).¹⁸ By tuning the kind of materials and deposition sequences, various nanostructured components with distinct structure and composition can be closely and harmoniously combined within the LbL assembled multilayer films, thereby resulting in hybrid nanostructures with promising collective and improved functional properties for target applications.



Scheme 1 The advantages and characteristics of the LbL assembly technique.

In light of the simplicity and versatility of the LbL assembly technique, a series of excellent reviews have appeared to discuss the extensive applications of the LbL assembly technique such as fabrication of thick polymeric films,¹⁹ assembly of



Fang-Xing Xiao

Fang-Xing Xiao obtained his BS and MS degrees from Huaqiao University in 2006 and 2009, respectively, and obtained his PhD degree from Fuzhou University in 2013. Currently, he is working as a research fellow in Prof. Dr Bin Liu's group at Nanyang Technological University. His research interests focus on the assembly of hybrid semiconductors for photocatalytic and photoelectrochemical applications.



Mario Pagliaro

Mario Pagliaro is a chemistry and energy scholar based at Institute of Nanostructured Materials, Italy. Co-founder of Sicily's Solar Pole, Mario has educated tens of students in nanochemistry, solar energy, energy efficiency and materials science in the last 15 years. Since 2011, his research team organizes annually in Sicily the SuNEC and FineCat premier meetings in solar energy and catalysis.



Yi-Jun Xu

Yi-Jun Xu is a full professor now working at the State Key Laboratory of Photocatalysis on Energy and Environment, College of Chemistry, Fuzhou University, P. R. China. His current research interests primarily focus on the assembly and applications of semiconductor-based and metal-based nanostructured materials, such as graphene-based, one dimension-based and core-shell structure-based composites, in the field of heterogeneous photocatalysis.



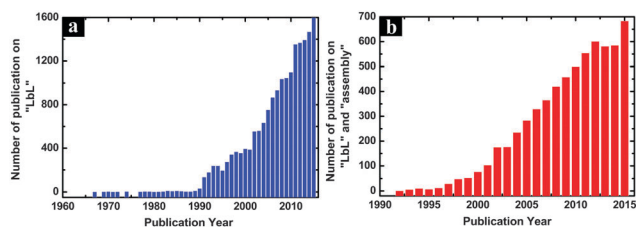
Bin Liu

Bin Liu received his BEng and MEng in chemical engineering from the National University of Singapore with Professor Hua Chun Zeng and PhD in chemical engineering from the University of Minnesota with Professor Eray S. Aydil. He worked as a post-doctoral researcher in the Department of Chemistry at University of California, Berkeley with Professor Peidong Yang. He is currently an Assistant Professor in the School of Chemical and Biomedical Engineering at Nanyang Technological University. His current research involves architected nanomaterials for solar-to-fuel and solar-to-electric conversion, photocatalysis for air and water treatment, and nanocomposites for electrocatalysis.

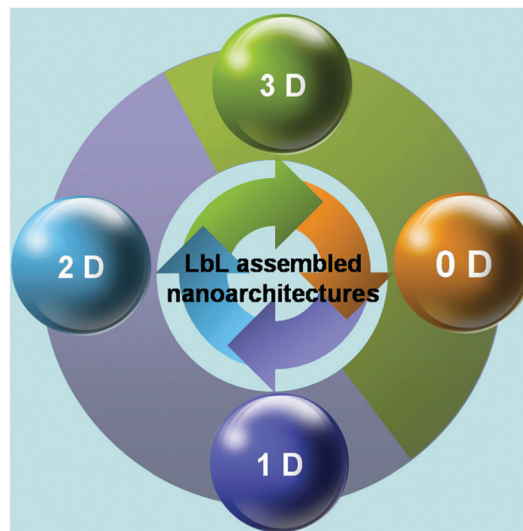
biomedical microcapsules,²⁰ design of proton exchange membrane fuel cells and supercapacitors,²¹ and applications in tissue engineering.²² Despite the intense endeavors, there is still a lack of a general and comprehensive overview of the design of various novel and robust multi-dimensional nanostructures *via* the assembly of an unprecedented choice of materials based on the LbL assembly concept. Additionally, it should be particularly noted that thus far there have been no elaborated reviews on the rational design of multilayer thin films or hybrid nanostructures with 2D inorganic nanosheets and graphene, which are two classes of very promising materials that have emerged in recent years as building blocks for LbL assembly of multi-functional materials. Furthermore, recent impressive advancements in conjunction with potential applications of the LbL assembly technique in diverse fields have seldomly been systematically reviewed. These factors strongly motivated us to write this up-to-date review on the history and development of using the LbL assembly technique as a versatile strategy for advanced nanostructure design toward multi-functional applications in a myriad of technological fields, such as transparent conducting films, field effect transistors, lithium ion batteries, supercapacitors, solar cells, sensors, proton exchange membrane fuel cells and catalysis.

On the other hand, the high importance and massive interest in the field of LbL assembly can be clearly exemplified by a simple search of the ISI Web of Knowledge database using the terms “layer-by-layer” or “layer-by-layer” and “assembly” as the topic keywords. It can be clearly seen from Scheme 2a that the number of publications per year over the past several decades demonstrates an exponential growth rate, and more than 1000 publications on LbL per year can be observed from 2008, indicating that the research on LbL has well received tremendous interest. When the topic keywords of “layer-by-layer” and “assembly” were combined with a view to highlighting the LbL assembly methodology in fabricating composite materials, it was found from Scheme 2b that the LbL assembly technique gradually increases from 1997 and then keeps a marvelous rate till now, suggesting the extreme significance and broad attraction of this subject.

In this review, we intend to afford an elaborated overview regarding the LbL assembly technique and highlight its merits as an easily accessible, facile, flexible, and promising bottom-up strategy to modify varied substrates and fabricate different novel multifunctional systems. Meanwhile, particular emphasis is devoted to the principle on how to design and prepare



Scheme 2 Number of yearly publications with topic keywords of (a) “layer-by-layer” since 1967 and (b) “layer-by-layer” and “assembly” since 1992.



Scheme 3 The theme of this review for LbL assembly of nanoarchitectures with diverse dimensionality including 0D, 1D, 2D, and 3D.

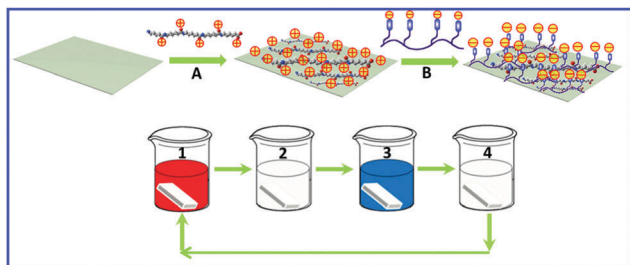
multilayer assemblies including various multi-dimensional hybrid nanostructures based on LbL assembly (Scheme 3). Furthermore, versatile applications of the LbL-assembled hybrid nanomaterials are itemized and elucidated in the light of specific technological field. Finally, we provide a brief perspective and potential future challenges of the LbL assembly technology. It is anticipated that our current review can provide enriched information on the LbL assembly technique and spark enlightened ideas for rational design of multilayer assemblies toward practical applications.

2. Development history of the LbL assembly technique and factors influencing the LbL assembly process

2.1 Development history and mechanism of the LbL assembly technique

It is generally conceived that the principle of LbL assembly involves the alternate deposition of interacting species on a solid or flexible substrate with an intervening rinsing step after each deposition, as shown in Scheme 4. This idea of repetitive adsorption of oppositely charged building blocks stems from the seminal work carried out by Iler and Kirkland in 1964–1966,^{23,24} which involves the assembly of inorganic films based on negatively charged silica particles and positively charged alumina fibrils. However, the lack of suitable analysis techniques at that time restricted further investigation of the LbL process. It was not until 1991 that Decher and Hong as pioneer researchers achieved full characterization of the LbL assembled multilayer thin films;²⁵ thereafter the idea of using polyelectrolytes (PEs) stacked in an alternate fashion rapidly revived and paved the way for precise control over the film architecture.²⁶

The use of the LbL strategy for the synthesis of biomolecule-based assemblies promotes the rapid development of the LbL



Scheme 4 Preparation of multilayer thin films using the LbL assembly technique: (A) deposition of positive PE (*i.e.*, polycation) and (B) deposition of negative PE (*i.e.*, polyanion). (1) Polyanion, (2 and 4) DI H₂O, (3) polyanion.

technique.^{27,28} In particular, the introduction of leading techniques including optical absorption, X-ray, and neutron reflectivity, which were initially introduced for LB films, made *in situ* determination of the growth of LbL assembled multilayer thin films easily accessible. Since then, these tools have been widely employed in the LbL assembly procedure involving a huge variety of systems including organic or inorganic materials and biomolecule assemblies.²⁹ The popularity of LbL films was revived in 1997 by the article entitled “*Fuzzy Nanoassemblies: Toward Layered Polymeric Multicomposites*” published by Decher in *Science*, which presented a facile and green LbL approach to electrostatically assemble the PE films.³⁰ In this case, electrostatic interaction serves as the predominant driving force to achieve the assembly buildup *via* surface charge inversion after alternating deposition of a PE in each step. In the following many years, electrostatic interaction has been regarded as a very popular driving force to fabricate LbL nanostructures since it can be combined with a wide variety of topologies and substrates (*e.g.* gold, quartz, silicon, or clay).³¹

Apart from the frequently used electrostatic interaction, many other molecular interactions have also been developed to create various novel multilayer nanoarchitectures through the LbL assembly technique. For example, the pioneering studies on using hydrogen-bonding interaction to prepare LbL assemblies were firstly demonstrated by Stockton *et al.* and Wang *et al.*^{32,33} The reversible and pH-triggered dissolution of the multilayer properties of hydrogen-bonding interaction renders the LbL assemblies favorable for controlled release from multilayer films and capsules.^{32,33} The coordination bonding³⁴ and charge transfer interactions³⁵ were introduced in 1997 and 1998, respectively. The hydrophobic interaction was determined by Kotov and Cochran in 1999 as the main driving force for LbL buildup.^{36,37} Besides, host-guest interaction has also been widely employed for LbL assembly of multilayer thin films in biomimetic systems.³⁸ Consequently, various kinds of noncovalent interactions that dominate the LbL process give rise to a diverse variety of systems. For detailed information on the different molecular interactions responsible for the LbL assembly, readers are suggested to refer to Section 2.3.

2.2 Parameters controlling the LbL assembly process

The structures of LbL assembled multilayer thin films could be greatly influenced by various parameters such as pH,

temperature, ionic strength, electrolyte type, solvent, and properties of PEs including charge density, molecular weight, concentration, and architecture. To gain deep insights into the LbL assembly process, the specific influences of these different factors on the growth of LbL multilayer thin films are concisely summarized in the following section.

2.2.1 pH. The pH value of a solution exerts profound influence on the composition, structure, and cross-link density of LbL multilayer thin films or hierarchical nanostructures owing predominantly to the difference in the ionization degree of PEs under varied pH circumstances. It is worthwhile that strong PEs with substantial charges are fully charged independent of pH; however, weak PEs with carboxylic acid or amine functional groups are highly sensitive to the pH of the external solution, for which the number of nonionized carboxylic acid groups either within the multilayer film or on the surface can be controlled by pH.^{39,40} Therefore, the conformation of weak PEs can drastically change with the change of charge density afforded by pH transformation, while the conformation of strong PEs will not be influenced. The unique responsive property of PEs features opportunities to achieve direct control over the thickness, roughness, and internal structure of multilayer thin films or nanostructures using the LbL assembly technique with respect to solution pH. For example, it was demonstrated that a tiny change in the solution pH for weak PEs of polyacrylic acid (PAA) and poly(allylamine hydrochloride) (PAH) could induce pronounced transformation in the growth mechanism, thickness, and composition of the LbL-assembled multilayer thin films.^{41–43} Moreover, as systematically explored by Burke and Barrett, the pivotal role of pH in determining the swelling behavior of multilayers containing weak PEs has been undoubtedly established.⁴⁴

2.2.2 Temperature. The influence of temperature on the thickness, internal structure, and stability of LbL multilayer assemblies has been specifically explored.^{45–47} In general, as assured by previous results, multilayer thin films assembled at high temperature were thicker than analogous films fabricated under ambient conditions due to the swelling of the films and increased interpenetration between PE layers.⁴⁸ Moreover, it is worthwhile that the effect of temperature on the stability and growth of LbL assembled multilayer thin films is universal for both 2D and 3D assemblies.^{49,50}

2.2.3 Ionic strength. Ionic strength has been determined to be another important parameter which remarkably affects the stability, permeability, and growth of LbL multilayer systems.^{51–53} During the past two decades, the correlation of salt type and concentration with the thickness of multilayer films was specifically probed by many researchers. It was found that substantial differences were observed within the multilayer thin films assembled in the solutions with low and high salt concentration on account of the conformational transition of PE solution from extended rod to globular coil at low and high salt concentration, respectively, thus leading to varied internal structures of multilayers. For example, with regard to the most frequently investigated PE system comprising the poly(diallyldimethylammonium chloride) (PDDA) and poly(sodium 4-styrene sulfonate) (PSS) pair,

there exists an optimum salt concentration (*ca.* 0.3 M) below which the thickness of assembled multilayer films increases with increasing salt concentration and finally complete disassembly of the multilayer occurs when salt concentration is higher than *ca.* 0.6 M due to the competition of PE pairs caused by external salt ions. Furthermore, it has been well-established that bilayer mass, stiffness, and swelling properties of the multilayer films were also dictated by ionic strength.^{54–56}

2.2.4 Solvent. The structure of PEs and growth of multilayer thin films or nanostructures are closely related to the solvent environment. For example, Poptoshev and co-workers studied the effect of solvent quality on the growth and structure of PE multilayer thin films composed of PSS and PAH by varying the ethanol amount in the aqueous PE solutions.⁵⁷ Their results suggested that decreasing the solvent quality through increasing the ethanol amount led to the increase of film thickness and mass loading, which could be attributed to the reduced solvating effect of aqueous solutions containing electrolyte ions. Thus, it is highly desirable to select a suitable solvent to prepare PE solutions for efficient LbL assembly buildup.

2.2.5 Properties of PEs. The charge density of PEs has been determined to be an important factor affecting the LbL assembly of multilayer systems. The influence of charge density of strong PEs on the growth of multilayer films was studied by Koetse's group using various cellulose derivatives.⁵⁸ The results revealed that film thickness increases with the decreasing charge density of PEs. The same trend was also observed in weak PEs such as PAA or PAH.⁵⁹

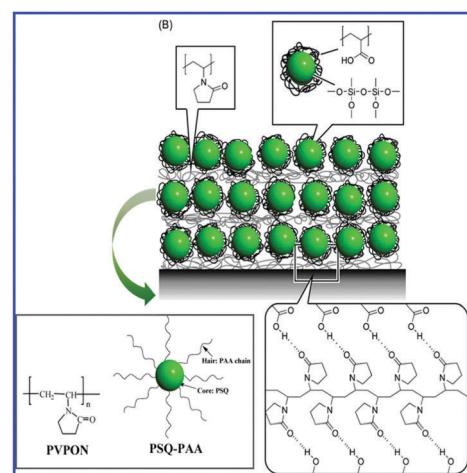
More recently, the influence of molecular weight (MW) of PEs on the structure of PE multilayer films with mobile polymer chains was evaluated.⁶⁰ The results indicated that an increase in polycation MW gave rise to an increase of the internal roughness of multilayer films and, meanwhile, the swelling and dissociation properties of multilayer films in response to pH could be precisely controlled by polyanion MW.⁶¹ Further study revealed that tunable control over MW of PEs could avoid the use of tedious post-treatment procedures to fabricate multilayer films, which would result in disassembly between internal deposition layers.^{62,63} Besides, chain architectures of PEs including chain conformation and chain interpenetration can also affect the formation of PE multilayer thin films. As unveiled by Liu *et al.*,^{64,65} chain conformation plays a pivotal role at low salt concentration in the growth of multilayer films and chain interpenetration dictates the assembly of films when the multilayers are composed of flexible or semi-flexible PE chains.⁶⁶

2.3 Molecular interactions dominating LbL assembly buildup

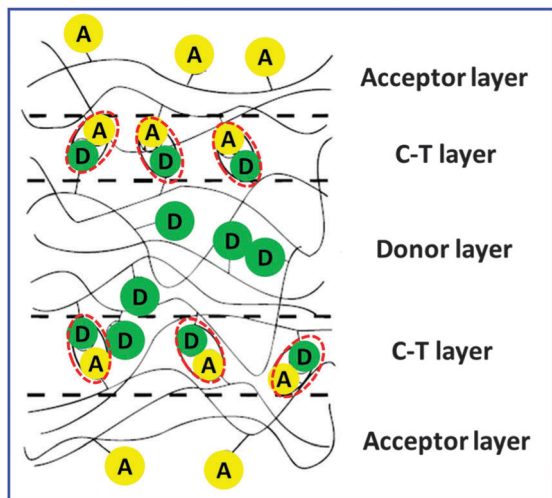
2.3.1 Hydrogen bonding interaction. Hydrogen bonding has been established to be one of the most investigated driving forces other than electrostatic interaction, which allows for the combination of various uncharged building blocks into multilayer films or nanostructures as long as they can serve as hydrogen bonding donors and acceptors. The pioneering work on hydrogen-bonded LbL multilayer films was demonstrated by

Stockton and Rubner's studies, in which multilayer thin films were fabricated by alternate deposition of polyaniline (PANI) and various non-ionic hydrophilic polymers.³² Their results indicate that PANI films assembled *via* hydrogen bonding contain higher PANI amounts adsorbed per deposition cycle and show enhanced performances in comparison with the counterpart films prepared through conventional electrostatic interactions. As reported in another interesting work from Chen's group (Scheme 5),⁶⁷ a spherical polymer brush consisting of a poly(methylsilsesquioxane) (PSQ) core and PAA hair chains, and poly(vinylpyrrolidone) (PVPON) were used as building blocks for LbL assembly of composite multilayer films *via* hydrogen bonding interaction. Selective dissolution and calcination of the films to remove PSQ and organic moieties, respectively, were harnessed to tune the composition and optical properties of the multilayer films. On the other hand, it should be emphasized that hydrogen-bonded LbL multilayer assemblies are sensitive to the surrounding environment including pH, ionic strength, temperature, external stress, and electrical field, thus indicating the intrinsic reversible properties.^{68–73} Alternatively, hydrogen-bonded LbL multilayer thin films can also be fabricated by depositing the same component such as dendrimers with various carboxyl groups which simultaneously act as hydrogen bonding donors and acceptors.⁷⁴ In general, multilayer assemblies prepared by hydrogen bonding interaction are less stable and robust than those attained by other molecular interactions, especially electrostatic interaction.

2.3.2 Charge-transfer interaction. LbL assembled multilayer thin films can be fabricated by charge-transfer (CT) interaction, which involves alternate deposition of two types of non-ionic molecules with electron-accepting and electron-donating functional groups in the side chains (Scheme 6). The growth of multilayer thin films by CT interaction was first presented by Shimazaki and co-workers,^{75–78} for which two kinds of polymers, *i.e.*, poly[2-(9-carbazolyl)ethyl methacrylate]



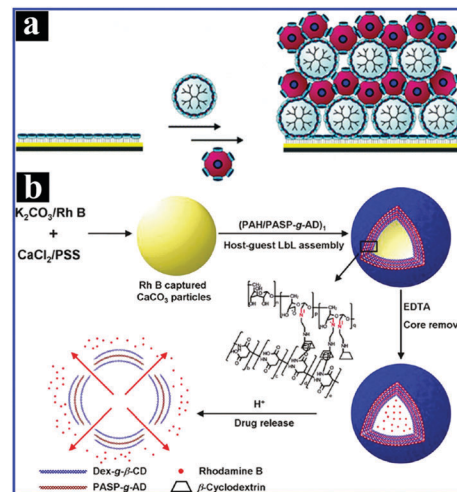
Scheme 5 Hydrogen bonding based LbL assembly between a polymer brush and a linear chain. (Reprinted with permission from ref. 67, Copyright 2006, Royal Society of Chemistry.)



Scheme 6 Side-view illustration of the LbL assembled multilayer thin film prepared by charge-transfer interaction. D and A denote a carbazolyl group and a 3,5-dinitrobenzoyl group, respectively. The interaction of D and A is highlighted with a red circle. (Reprinted with permission from ref. 75, Copyright 1997 American Chemical Society.)

and poly[2-[(3,5-dinitrobenzoyl)oxy]ethyl methacrylate], both possessing nonionic pendant groups in the side chains with electron-donating and electron-accepting characteristics were selected as the building components. The pronounced CT interaction between these groups at the solid-liquid interface induced the formation of multilayers with periodic layers of CT complexes which confer unique physical properties. Moreover, it should be stressed that LbL films assembled through CT interaction can be prepared in organic solvents apart from the conventional aqueous environment, which is beneficial for incorporating various hydrophobic groups within the films and extending the potential applications of these nanostructured multilayer thin films.^{79–81} Furthermore, CT interaction could also facilitate the production of supramolecular LbL assemblies for preparing smart materials. It should be stressed that charge-transfer interaction is limited to molecules which exhibit electron-accepting and electron-donating groups. In addition, most of the charge-transfer complexes show low association constants which limit their potential for construction of well-ordered and stable multilayer assemblies.

2.3.3 Host-guest interaction. Host-guest interaction can be utilized to fabricate LbL multilayer assemblies through strong interaction between host (*e.g.* cyclodextrins, cucurbiturils, calixarenes, pillararenes, crown ethers, or porphyrins) and guest (*e.g.* ferrocene, adamantane, or azobenzene) molecules because of its highly selective and specific features.^{11,82,83} As carried out by Husken's group (Scheme 7a), a novel organic/inorganic multilayer assembled in the presence of supramolecular interactions between guest-functionalized dendrimers and host-modified gold (Au) nanoparticles (NPs) was stepwise constructed. The growth of the multilayer films can be easily monitored by surface plasmon resonance spectroscopy.⁸⁴ Apart from 2D multilayer thin films, the assembly of 3D multilayers *via* host-guest interaction is now becoming the focus for the



Scheme 7 (a) Schematic illustration for LbL alternating adsorption of adamantyl-terminated dendrimer and Au NPs. (b) Flowchart depicting LbL assembly of Dex-*g*- β -CD/PASP-*g*-AD multilayers by using CaCO₃ NPs as a template, formation of hollow microcapsules, and the drug release process. (Reprinted with permission from ref. 84 and 85, Copyright 2005 and 2011 American Chemical Society.)

fabrication of pH-responsive and degradable microcapsules. For example, Li and co-workers fabricated biodegradable microcapsules with pH sensitivity by host-guest interaction between β -cyclodextrin (β -CD) and adamantane (AD), as shown in Scheme 7b. In their work, two types of biocompatible polymers including dextran-*graft*- β -CD (Dex-*g*- β -CD) and poly-(aspartic-*graft*-adamantane) (PASP-*g*-AD) were employed as the building blocks for LbL assembly buildup,⁸⁵ and the thus-assembled pH-sensitive Dex-*g*- β -CD/PASP-*g*-AD microcapsules exhibited promising potential in cancer drug delivery. Noteworthy, host-guest interaction generally requires a perfect recognition afforded by selective and strong interactions between host cavities and guest molecules, which limits its extensive applications.

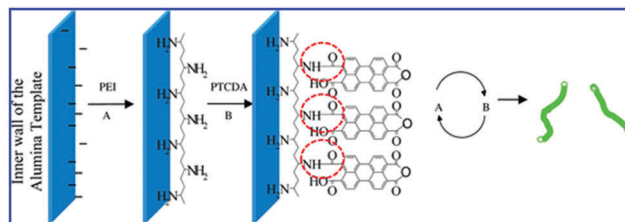
2.3.4 Biospecific interaction. The first work on fabrication of alternating multilayer assemblies through biospecific interactions was reported by Decher and K. Lowack in the early 1990s.⁸⁶ In this pioneering work, the authors extended the LbL assembly concept to integration of protein layers into synthetic PE films. As a first and extremely simple example, the well-established biotin/streptavidin system was used by the authors to construct such multilayers through biospecific recognition. Specifically, poly-L-lysine (PLB) was biotinylated and subsequently used for the construction of multilayer assemblies by biospecific recognition between biotin groups and streptavidin. The binding constant of the two entities is very high ($k \approx 10^{15} \text{ M}^{-1}$) which makes the process essentially irreversible.^{86,87} In a following study, Decher and K. Lowack fabricated the protein/polymer hybrid films by the LbL assembly technique based on combined electrostatic and biospecific interactions.⁸⁸ From then on, tremendous attention has been devoted to the fabrication of various alternating multilayer assemblies based on biospecific interactions. For example, as

performed by Yang's group,⁸⁹ protein multilayers composed of avidin and biotin-labeled antibody have been prepared on the gold substrate by the LbL assembly technique on account of the high specific binding constant between avidin and biotin afforded by biospecific recognition. Moreover, it was revealed that these biospecific interaction-dominated antibody multilayers remarkably enhance the binding ability compared to the conventional immobilized monolayer antibody, thus significantly boding well for their promising applications as immunosensors or biosensors. Alternatively, varied protein architectures and biotinylated protein networks have also been crafted by means of biospecific interactions giving rise to a large variety of molecularly layered multicomposite films.^{90,91}

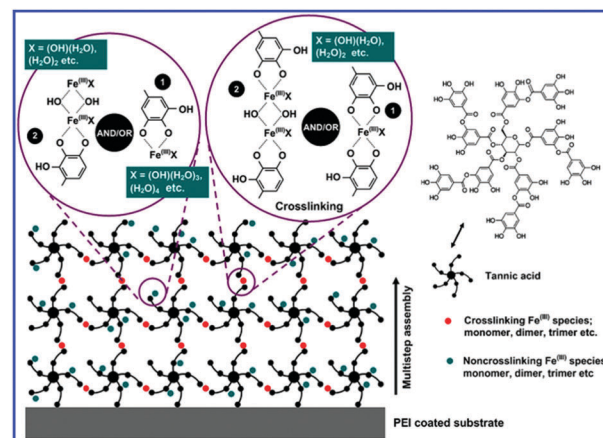
2.3.5 Covalent bonding interaction. Covalent bonding offers an alternative interaction to assemble LbL multilayer thin films, and has many intrinsic advantages. In particular, the stability and structure of multilayer films can be significantly strengthened with the introduction of covalent bonding. Moreover, it enables the integration of various functional groups in the assembled films which is in favor of fabricating a large amount of multifunctional assemblies.

The work on covalent bonding for LbL assembly was firstly reported by Crooks and co-workers,⁹² in which dendrimers and maleic anhydride were utilized as the constructing ingredients for LbL assembly of multilayer thin films with a thickness of 10–50 nm on various substrates (*e.g.*, glass, silicon, or gold-coated silicon wafers). In recent years, Caruso and co-workers creatively introduced the click chemistry concept to achieve efficient covalent LbL assembly under mild conditions.^{93,94} In these studies, LbL assembly was carried out by the copper(I)-catalyzed click reaction of azide and alkyne to form an extremely stable 1,2,3-triazole linkage, thereby resulting in covalently linked multilayer thin films with tailored structures. In another work, Li and co-workers developed a press-filter-template approach to prepare fluorescent nanotubes consisting of PEI and 3,4,9,10-perylenetetracarboxyldianhydride (PCTDA) *via* alternating deposition and covalent bonding interaction, as shown in Scheme 8.⁹⁵ The obtained nanotubes could be used in diverse fields such as catalysis, drug delivery, and design of optical devices. The covalent bonding based LbL assembly *via* click chemistry extends the number and diversity of materials that can be incorporated within the films, therefore contributing to the fabrication of highly stable and robust multilayer thin films that can resist a wide range of hash conditions. Despite the above properties, covalent bonding interaction is limited to molecules demonstrating complementary functional groups and, moreover, some side products might be introduced in the multilayer assemblies, thereby making it a more complex methodology.

2.3.6 Coordination chemistry interaction. Coordination chemistry interaction is a strong molecular interaction established between a diversity of metal ions and organic ligands, which has been utilized to construct highly oriented and robust 2D multilayer thin films and hierarchical 3D nanoarchitectures comprising polymers, metal oxides, and/or inorganic/organic hybrid nanocomposites.^{96–100} The assembly of coordination



Scheme 8 Chemical reaction procedures between PEI and PCTDA molecules. (Reprinted with permission from ref. 95, Copyright 2006, American Chemical Society.)

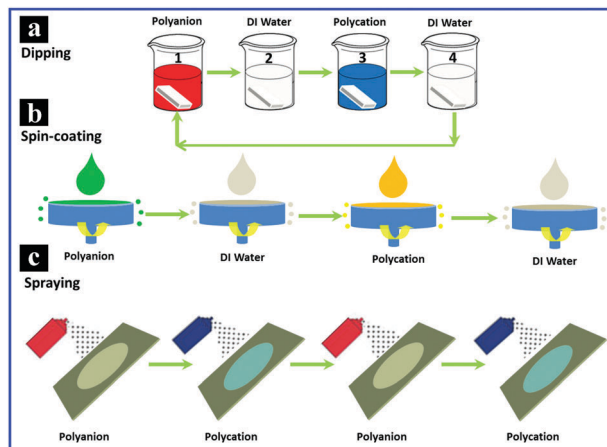


Scheme 9 Schematic illustration of the proposed growth mechanism for multistep assembly of Fe–tannic acid complex films. (Reprinted with permission from ref. 101, Copyright 2014 American Chemical Society.)

multilayers can be achieved by solution-based LbL growth methods, which render the fabrication of precisely tailored surfaces with long-range 2D ordering and orientation. Recently, Caruso's group (Scheme 9) reported the assembly of metal-polyphenol multilayer films and capsules *via* sequential deposition of iron(III) ions and tannic acid through metal–ligand coordination, which gives rise to lateral and longitudinal cross-linking of tannic acid by Fe(III) within the film architecture.¹⁰¹ Notably, the utilization of coordination chemistry interaction is restricted by its limited material selections and, moreover, it offers a slow assembly process for fabricating multilayer nanostructures depending on the type of organic ligand, metal ion, and solvent used. Moreover, some impurities may be incorporated in the final multilayer nanoarchitectures.

2.4 Assembly methods for LbL construction

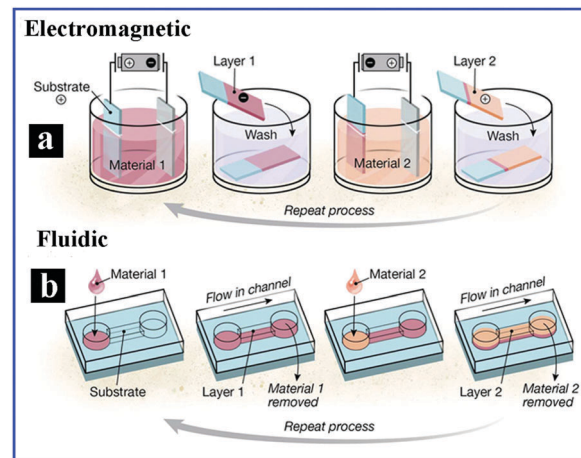
It has been well-established that the assembly method used in the LbL assembly process not only determines the process properties (*e.g.*, time, scalability, and manual intervention) but also remarkably influences the physicochemical properties of assembled films (*e.g.*, thickness, homogeneity, and inter- and intralayer film organization). With the development of the LbL assembly technique, many assembly methods have been developed to fabricate multilayer assemblies such as dip-coating, spin-coating, spraying,^{102–106} and perfusion,¹⁰⁷ which add additional versatility to the LbL assembly technique (Scheme 10).



Scheme 10 Schematic illustration of the LbL assembly process with (a) dipping method, (b) spraying method, and (c) consecutive spin-coating process of anionic and cationic PEs.

Among the various methods, dip-coating is advantageous for coating substrates with varied geometries (Scheme 10a), but the possible residual for each deposition step and relatively tedious procedures limit its efficiency for practical applications. Recently, spin- and spray-assisted LbL assemblies have been determined to be promising alternatives for LbL construction,^{108,109} which are beneficial for rapidly producing low cost and uniform LbL assembled films by reducing the processing time, thereby being more suitable for industrial applications (Scheme 10b and c).^{110,111} In particular, the spin-assisted LbL deposition method can introduce intimate interactions between PEs in the presence of simultaneous interaction forces including strong centrifugal, viscous, and air-shear forces. Therefore, it exhibits intrinsic advantages in terms of low chain interpenetration and dense packing coverage in comparison with conventional dipping methods. Moreover, the spray-assisted LbL deposition method can be applied not only to 2D but also to 3D substrates, and the structural properties of the multilayer films can be tuned by modulating the flow rate, sample to nozzle distance, and drainage time.¹⁸ Besides, other combined assembly methods including inkjet printing-assisted LbL assembly method^{112,113} and hydrodynamic dip-coating approach^{114,115} have also been developed for the fabrication of multilayers which remarkably improve the efficiency of the LbL assembly process. Alternatively, it is worth noting that newly developed vapor-based LbL growth methods, including atomic layer deposition (ALD),^{116–119} molecular layer deposition (MLD),^{120–123} and their combined methods,^{124–127} as efficient routes to assemble multilayer thin films have emerged for accurate control over film thickness, conformality, and uniformity, hence giving rise to high-quality multilayer films with densely packed and well-ordered internal structure.

More recently, two newly explored assembly methods including electromagnetic assembly and fluidic assembly have been developed to promote LbL assembly of multilayered films, as displayed in Scheme 11. To be specific, an applied electric or magnetic field was used in electromagnetic assembly to access



Scheme 11 (a) Electromagnetic assembly and (b) fluidic assembly for LbL assembly buildup. (Reprinted with permission from ref. 134, Copyright 2015 Science group.)

layering, *e.g.*, electrodes coated with polymer solutions or magnetic particulate substrates can be moved in and out of the coating solution.^{128,129} In a standard setup for electromagnetic assembly, two electrodes are immersed in a PE solution and an electric current is then applied to trigger electrodeposition. Subsequently, the electrodes are thoroughly washed and put into another PE solution with opposite charge, and the process can be repeated to attain the desired assembly layer (Scheme 11a).¹³⁰ Electromagnetic assembly based on electrodeposition can rapidly assemble ions, polymers, and colloids with much less time in comparison with many other conventional assembly approaches. Besides, the magnetic effect in electromagnetic assembly facilitates LbL assemblies on sensitive particulate or small templates which are difficult to be centrifuged.¹³¹ Although electromagnetic assembly has not been extensively applied in fabricating nanomaterials as other conventional assembly technologies owing to the requirement of special equipment and expertise, it provides a novel approach to efficiently construct multilayer systems and thus provides alternative opportunities for assembling films.

Fluidic assembly which involves coating of channel walls and a substrate placed in a fluidic channel can be used to deposit multilayers with fluidic channels.¹³² The method is featured with step-by-step moving PE using pressure or vacuum and washing solutions through the channels, such as tubing or capillaries, or designed microfluidic networks (Scheme 11b).¹³³ Fluidic assembly is typically accompanied by a pump or spinning to transport the liquid through the channels, which makes it a viable alternative for centrifugation-free assembly on particulate substrates. In general, fluidic assembly affords a means to assemble multilayers on surfaces which are not easily accessible by other methods, thus offering a new means for region-specific patterning and for boosting the industrial capacity of multilayer assemblies. Although fluidic assembly needs specialized equipment and expertise to build up fluidic systems, unique advantages of fluidic assembly make it extremely attractive for a diverse range of applications.¹³⁴

3. LbL assembly of 0D nanoparticulate assemblies

Surface properties of colloidal materials are of paramount importance to their potential applications in a myriad of technological research areas encompassing studies in the pharmaceutical, biological, and medical fields.¹³⁵ One of the requirements for realizing functional materials based on nanoparticles especially for metal and semiconductor nanoparticle systems is the availability of suitably modified nanoparticle building blocks. Nanoparticles with tailored properties have been prepared by surface modification with biomolecules (*e.g.*, DNA and protein),^{136,137} inorganic,¹³⁸ and organic materials.¹³⁹ Among these, polymer modification of nanoparticulate materials provides an effective method to tune the surface properties of the particles. Although various techniques have been developed to encapsulate metal nanoparticles with polymers and have gained varying success during the past one decade, it was not until 2001 that Caruso's group achieved controlled adsorption of preformed polymers (*i.e.*, PEs) to form uniform coating on metal nanoparticles based on electrostatic interactions afforded by the LbL assembly approach.¹⁴⁰ In this work, the authors reported the PE coating of gold nanoparticles with varying monodispersity and with diameter ranging from 10 to 50 nm, focusing predominantly on nanoparticles with diameter greater than 30 nm. This work surmounts the difficulty in the assembly of PEs onto nanoparticles with diameter less than 100 nm in order to form uniform and stable surface coatings regardless of the small size of the particles and high curvature of their surfaces.¹⁴¹ More significantly, LbL assembly of zero-dimensional (0D) metal nanoparticle/PE assemblies provides a versatile method that permits the controllable surface functionalization of a broad range of nanoparticles.

In a following study, the authors achieved uniform PE coating by the LbL assembly approach on nanoparticles with much smaller size (<10 nm). As shown in Fig. 1, intrinsic negatively charged mercaptoundecanoic acid (MUA)-capped gold nanoparticles with a mean diameter of *ca.* 7 nm were used as the substrate, and PEs of PDDA and PSS were used to step-by-step modify the surface properties of gold nanoparticles *via* the LbL assembly adsorption technique. It was found that the surface charge of gold nanoparticles can be easily inverted by adsorption of oppositely charged PEs without sacrificing the monodispersity of nanoparticles and, moreover, the surface plasmon peak of gold nanoparticles can be tuned by the assembly layer and ionic strength of the nanoparticle dispersion.

Furthermore, adsorption of PE-coated MUA-capped gold nanoparticles onto an oppositely charged planar substrate has also been achieved and the surface loading amount of gold nanoparticles can be tuned by varying the salt concentration in the nanoparticle dispersions used for adsorption. The LbL assembly strategy used in this work is anticipated to be applicable to modify other 0D nanoparticles or quantum dots (*e.g.*, semiconductors, phosphors), thereby offering a facile method for their controlled surface modification through PE nanolayering. Such 0D nanoparticles are envisaged to have extensive applications

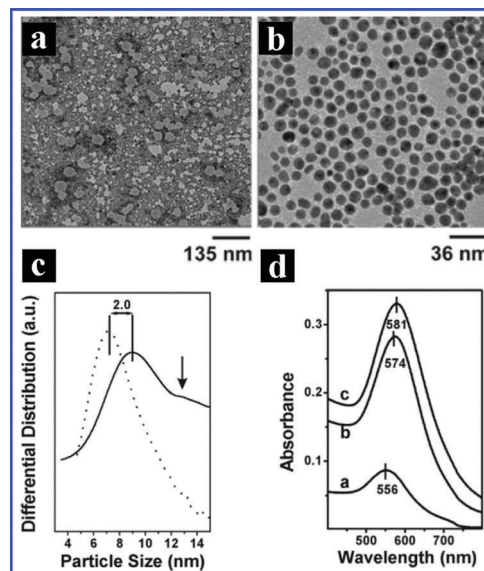


Fig. 1 (a) TEM image of MUA-capped gold nanoparticles coated with two PE layers (PDDA/PSS) and (b) higher magnification TEM image of (a). (c) Particle size distribution of MUA-capped gold nanoparticles before (dotted line) and after (solid line) coating with two layers of PEs (PDDA/PSS). (d) UV-vis spectra of multilayered thin film composed of (PDDA/PSS)-coated MUA-capped gold nanoparticles which were assembled on PEI-coated quartz substrates. The gold nanoparticles were deposited from aqueous solutions containing varied NaCl concentration: (a) 0, (b) 10, and (c) 20 mM. (Reprinted with permission from ref. 141, Copyright 2003 John Wiley & Sons, Inc.)

in the biomedical and bioanalytic fields, and to be useful building blocks for the construction of advanced nanoparticle-based films.

4. LbL assembly of 1D nanoarchitectures

The utilization of 1D nanostructures as templates for LbL assembly facilitates the creation of composite materials with well-defined tubular structures. The size, length, component, and thickness of the tubes can be tuned by the diameter and length of the templates, types of species deposited, and assembly cycles.

Generally, the two-step synthetic procedure is harnessed to access the LbL assembly of two oppositely charged components in the nanoscale range. For example, a layer of a PE pair (such as PDDA and PSS) can be firstly deposited on the surface of 1D nanostructures using LbL assembly, which affords positively or negatively charged surface. Subsequently, the oppositely charged ions in the precursor solution are adsorbed on the surface of the 1D nanostructures by virtue of pronounced electrostatic attraction between the charged species. Based on this, *in situ* reactions will occur on the 1D nanostructure surface giving rise to core-shell nanostructures, in which the electrostatic attraction between the charged species and the *in situ* reaction on the surface contribute to the formation of core-shell nanostructures with uniform coating layers. Finally, the

transformation of core-shell nanostructures to uniform nanotubes can be achieved by removing the templates.¹⁴² The thus-prepared core-shell or hollow 1D nanostructures with large surface-to-volume ratios hold great potential for extensive applications.

4.1 LbL assembly on conventional 1D templates

The utilization of nanoporous templates for LbL assembly of 1D nanostructures has gained enormous attention during the past few decades. Conventional 1D nanoporous templates including polycarbonate (PC) membranes, polystyrene (PS) fibers, and anodic aluminum oxide (AAO) membranes have been well and widely studied. PC membranes containing cylindrical pores with a mean diameter of 400 nm were frequently used as the template for the fabrication of nanotubes. In general, PEs were firstly LbL deposited within the nanopores of the templates, followed by PC template removal to generate free-standing nanotubes with desired diameter, wall thickness, and composition.¹⁴³ As a typical example, anatase and rutile titania nanotubes were prepared by LbL alternating deposition of negatively charged titanium(IV) bis(ammonium lactato)-dihydroxide (TALH) and positively charged PEI into the cylindrical pores of a PC membrane template, followed by calcination at different temperatures to produce TiO₂ nanotubes with varied crystal phases, as shown in Fig. 2.¹⁴⁴ Electrospun PS microfibers were also employed to fabricate PE multilayer microtubes by alternately coating the template with PAH/PSS PE pairs and finally removing the template with tetrahydrofuran to yield PAH/PSS PE microtubes.¹⁴⁵

A large variety of materials have been deposited within the cylindrical nanopores of AAO *via* the LbL assembly technique to produce nanotubes. Guo and co-workers (Fig. 3)¹⁴⁶ fabricated TiO₂ and TiO₂-based nanocomposite (*i.e.*, TiO₂-CdS and TiO₂-Au) nanotube arrays *via* LbL assembly of building blocks (TALH, CdS quantum dots, and Au NPs) onto the AAO template. In another

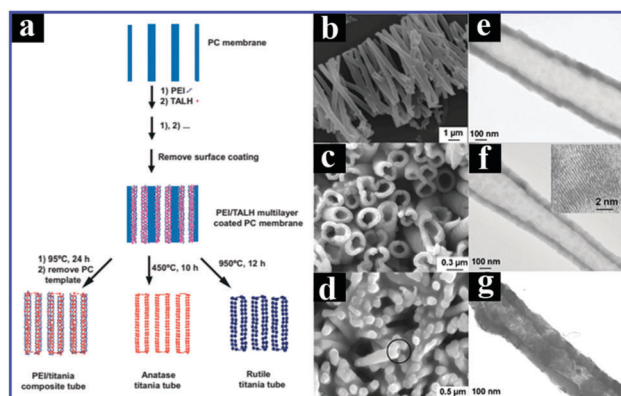


Fig. 2 (a) Schematic illustration of the preparation of titania nanotubes using the PC membrane as a template. SEM (b–d) and TEM (e–g) images of titania nanotubes prepared by calcining the (PEI/TALH)₁₂ multilayers coated on the PC membrane under varied temperature, (b and e) 95 °C for 24 h, (c and f) 450 °C for 10 h, and (d and g) 950 °C for 12 h in air. (Reprinted with permission from ref. 144, Copyright 2007 John Wiley & Sons, Inc.)

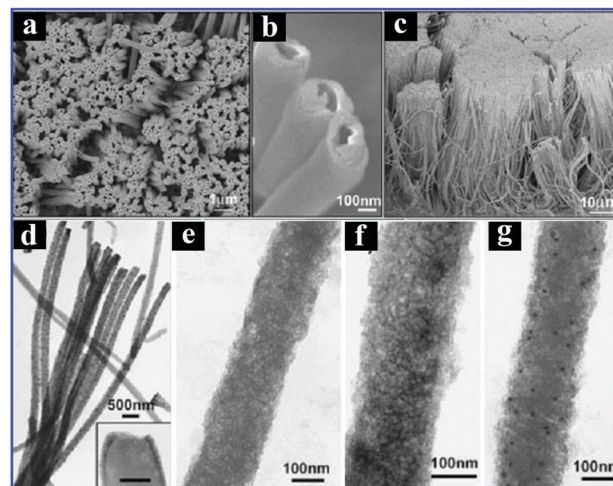


Fig. 3 (a–c) SEM and (f) TEM images of AAO/PSS/PDDA/(TALH/PDDA)/CdS/PDDA₅ after refluxing, TEM image of AAO/PSS/PDDA/(TALH/PDDA)₆ (d) before and (e) after refluxing, and (g) TEM image of AAO/PSS/PDDA/(TALH/PDDA)/Au/PDDA₅ after refluxing. (Reprinted with permission from ref. 146, Copyright 2005 John Wiley & Sons, Inc.)

case, a LbL assembly strategy for fabricating protein nanotubes within the pores of an AAO membrane was developed, in which the AAO template was alternately immersed in protein and glutaraldehyde solution with the latter acting as the cross-linking agent to combine the protein layer together.^{147,148} The numbers of protein layers that make up the nanotube walls can be tuned by changing the number of alternately deposited protein/glutaraldehyde cycles. Despite the significant endeavors in the previous studies, a key problem in preparing tubular nanomaterials through AAO pore templating is the aggregation upon membrane removal. Thus, it is highly desirable to develop more efficacious LbL assembly strategies to circumvent this problem. Alternatively, macroporous cellulose acetate membranes consisting of interconnected fibers have also been used as a template for preparing inorganic nanotubes, by which interconnected nanotubes with high surface areas within a framework can be attained through LbL assembly.¹⁴⁹

4.2 LbL assembly on carbon nanotubes

Although a large number of metal oxide nanotubes have been prepared by conventional template-assisted LbL approaches, there still exist several disadvantages in this respect. For example, the diameters of metal oxide nanotubes prepared based on the AAO template are generally larger than 100 nm which makes preparation of nanotubes with controllable diameters difficult. Additionally, it is rather difficult to completely remove the template. In recent years, carbon nanotubes (CNTs) have been explored as an ideal alternative template for LbL assembly of metal oxide nanotubes, which could circumvent the disadvantages caused by conventional templates.

The overall synthetic procedure for LbL assembly of metal oxide/CNT core-shell nanostructures or hollow metal oxide nanotubes is presented as follows. The intrinsic negatively charged surface of CNTs afforded by acid treatment is firstly

modified by PEs to render the CNT surface positively charged, which enables the adsorption of negatively charged complexes of metal ions and citric acid. The pronounced adsorption between CNTs and metal ions facilitates the *in situ* redox reactions occurring on the CNT surfaces, thus leading to uniform deposition of metal and metal oxide layers. Furthermore, hollow metal or metal oxide nanostructures can be fabricated by calcining the thus-assembled CNT@metal/metal oxide nanocomposites.

As carried out by Yang's group,¹⁵⁰ indium (In) NPs were uniformly deposited onto CNTs in which negatively charged sodium borohydride (*i.e.* BH_4^-) was used to reduce the metal ions (In^{3+}) pre-adsorbed on the positively charged PDDA/PSS/PDDA modified CNTs. The deposited In NPs were immediately oxidized to In_2O_3 under an oxygen atmosphere in solution, leading to well-defined CNT@ In_2O_3 core-shell nanostructures, as shown in Fig. 4. This LbL assembly strategy combined with an *in situ* reduction reaction has been established to be rather effective to fabricate many other hollow metal oxide or metal oxide/CNT core-shell nanostructures, such as NiO and NiO/CNTs, SnO_2 and SnO_2 /CNTs, Fe_2O_3 and Fe_2O_3 /CNTs, and CuO and CuO/CNTs.¹⁴² Moreover, assemblies of metal/CNTs and metal sulfide/CNTs can also be prepared using analogous LbL assembly approaches, thereby corroborating the versatility of this synthetic protocol.^{151–154} Apart from binary core-shell nanostructures, 1D ternary heterostructures can also be prepared with similar technical routes. For example, SnO_2 /Au/CNT core-shell nanostructures were synthesized *via* LbL assembly, for which Au NPs were firstly deposited onto the CNT substrate *via* a controlled *in situ* reduction reaction. Subsequently, a dense nano-layer of SnO_2 was coated on the CNT@Au through another *in situ* reduction reaction resulting in CNT@Au@ SnO_2 ternary nanostructures.¹⁵⁵ In this work, the two *in situ* reduction reactions integrated with the LbL process are conducive to precisely control the deposited amount and uniform distribution of metal oxide layers. Analogous synthetic procedures were reported by the same group for the preparation of CeO_2 / SnO_2 /CNT and Ag/NiO/CNT ternary core-shell heterostructures.¹⁵⁶ Besides, carbon fibers can also serve as a template to prepare various 1D nanostructures. As reported by Wang and co-workers,

zeolite microtubes were attained by LbL assembly of zeolite nanocrystals and PDDA on carbon microfibers, followed by removal of the template and PE through calcination.¹⁵⁷

It should be emphasized that the *in situ* reduction reaction based LbL assembly strategy exhibits several advantages over conventional LbL assembly methods which usually involve pre-synthesis of two oppositely charged components followed by simply assembling them in a well-designed fashion. To be specific, firstly, the *in situ* reduction reaction based LbL assembly strategy can afford complete adsorption and pronounced electrostatic interaction between two oppositely charged species which is beneficial for uniform deposition of stable and dense layers. Secondly, the thickness of the deposited ingredients can be easily tuned by adjusting the molar ratio of one species to the other precursor ions. Thirdly, the efficiency of the LbL assembly process based on *in situ* reduction reaction can be remarkably reinforced by reducing the complexity of the synthetic procedures.

4.3 LbL assembly on 1D semiconductors or metals

In addition to using conventional nanoporous materials and CNTs as templates, high-aspect-ratio 1D semiconductors or metal nanostructures such as nanorods and nanofibers can also be utilized as templates for LbL assembly buildup. The utilization of high-aspect-ratio templates can retard the pore blockage and non-uniform pore coating which are frequently observed when using conventional membrane templates. As reported by Caruso and co-workers (Fig. 5),¹⁵⁸ titania nanotubes were fabricated *via* alternating deposition of TALH and PDDA onto nickel nanorods, followed by hydrolysis of TALH through refluxing treatment and decomposition of the template. Alternatively, other 1D semiconductors such as zinc oxide (ZnO) nanorods were also adopted as the template for LbL assembly of 1D hybrid nanostructures.

On the other hand, apart from various 1D templates, template-free LbL assembly of 1D nanostructures has also been achieved. For example, Liu and co-workers developed an effective LbL assembly technique to prepare novel TiO_2 heterostructures

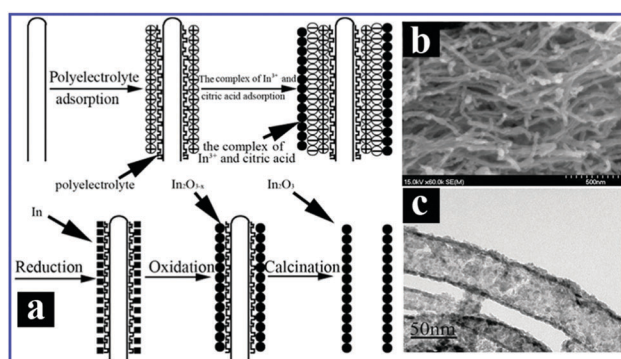


Fig. 4 (a) Schematic illustration depicting the preparation of In_2O_3 nanotubes, and (b) SEM and (c) TEM images of In_2O_3 nanotubes prepared by calcination of In_2O_3 /PE/CNT nanocomposites. (Reprinted with permission from ref. 150, Copyright 2007 John Wiley & Sons, Inc.)

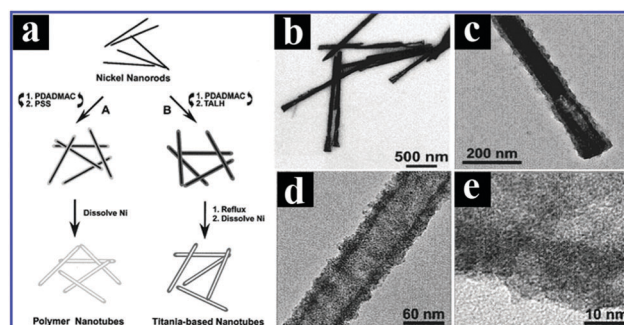


Fig. 5 (a) Schematic illustration of the fabrication of polymer and inorganic/organic composite nanotubes by the LbL assembly strategy. (b) TEM image of nickel nanorods coated with titania/PDDA. (c) TEM image of nickel nanorods coated with titania/PDDA. (d) TEM and (e) HRTEM images of a titania nanotube after removing the template. (Reprinted with permission from ref. 158, Copyright 2001 the American Chemical Society.)

via electrostatic interaction using PSS as a bridging or adhesion layer combined with calcination, in which anatase NPs were uniformly assembled on the rutile nanorods.¹⁵⁹

5. LbL assembly of 2D nanoarchitectures

To date, 2D metal oxide or non-oxide nanosheets have sparked worldwide interest by virtue of their peculiar electronic structures and distinctive physicochemical properties inherited from the layered parent compounds.^{160–163} It has been well-established that these nanosheets demonstrate exceptionally high 2D anisotropy with a molecular thickness of *ca.* 0.5–3 nm and lateral size of several hundred nanometers. Moreover, 2D configuration provides an extremely high percentage of exposed specific crystal facet, huge surface area, and large fraction of unsaturated surface metal sites which can act as active centers.^{164–167} Consequently, the excellent features of the 2D nanosheets offer abundant opportunities for researchers to rationally design innovative nanoarchitectures when they are used as building blocks during the LbL assembly process. In this section, we will summarize the latest developments of 2D nanosheets including transitional metal oxide nanosheets, non-metal oxide nanosheets, and graphene nanosheets for LbL assembly of multilayered thin films.

5.1 LbL assembly of multilayer assemblies using inorganic nanosheets as the main building blocks

5.1.1 Titanium dioxide nanosheets. TiO₂ possesses various polymorphs, among which anatase, rutile, and brookite have been established to be the most investigated structures. In recent years, metastable monoclinic TiO₂-B has also received increasing attention owing predominantly to its intriguing photo- and electrochemical properties.^{168–171} Apart from these well-documented structures, TiO₂ can also be derived from exfoliation of some Ti–O-bearing layered compounds to obtain a unique 2D anisotropy. TiO₂ single nanosheets which resemble the structure of graphene have been explored for almost twenty years. The swelling-exfoliating behaviors of layered titanates have been systematically studied by Sasaki and co-workers since the mid-1990s.^{172–175} The layered parent titanates can be exfoliated into single nanosheets through diverse approaches including ion exchange, intercalation, and mechanical shaking, by which single TiO₂ nanosheets with a thickness of *ca.* 1 nm and lateral size up to several tens of micrometers are prepared. In particular, TiO₂ nanosheets obtained from the wet-chemical exfoliation process retain a high single crystallinity and possess substantial surface charges for stable colloidal dispersion. More significantly, owing to the unique 2D nanostructure, distinctive properties of single TiO₂ nanosheets that are difficult to acquire in its bulk counterparts have been achieved.¹⁷⁶ As the composition of the exfoliated TiO₂ nanosheets slightly deviates from the theoretical stoichiometry of TiO₂ which is strongly dependent on the layered parent titanate compounds, a general formula of Ti_{1-x}□_xO₂^{δ-} (*e.g.* Ti_{0.91}O₂^{0.36-} or Ti_{0.87}O₂^{0.52-}) is generally used

to describe the nanosheets in which □ represents titanium vacancies.¹⁷⁷

Owing to the 2D planar characteristic of exfoliated nanosheets, it is highly intriguing to fabricate multilayer thin films comprised of closely integrated nanosheets with different compositions. Particularly, the ultra-thin exfoliated TiO₂ nanosheets can be used as fascinating building blocks for LbL assembly. As performed by Sasaki's group, pure Ti_{0.91}O₂^{0.36-} nanosheet multilayer thin films were fabricated *via* LbL stepwise assembly, for which PEI, PDDA, and Ti_{0.91}O₂^{0.36-} nanosheets were used as ingredients for the growth of multilayer films with sandwich-like structure.¹⁷⁸ Similarly, colloidal TiO₂ NPs were LbL assembled with Ti_{0.91}O₂^{0.36-} nanosheets using PDDA and PSS as “glue molecules”, thus resulting in TiO₂ NPs/Ti_{0.91}O₂^{0.36-} nanosheet films in an alternate deposition fashion by the same group.¹⁷⁹ Apart from single-component films, hybrid multilayer films consisting of Au NPs and Ti_{0.91}O₂^{0.36-} nanosheets were LbL assembled on the glass or ITO substrate in an arbitrary layering order with the addition of PEI and PDDA.¹⁸⁰ The plasmon resonance of the multilayers can be tuned by the varied intercalated layer of TiO₂ nanosheets and plasmon coupling of Au NPs. More recently, this technique was applied to LbL assembly of exfoliated Ti_{0.91}O₂^{0.36-} nanosheets with graphene (GR) nanosheets using PEI as a binder (Fig. 6), by which exfoliated Ti_{0.91}O₂^{0.36-} and graphene oxide (GO) nanosheets were deposited in an alternating fashion giving rise to multilayered structures.^{181,182} GO can be readily reduced to GR by exposing the films to UV light which generates Ti_{0.91}O₂^{0.36-}/GR composite films. This work signifies the accessibility of using exfoliated Ti_{0.91}O₂^{0.36-} and other 2D inorganic nanosheets (*e.g.*, MnO₂^{δ-},¹⁸³ Nb₃O₈,¹⁸⁴ layered double hydroxides,¹⁸⁵ and CdS¹⁸⁶) as building blocks for LbL assembly of multilayer thin films for photoelectrochemical (PEC) applications.

Besides the commonly used PEs for LbL assembly, conducting polymers have been recently utilized as binders to assemble Ti_{0.91}O₂^{0.36-} nanosheets, which avoids the post-removal of PEs *via* calcination or UV irradiation treatment.¹⁸⁷ Wang's group directly applied polyaniline (PANI) as the building block to LbL

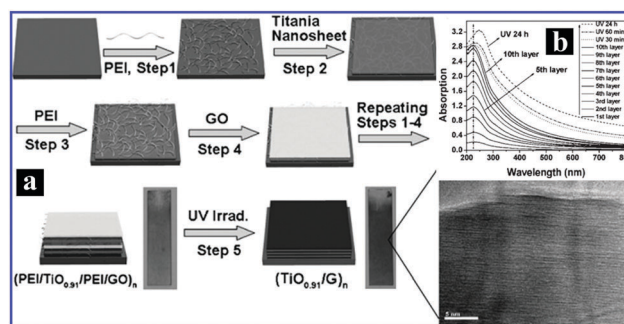


Fig. 6 (a) Schematic illustration of the fabrication of LbL assembled Ti_{0.91}O₂^{0.36-}/GO multilayer thin films followed by UV photoreduction. The inset shows the HRTEM image of Ti_{0.91}O₂/GO multilayer films. (b) UV-vis absorption spectra of the (Ti_{0.91}O₂/GO or GR) multilayer films with variation of the deposition layer. (Reprinted with permission from ref. 181, Copyright 2009 John Wiley & Sons, Inc.)¹⁸¹

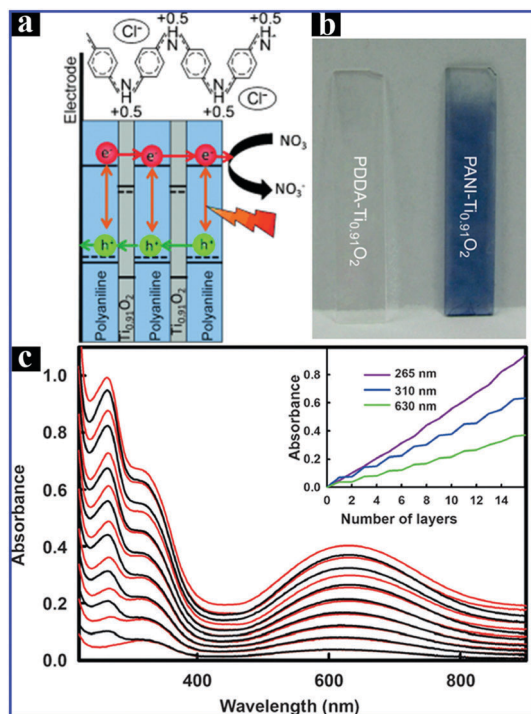


Fig. 7 (a) Schematic illustration showing the LbL assembly of TiO₂ nanosheets and PANI, and the corresponding photoelectrochemical mechanism. (b) Digital photographs of blank Ti_{0.91}O₂ nanosheet multilayer films and (PANI-Ti_{0.91}O₂)₈ multilayer films. (c) UV-Vis absorption spectra of PANI/Ti_{0.91}O₂ multilayer films. The inset shows the absorbance of a particular wavelength with the number of deposited layers. (Reprinted with permission from ref. 188, Copyright 2013 John Wiley & Sons, Inc.)

assemble with Ti_{0.91}O₂^{0.36-} nanosheets through carefully adjusting the pH value of the PANI solution, which produced PANI/Ti_{0.91}O₂^{0.36-} nanosheet multilayer thin films (Fig. 7). The thus-assembled multilayer films exhibited unique switchable photocurrents from n-type to p-type under different pH conditions, which was principally ascribed to the remarkable transformation in the structural configuration and conductivity of PANI molecules upon protonation within the composite multilayer film.¹⁸⁸ This work provides a new strategy to probe the electronic property of TiO₂ nanosheets without the interference of PEs. In addition, other inorganic species including Al₁₃ Keggin ions and ruthenium red have also been exploited for LbL assembly of Ti_{0.91}O₂^{0.36-} nanosheet-based nanoporous multilayer composite films with improved thermal stability and functionalities.^{189,190}

5.1.2 Other transitional metal oxide nanosheets. Besides titania-based nanosheets, perovskite nanosheets with large dielectric constants have also been widely explored for LbL assembly. Till now, various exfoliated layered perovskite nanosheets have been reported such as LaNb₂O₇, (Ca, Sr)₂Nb₃O₁₀, CaLaNb₂TiO₁₀, La₂Ti₂NbO₁₀,^{191–196} and some others with Ruddlesden-Popper (Eu_{0.56}Ta₂O₇, SrLaTi₂TaO₁₀, Ca₂Ta₂TiO₁₀), Aurivillius (Bi₂WO₆, SrBi₂Ta₂O₉, Bi₄Ti₃O₁₂),^{197–200} and rock-salt (K₂NbO₃F) phases.^{201–206} LbL assembly of layered perovskite nanosheets affords a promising approach for the fabrication of dielectric and ferroelectric films

with precisely controlled thickness and composition. Noteworthy, the work on LbL assembly of perovskite nanosheets has seldomly been reported until very recently. To this end, Osada and co-workers (Fig. 8) fabricated multilayer thin films using perovskite nanosheets (CaNb₃O₁₀, LaNb₂O₇, and Sr₂Nb₃O₁₀) as building blocks for LbL assembly,^{207–209} in which delaminated layered perovskite nanosheets were stacked on atomically flat SrRuO₃ and Pt substrates to create films with thicknesses of ca. 5–20 nm. Moreover, it was found that the CaNb₃O₁₀ and Sr₂Nb₃O₁₀ multilayers exhibited large dielectric constants (>200 s) and low leakage current densities (<10⁻⁷ A cm⁻²) even in films with thickness less than 5 nm, which showed great potential applications as electric devices. Similarly, multilayer films consisting of perovskite-type (Ca₂Nb₃O₁₀)_n (n = 1–10) nanosheets were also prepared *via* the LbL assembly approach, which exhibited excellent dielectric properties.²¹⁰ These results suggest that perovskite nanosheets could provide new opportunities for applications ranging from electronics to energy-storage devices. In addition, a Bi₂WO₆ nanoplate multilayer film as an efficient visible-light-driven photocatalyst was prepared by LbL assembly of negatively charged Bi₂WO₆ nanoplates and PEI.²¹¹

5.1.3 Non-metal oxide nanosheets. More recently, a large number of exfoliated non-metal oxide nanosheets have been extensively investigated, among which the nanosheets of MoS₂, WS₂, BN, MoSe₂, NbSe₂, NiTe₂, and Bi₂Ti₃ arising from layered dichalcogenides and nitrides are experiencing exponential growth in various research fields.^{212–218} The diversity of monolayer non-metal oxide nanosheets provides new options for the selection of building ingredients for LbL assembly of composite films. As reported by Sun and co-workers,²¹⁹ MoS₂-GR multilayers were

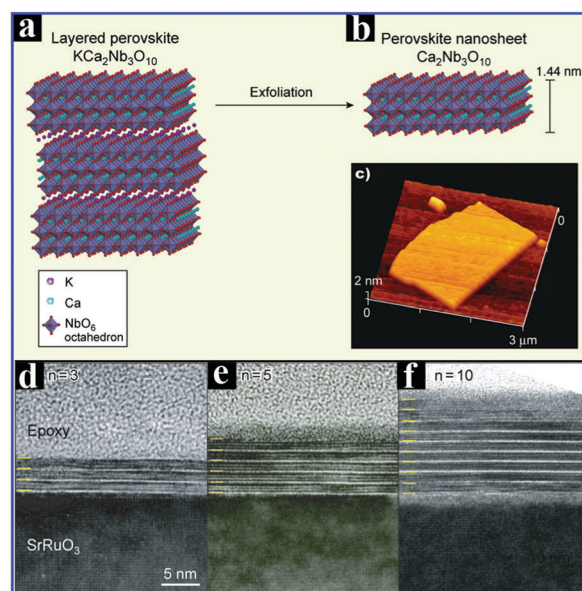


Fig. 8 Structure of the starting layered (a) perovskite KCa₂Nb₃O₁₀ and (b) Ca₂Nb₃O₁₀ perovskite nanosheets. (c) AFM image of a single Ca₂Nb₃O₁₀ nanosheet deposited onto a Si substrate. (d–f) HRTEM images of the (Ca₂Nb₃O₁₀)_n (n = 3, 5, 10) films deposited on the SrRuO₃ substrate. The lines show the layer stacking. (Reprinted with permission from ref. 207, Copyright 2010 American Chemical Society.)

LbL assembled *via* vacuum assisted filtration of a mixture of MoS₂ and GR nanosheets suspended in *N*-methyl-pyrrolidinone and water, respectively, by which MoS₂ nanosheets were evenly dispersed between the GR nanosheets and *vice versa*. Moreover, it was found that the as-assembled MoS₂-GR multilayer thin films could be used as high-performance lithium ion battery anodes. Although intense efforts have been devoted to the synthesis of 2D non-metal oxide nanosheets, thus far, the potential applications of these nanosheets for LbL assembly are still in their infancy. It is possible that intriguing properties would emerge from these non-metal oxide nanosheets in that quantum confinement effects might become dominant at atomic thickness and make them behave very differently.

5.2 LbL assembly of multilayer assemblies using GR as the main building block

GR represents a unique category of 2D nanosheets based on its single-layer property with carbon atoms arranged in tightly bound hexagons.^{220–237} The 2D structure of GR nanosheets in conjunction with atomic thickness imparts unique properties to GR which are distinctly different from conventional 1D carbon allotrope counterparts (*e.g.*, CNT). GR is featured with various stimulating properties including extremely efficient transportation of electrons, mechanical properties and high surface-to-volume ratio. In particular, the 2D nanosheet-like morphology of GR makes it more applicable to combine with many other planar substrates using intimate face-to-face stacking as compared with other counterparts which are typically randomly distributed on the substrate.²³⁸

It should be stressed that the extraordinary properties of GR are merely observed in the mechanically exfoliated GR with nearly perfect structure; however, tedious synthetic procedure, low yield, and high-temperature processing conditions make the preparation of GR nanosheets with comparable properties rather difficult. Therefore, in this regard, various synthetic strategies have been developed such as chemical vapor deposition (CVD),²³⁹ epitaxial growth,²⁴⁰ and solution-based synthesis,²⁴¹ among which the solution-based synthesis of GR has received tremendous attention by virtue of its inexpensive sources, high yield and, more significantly, stable colloidal dispersions for easy and flexible preparation of hybrid multilayer thin films. In general, two methods are adapted to prepare solution processed graphene (SPG) nanosheets. One involves the dispersion of graphite in a liquid medium (*e.g.*, *N*-methylpyrrolidone) followed by sonication and separation by centrifugation to remove the non-exfoliated graphite.²⁴² The other method involves the utilization of graphene oxide (GO) as a precursor, which has been determined to be the most efficient way to produce SPG.^{243,244}

The most obvious difference between SPG and GR synthesized from the mechanical exfoliation method is the amount of oxygen containing functional groups. On SPG, there exist a large amount of oxygen-containing functional groups including hydroxyl and epoxy groups on the basal plane and carboxyl and carbonyl groups at the edges.²⁴⁵ These polar functional groups provide various opportunities for GO to act as a building block for LbL assembly through hydrogen bonding or electrostatic

attractive interaction. Additionally, the pronounced interaction between the basal planes of SPG owing to pronounced van der Waals and π - π stacking forces could further reinforce the stability of LbL assembled multilayer thin films. Therefore, the intrinsic structural characteristics of GO (or SPG) set up a solid foundation for LbL assembly of various multilayer thin films.

5.2.1 GO or GR-polymer multilayer assemblies. The layered assemblies of GR or GO were firstly demonstrated by Kotov and co-workers,²⁴⁶ in which positively charged PDDA was used as the partner PE of GO to trigger the electrostatic interaction-based LbL assembly buildup. It was estimated that the average thickness of the PDDA and GO layer was around 16 ± 3 Å and 22 ± 5 Å, respectively. This pioneering work signifies the feasibility of preparation of GO multilayer ultrathin films through the LbL assembly strategy. The stable GR dispersion affords the preparation of GR-based multilayers without undergoing the post-reduction treatment to transform GO to GR within the film. For example, as performed by Ye's group,²⁴⁷ PAA functionalized negatively charged GR and poly(acrylamide) (PAA) modified positively charged GR were prepared by radical polymerization and used as building blocks for LbL assembly of pure GR multilayer films. In another work, as reported by Zhao and co-workers (Fig. 9),²⁴⁸ (PVA/GO)_{*n*} multilayer ultrathin films were constructed by LbL assembly of poly(vinyl alcohol) (PVA) and GO nanosheets based on hydrogen bonding interaction, in which only GO nanosheets were used as the building blocks. It was found that the mechanical properties of the film were significantly enhanced including a 98.7% improvement of elastic modulus and a 240.4% increase of hardness, which could be attributed to the well-defined layered architecture of hybrid multilayers with a high degree of planar orientation and nanoscale assemblies of GO nanosheets in the polymer matrices. Analogously, Davis's group²⁴⁹ prepared GR/polymer multilayer films by the LbL assembly of pyrene-terminated poly(2-*N,N'*-dimethyl amino ethyl acrylate) (PDMAEA) and PAA-modified GR *via* π - π stacking.²⁵⁰ The resulting GR/polymer films were revealed to show phase transfer behavior between aqueous and organic media under different pH conditions. The incorporation of charged block copolymers into GR multilayers through LbL assembly was also reported.²⁵¹

5.2.2 GR-metal NP multilayer assemblies. The unique physical properties of GR nanosheets make them excellent substrates for immobilizing metal NPs. Over the past few years, considerable progress has been made in the synthesis of GR-metal NP composites.^{252–255} In particular, GR nanosheets as building blocks have recently been combined with various metal NPs to prepare composite films by the LbL assembly method.²⁵⁶ For example, GR-platinum (Pt) NP multilayer thin films were constructed by alternately LbL assembling ionic liquid modified GR nanosheets and Pt NPs for electrocatalytic oxygen reduction.²⁵⁷ Jung and co-workers developed an efficient LbL assembly strategy combined with a vacuum filtration technique to prepare GR/Au NP multilayer thin films, in which Au NPs with a mean particle size of *ca.* 200 nm were *in situ* formed through spontaneous reduction of gold ions on GR films.²⁵⁸ Moreover, as carried out by Roy's group,

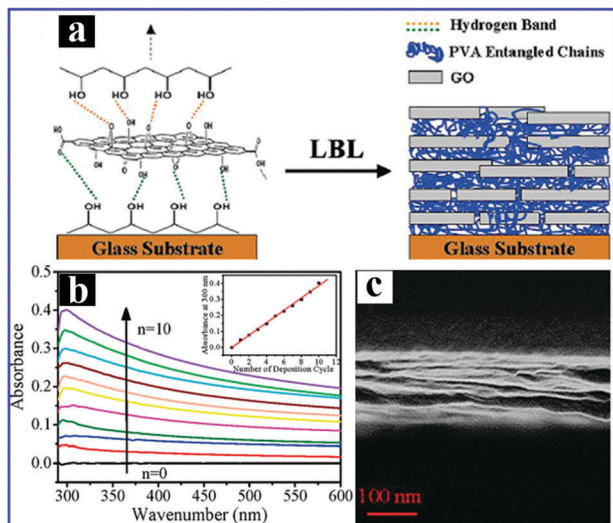


Fig. 9 (a) Schematic illustration of the LbL assembly process (top left) with GO nanosheets and architecture of the PVA/GO multilayer thin films (top right), (b) UV absorption spectra of (PVA/GO)_n films as a function of the stacking layer. Inset: Absorbance of (PVA/GO)_n films at 300 nm as a function of deposition cycles, and (c) cross-sectional SEM image of (PVA/GO)₅₀ films. (Reprinted with permission from ref. 248, Copyright 2010 American Chemical Society.)

a novel nanoarchitecture for low-voltage flash memory based on solution-processed GR/Au NP hybrid films LbL assembled on flexible poly(ethylene terephthalate) (PET) substrates was systematically demonstrated.²⁵⁹ In addition to Pt and Au NPs, Ag NPs can also be integrated within the LbL assembly system. For instance, transparent and conductive GR/Ag NP multilayer thin films were LbL assembled on a quartz substrate using homogeneous Ag NPs@PDDA and GO nanosheets as constructing components followed by a thermal reduction process.²⁶⁰ More recently, growing interest has been devoted to the development of porous GR for LbL assembly of 3D multilayer films. Typically, Yang and co-workers reported the fabrication of a uniform 3D Au NP-embedded porous GR (Au-EPG) hybrid multilayer thin film by electrostatic LbL assembly of Au NPs and bovine serum-modified GR nanosheets followed by a thermal annealing treatment (340 °C, in air, 2 h).²⁶¹ It was found that the thus-assembled multilayer thin films demonstrated significantly improved electrochemical sensing performances for H₂O₂ detection as compared with nonporous Au NP-GR film-modified electrodes, which was attributed to the advantages imparted by the porous structure of Au-EPG. This work opens up a new and facile way to directly prepare metal NP-embedded porous GR composite films. Additionally, it should be noted that the synthetic process for LbL assembly of GR and metal NPs can be remarkably speeded up by combing with spin-coating instead of being limited to conventional simple static deposition.²⁶²

Alternatively, the electrodeposition strategy has also been established to be an efficient and rapid approach for LbL assembly of GR-metal multilayer composite films. For example, Luo and co-workers achieved one-step co-electrodeposition of GR-Au NP composite multilayer films in which both GO and

metal reduction reactions occur simultaneously under cathodic conditions.²⁶³ As shown in Fig. 10, the as-prepared multilayered composite thin film demonstrated characteristic layered nanostructures composed of alternating layers of Au NPs and GR nanosheets, in which the intercalation of Au NPs between GR nanosheets prevented the agglomeration of GR nanosheets and improved the conductivity of the GR film.

5.2.3 GR-carbon multilayer assemblies. GR/carbon hybrid nanomaterials have been extensively explored owing to their respective structural advantages and extraordinary application potential arising from synergistic interaction.²⁶⁴ Among them, GR/carbon multilayer thin films prepared by the LbL assembly approach have been shown to be a unique platform for integrating diverse carbon nanomaterials for multifunctional electronic and energy applications.²⁶⁵ For example, Yu and co-workers achieved the intimate combination of GR nanosheets and CNTs based on an efficient and easily accessible LbL self-assembly strategy, in which positively charged PEI-modified GR nanosheets were alternately deposited with negatively charged CNTs, thus producing GR/CNT multilayer composite films with an interconnected network of carbon structures and well-defined nanopores.²⁶⁶ Moreover, it was revealed that these hybrid films could serve as efficient supercapacitor electrodes. This work provides a convenient synthetic protocol for the preparation of GR/CNT multilayer thin films.

Although recent efforts are geared toward the production of GR-based multilayer thin films with LbL assembly techniques, most of these are limited to composite structures associated with various polymer PEs. Thus, it is highly desirable to achieve a uniform blend of 2D GR nanosheets with other ingredients in a well-defined structure by a direct LbL deposition approach. As performed by Min's group,²⁶⁷ large-area ultrathin transparent films comprised of double layers of GR nanosheets

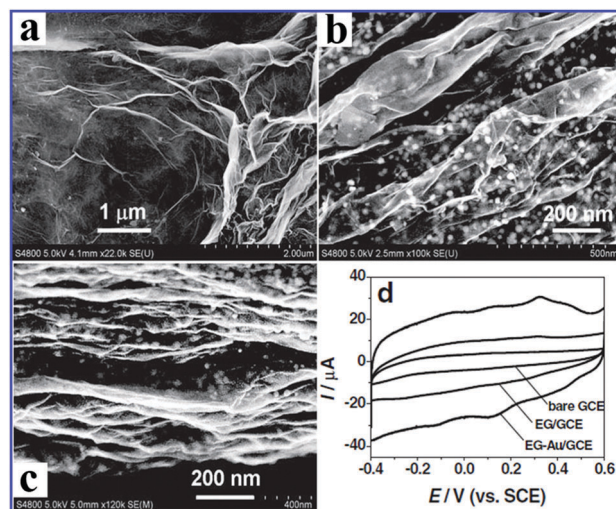


Fig. 10 (a) SEM images of electrogenerated GR (EG) and (b) EG-Au multilayer films. (c) Cross-sectional SEM image of the EG-Au multilayer film. (d) CV curves of the bare glassy carbon electrode (GCE), EG/GCE, and EG-Au/GCE in 1.0 M KCl at a scan rate of 50 mV s⁻¹. (Reprinted with permission from ref. 263, Copyright 2011 John Wiley & Sons, Inc.)

and multi-walled CNTs (MWNTs) were prepared through a LbL self-assembly process, in which negatively charged GO and positively charged MWNTs were directly utilized as building blocks for LbL buildup without the involvement of any polymers. This work offers a conceptual guideline for integrating various active carbon materials. In a similar study, Hong and co-workers developed a simple method to fabricate hybrid films by integrating GR nanosheets with MWNTs *via* LbL assembly which involves the electrostatic attractions of two oppositely charged suspensions of GR nanosheets and MWNTs.²⁶⁸ The GR/MWNT hybrid multilayer thin films were shown to serve as highly flexible and transparent electrodes.

In addition, multilayer thin films consisting of exclusively GR nanosheets have also been prepared through the LbL assembly strategy. For example, Kim's group fabricated pure GR multilayer thin films by sequential LbL assembly of positively and negatively charged GO nanosheets.²⁶⁹ In a following study, the same group made use of the thus-assembled multilayer GR films as transistors, and the result showed that either ambipolar or unipolar (both n- and p-type) transport behavior could be tuned by the bilayer number of thermally reduced GO films, as shown in Fig. 11.²⁷⁰ These two studies provide a versatile method to prepare controllable GR multilayer thin films on a large scale and, more importantly, to control the charge transport in GR multilayer films.

5.2.4 GR-inorganic materials multilayer assemblies. Multilayer composite films consisting of alternating GR nanosheets and inorganic nanosheets or NPs have been widely prepared through the LbL assembly strategy and show fascinating potential applications. It has been generally assumed that intercalation of a foreign inorganic layer in GR can efficiently prevent π - π stacking between the layers and create functional separation of individual GR nanosheets. Such multilayer stacked films allow for the periodic control of the refractive index as well as the interplay of photon and electron transport,²⁷¹ which can be utilized in the fabrication of broadband antireflective coating or Bragg mirrors.²⁷² Ultrathin monolayer inorganic nanosheets prepared by exfoliation of bulk layered compounds have attracted considerable attention nowadays as nanobuilding blocks for LbL assembly of multilayer films.²⁷³ To date, a variety of LbL assembled multilayer hybrid systems have been constructed by using inorganic nanosheets (*e.g.*, $\text{Ti}_{1-\delta}\text{O}_2$, MnO_2 , or hydroxide) as ingredients.²⁷⁴ As aforementioned in Section 5.1.1, highly crystalline TiO_2 nanosheets exhibit very high 2D anisotropy with a thickness of 0.75 nm and lateral dimensions of up to several tens of micrometers.²⁷⁵ Therefore, it is highly desirable to prepare multilayer thin films by alternating deposition of such TiO_2 lamellar structure and GR nanosheets which would contribute to intimate 2D-2D composite multilayer thin films with versatile functionalities.

Loh's group fabricated alternating GR and titania ($\text{Ti}_{0.91}\text{O}_2$) multilayered hybrid nanosheet systems using the LbL electrostatic deposition route in conjunction with UV irradiation, in which GO nanosheets, $\text{Ti}_{0.91}\text{O}_2$ nanosheets, and PEI were used as building blocks.¹⁸¹ The as-assembled hybrid nanosheet films showed ultrafast photocatalytic electron transfer between

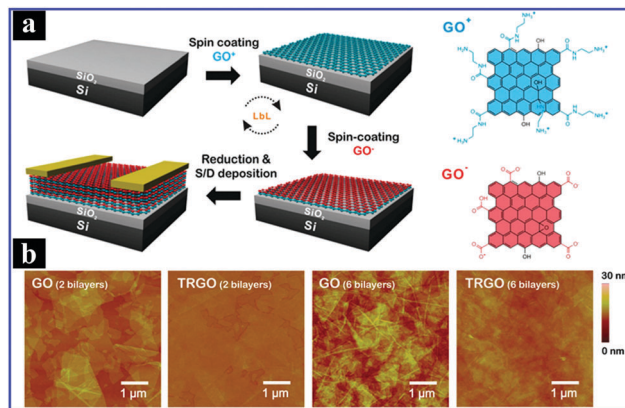


Fig. 11 (a) Schematic representation of a LbL-assembled GR-based field-effect transistor, and (b) AFM images of two- and six-bilayered GO and thermally reduced GO (TRGO). (Reprinted with permission from ref. 270, Copyright 2012 American Chemical Society.)

$\text{Ti}_{0.91}\text{O}_2$ and GR nanosheets. In an analogous work, inspired by the structure and function of granum, Yang and co-workers fabricated alternate stacking structures with TiO_2/GR nanosheets *via* LbL assembly to improve the photoelectric conversion efficiency (Fig. 12), in which exfoliated TiO_2 nanosheets, GO nanosheets, and PDDA served as constructing components.²⁷⁶ Furthermore, the photoelectric effect of the composite multilayer films was exploited by monitoring the variation of photocurrent which indicates that the photoelectric response of the TiO_2/GR composites is about 20 times higher than that of pure TiO_2 film with the same stacking thickness. More significantly, the photocurrent of the composite film can be changed from cathodic to anodic as film thickness increases, which shows profound implications for solar cells. With this improvement, it is envisaged that TiO_2 -based solar cells could break the thickness bottleneck and achieve higher efficiency. Consistently, Yu's group applied multilayer films consisting of alternately stacked titania and GR nanosheets to fabricate photoconductive patterns, which exhibited high photocurrent generation and good reversibility.²⁷⁷

Apart from TiO_2 , as another quintessential visible light sensitizer, quantum dots (QDs) can also be integrated into GR films during the LbL assembly process. For example, Li's group developed a simple bottom-up approach to fabricate a novel layered CdS QDs/GR multilayer system, in which GR and *in situ* formed CdS QDs were LbL deposited in an alternate way, resulting in multilayer thin films with intimate interfacial interaction.²⁷⁸ The novel CdS QDs/GR multilayer composite films demonstrated a high photocurrent density of 1.08 mA cm^{-2} under simulated solar light illumination (100 mW cm^{-2}), which is the highest among all reported QD/carbon solar cells. This work provides a new direction toward the development of high-performance light-harvesting devices. More recently, our group developed an efficient synthetic approach for LbL assembly of CdS QDs/GR nanosheet multilayer films based on electrostatic interactions, for which tailor-made monodispersed CdS QDs and PAH-modified GR nanosheets were utilized as building blocks.²⁷⁹ The thus-assembled multilayer nanocomposite films

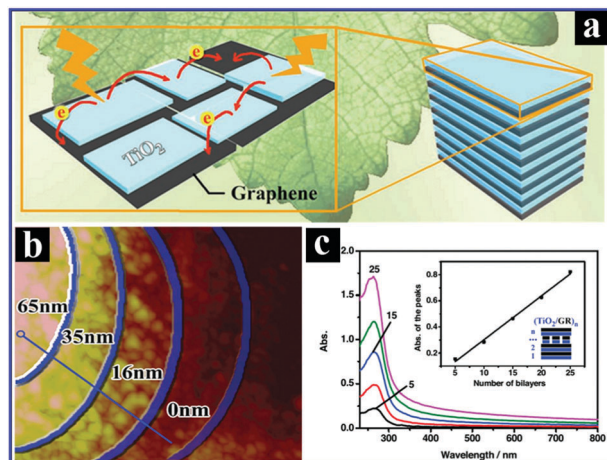


Fig. 12 (a) Schematic illustration of the stacked structure of the $(\text{TiO}_2/\text{GR})_n$ multilayer thin film, (b) AFM image of $(\text{PDDA}/\text{TiO}_2/\text{PDDA}/\text{GR})_{25}$ multilayers, and (c) UV-vis absorption of $(\text{TiO}_2/\text{GR})_n$ multilayer films with different number of layers and absorption of TiO_2 peak versus number of bilayer. (Reprinted with permission from ref. 276. Copyright 2012 John Wiley & Sons, Inc.)

demonstrated promising photocatalytic and PEC performances under visible light irradiation ($\lambda > 420$ nm). Noteworthily, multilayer composite thin films comprising conjugated polymers and CdSe NPs have also been prepared *via* the LbL assembly strategy based on covalent coupling reactions.²⁸⁰ Thus, it is anticipated that 2D GR/CdX (X = Te, Se) multilayer films would be attained through the LbL assembly strategy for multifunctional photovoltaic applications. Alternatively, free-standing LbL assembled GR/MnO₂ nanotube hybrid films were also fabricated by an ultrafiltration technique and used as anodes for lithium ion batteries, for which the unique structures of the multilayer films provided porous structures that could enhance Li ion diffusion.²⁸¹ Consequently, LbL assembled GR/inorganic materials bode well for multifunctional applications.

6. LbL assembly of 3D nanoarchitectures

LbL assembly of 3D structures has gained enormous research attention on account of their spatially hierarchical structures and recent years have witnessed their extensive applications in a myriad of research fields such as electrocatalysis, photoelectrocatalysis, photocatalysis and biomedical penetration. The versatility of LbL assembly has rendered a large variety of materials such as polymers, inorganic NPs, and biomolecules to be assembled on various substrates based on different molecular interactions.^{282–284} The synthetic strategy for LbL assembly of hierarchical 3D assemblies generally includes two routes. One involves LbL assembly on various microsized sacrificial colloidal or hierarchical templates and finally removal of the templates *via* calcination or solvent treatment giving rise to LbL assembled 3D inorganic or polymer assemblies. The frequently used sacrificial colloidal templates are mainly

centered on polystyrene (PS), melamine formaldehyde (MF), liquid droplets, gas bubbles, and silica.¹²⁸ Besides, tailor-made hierarchical templates consisting of orderly arranged colloidal particles (*e.g.*, SiO₂ and PS) or 1D nanostructures (*e.g.*, ZnO) can also be used as sacrificial templates. Therefore, LbL assembled microsized 3D hollow spherical capsules or spatially hierarchical nanostructures can be achieved by this templating technique which affords tunable control over size, component, thickness, and penetration of 3D assemblies *via* rational selection of appropriate templates. The other one is based on direct LbL assembly of 3D polymer capsules consisting of intertwined PE building blocks. Aside from 3D polymer and inorganic capsules, a large variety of other 3D assemblies can also be fabricated through the LbL assembly approach such as 3D graphene-based assemblies, metal-based assemblies, and polymer–metal assemblies, which will be elucidated in the following.

6.1 3D inorganic multilayer assemblies

Inorganic capsules, as a typical category of 3D colloidal template-based assemblies, can be prepared by a variety of spherical templates, which exhibit superior mechanical and thermal stability. Hollow spherical inorganic capsules can be prepared by LbL assembly of various tailor-made NPs which act as building blocks. Generally, inorganic capsules were fabricated by alternate deposition of PEs and semiconductor NPs onto PS spheres, followed by calcination to remove the organic components and templates leading to hollow spherical structures.^{285,286} In this way, both the size and shell thickness of inorganic capsules can be tuned *via* the assembly cycle of NP components. Moreover, post-calcination treatment can enhance the mechanical strength of the hollow capsules. Thus far, several inorganic precursors with specific charge properties have been directly applied to construct 3D hollow spherical inorganic capsules through the LbL assembly strategy based on the colloid-templating strategy. For example, as illustrated in Fig. 13, anatase titania capsules were prepared by alternate deposition of negatively charged titanium precursor, TALH, and positively charged PDDA on the PS substrate, after which the template and polycation were removed by calcination.²⁸⁷ Besides, calcium carbonate (CaCO₃), as another frequently used template for fabrication of various nanostructures, can also serve as a promising alternative sacrificial template for fabricating a large variety of 3D inorganic hollow capsules *via* the LbL assembly approach, owing to its excellent biocompatibility and easy removal in milder ways than PS and SiO₂.^{288,289}

On the other hand, porous colloidal templates such as mesoporous silica particles (MSP) have attracted increasing interest for LbL assembly of biomaterials because the highly porous interior of MSP can be harnessed to encapsulate various materials.^{290–293} For example, 3D hollow zeolite capsules decorated with metal NPs, metal oxides, and carbon have been prepared using MSP owing to their high specific surface area and large nanopore volume.^{294,295} Among them, palladium NP-loaded zeolite capsules have been demonstrated to exhibit high activity and favorable stability toward catalyzing a series of Heck-coupling reactions.²⁹⁶ Alternatively, as another fascinating

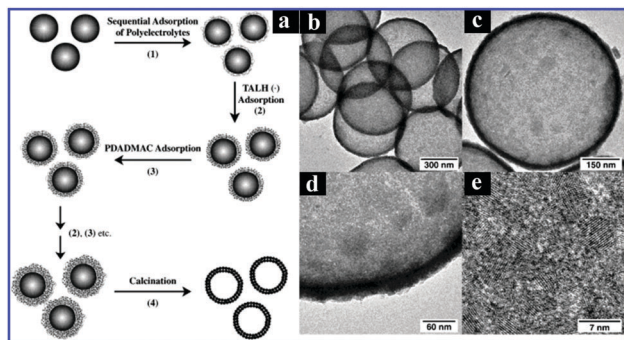


Fig. 13 (a) Schematic illustration of the procedure for constructing hollow titania spheres on PS spheres as the template. (b–d) TEM and (e) HRTEM images of hollow titania spheres after calcining the composite particles consisting of a PS core coated with TALH and PDADMAC at 450 °C. (Reprinted with permission from ref. 287, Copyright 2001 John Wiley & Sons, Inc.)

3D spatially hierarchically ordered template, 3D ordered macroporous (3DOM) materials have ignited massive interest in recent years due to their unique properties and promising potential applications, ranging from photonic crystals to advanced adsorbents and catalysts.²⁹⁷ For example, as demonstrated by Caruso's group,²⁹⁸ a 3DOM structure composed of highly ordered interconnected hollow spheres was fabricated by infiltrating a titania precursor (titanium isopropoxide) into a crystalline array of LbL assembled PE/silica-coated colloidal particles, followed by calcination to remove the PE moieties. The wall thickness of the macropore could be easily tuned by changing the number of deposition layers onto the colloids during the LbL assembly buildup. Alternatively, the LbL assembly technique was further applied to modify 3DOM titania membranes with PAH and cadmium telluride.²⁹⁹ By applying a similar method, as shown in Fig. 14, a 3DOM zeolite membrane was fabricated by LbL alternate coating of a crystalline array of MSP, followed by hydrothermal treatment, thereby yielding highly ordered and hierarchically porous multilayer thin films.³⁰⁰

6.2 3D GR and GR–metal multilayer assemblies

More recently, 3D multilayer thin films and capsules have raised increasing interest by virtue of their unique architectures and properties. Particularly, 2D structural advantages and tunable surface charge properties of GR nanosheets provide promising opportunities for the creation of 3D LbL assembled multilayer thin films and capsules. For example, as reported by Kim's group,³⁰¹ 3D electrocatalytic multilayer thin films were prepared by LbL assembly of electroactive Au NPs with GO nanosheets toward methanol oxidation, which involved the alternating assembly of two oppositely charged suspension of Au NPs and GO nanosheets in the presence of pronounced electrostatic interaction. It was found that intercalation of GO nanosheets in the hybrid thin films remarkably improves the utilization and dispersion of Au NPs and the high catalytic activity of Au NPs as well as the excellent electronic conduction of GR nanosheets contributed to the significantly enhanced methanol oxidation performance of composite films. Most recently, a 3D

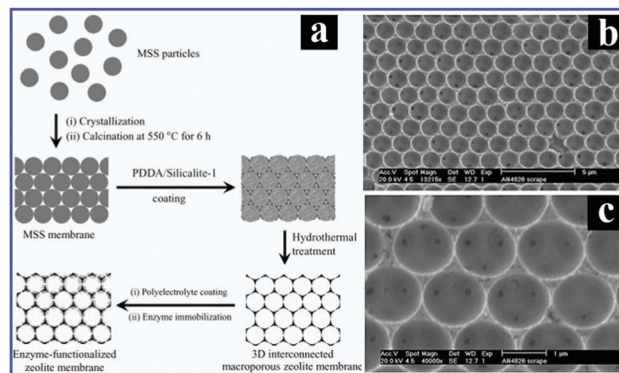


Fig. 14 (a) Schematic illustration of the fabrication of a 3D macroporous zeolitic membrane via the LbL assembly strategy, and (b and c) SEM images of the membrane at different magnifications. (Reprinted with permission from ref. 298, Copyright 2001 John Wiley & Sons, Inc.)

LbL GR/Au NP hybrid architecture was constructed by Xue and co-workers, for which the interlayer distance between GR nanosheets was tuned by Au NPs with different particle sizes.³⁰² This work provides an exciting impetus for building a tunable 3D carbon nanostructure with tailored functionality. LbL assembly of GR and other noble metal (Au, Pt, or Pd) 3D multilayer hybrid films has also been reported.^{248,252} These studies concurrently present the general concept for LbL assembly of GR-based 3D multilayer films. Besides, in another work, strikingly, Kim's group introduced a novel and versatile approach for LbL assembly of 3D GR capsules in which positively and negatively charged GR nanosheets were utilized as building blocks for the fabrication of multilayered capsules on sacrificial PS colloids, as shown in Fig. 15.³⁰³ More significantly, Au NPs can be further evenly incorporated into the interior surface of the GR capsules, which provides a basis for rationally designing 3D GR–metal capsules to open new possibilities in diverse promising fields such as drug delivery, catalysis, and electrochemistry.

6.3 3D polymer multilayer assemblies

3D polymer capsules prepared by the LbL assembly technique were firstly developed by Donath *et al.* in 1998 and have rapidly emerged as a new kind of materials for extensive biomedical applications.³⁰⁴ The main polymer capsules are prepared by alternate deposition of positively and negatively charged polymers on colloidal templates, in which the formation of multilayer assemblies is controlled by electrostatic attractive interactions. Alternatively, covalent bonding or complementary base pairing interactions can also be utilized to prepare polymer capsules.^{305,306} To date, various biocompatible polymer pairs have been developed to LbL assemble 3D polymer capsules, such as poly(L-lysine)/poly(L-glutamic acid),³⁰⁷ chitosan/dextran sulfate,³⁰⁸ poly(DL-lactic acid)/poly(DL-lactic-co-glycolic acid),³⁰⁹ chondroitin sulfate/poly(L-arginine),³¹⁰ and dextran sulfate/protamine.³¹¹ The typical morphology of 3D hierarchical polymer capsules consisting of PE multilayer films is displayed in Fig. 16. Notably, these polymer capsules are cross-linked via disulfide bonds and thus they are stable at physiological pH but can be disassembled

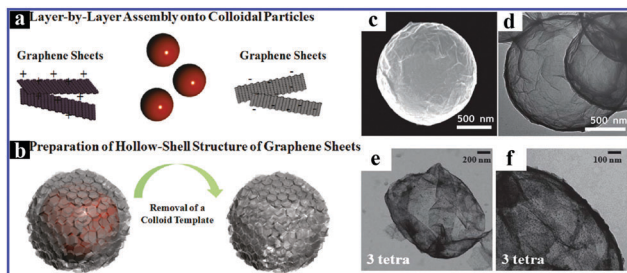


Fig. 15 Schematic illustration of (a) LbL assembly of GR nanosheets onto PS colloidal particles and (b) fabrication of GR multilayer hollow capsules after removing the sacrificial template. (c) SEM image of a core-shell composite particle containing GO nanosheets on the PS template (1 μm) before removing the core template. (d) TEM image of GR-based hollow capsules after removing the PS templates in (c) with THF. (e) Low and (f) high-magnification TEM images of GR-based capsules containing 3 tetralayers (GR-NH³⁺/GR-COO⁻/Au NPs/GR-COO⁻)₃. (Reprinted with permission from ref. 303, Copyright 2010 American Chemical Society.)

in response to thiol/disulfide, therefore showing great potential for *in vivo* penetration.^{312,313}

Liquid droplets can also be utilized as colloidal templates for LbL assembly of polymer capsules. For instance, it was reported that polymer membranes consisting of chitosan, pectin, or gelatin had been deposited on corn oil droplets dispersed in water, showing the great potential of the emulsion droplets as effective templates for 3D capsule preparation.^{314–317} Another amazing colloidal template that has been explored for LbL assembly is the gas bubble. As judiciously performed by Shchukin and co-workers,³¹⁸ detergent-capped air bubbles were used as templates to fabricate PE microcapsules, which prevents the collapse of air microsuspensions. The use of gas bubbles as templates for the creation of 3D polymer capsules makes the removal of the core moiety unnecessary; however, the relatively low stability and poor polydispersity of bubbles retard their extensive potential applications.

On the other hand, 3D hierarchical polymer capsules have also been fabricated using the LbL assembly strategy. For instance, as shown in Fig. 17b, Wang and co-workers reported LbL uniform coating of porous silica with PEs followed by removal of silica templates to obtain 3D micrometer-sized nanoporous PE capsules (Fig. 17c).³¹⁹ The detailed procedure

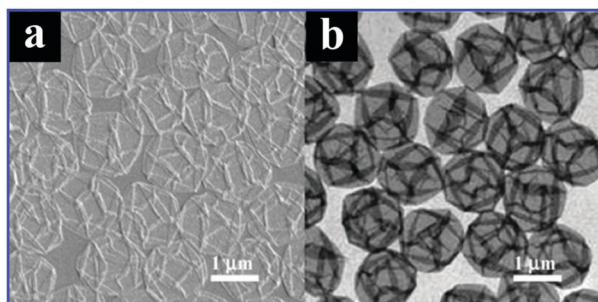


Fig. 16 (a) SEM and (b) TEM images of LbL assembled PSS/PAH polymer capsules. (Reprinted with permission from ref. 313, Copyright 2005 American Chemical Society.)

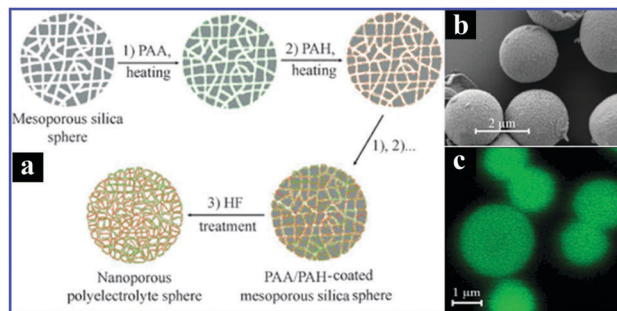


Fig. 17 (a) Schematic illustration of the preparation of nanoporous 3D PE capsules, (b) SEM image of (PAA/PAH)₂/PAA capsules, and (c) confocal laser scanning microscopy (CLSM) image of PE capsules which were partially cross-linked by heating (160 $^{\circ}\text{C}$, 2 h) after each PE deposition. (Reprinted with permission from ref. 319, Copyright 2005 John Wiley & Sons, Inc.)

to prepare the 3D nanoporous PE spheres normally involves two steps, as clearly illustrated in Fig. 17a. The first one involves LbL assembly of oppositely charged PEs (PAA and PAH) onto the surface of silica spheres followed by spatial cross-linking of each PE layer with heat treatment. The second step involves the removal of the silica template using hydrofluoric acid. This approach affords a general route towards the preparation of 3D nanoporous polymer capsules with tailored composition based on sequential LbL self-assembly.

6.4 3D all metal multilayer assemblies

Bimetallic alternating systems have been designed for tailored functions, such as superior electrocatalysis. In particular, Pt-based bimetallic materials have recently attracted considerable attention owing to their advanced performances in a myriad of fields. As demonstrated by Wang *et al.*,³²⁰ Pt/Pd alternating layers with accessible mesopores were prepared *via* a facile LbL electrochemical deposition method with the assistance of micelle assembly in a dilute surfactant electrolyte (Fig. 18A). It was ascertained by the authors that forming alternating layer structures with nanometer-level layer thickness is highly advantageous for achieving an abundant heterointerface by atom-level interfacial contact. Moreover, introducing mesopore structures into the bimetallic layers further boosts the electrocatalytic performance of Pt/Pd alternating layers toward methanol oxidation. More significantly, the amount (or thickness) of Pt and Pd components in the alternating layer can be easily controlled by electrochemical deposition time (Fig. 18B). In anticipation, the synthetic concept presented in this work can be applied to more complicated multilayer mesoporous films with various metal and alloy layers.

6.5 3D polymer-metal multilayer assemblies

Polymer-metal hybrid multilayer films with catalytic NPs embedded in multilayered PEs offer a versatile platform for potentially controlling catalyst properties, which simply involves alternating adsorption of polycations and polyanions. Generally, there are two strategies to prepare NP-containing 3D polymer-metal capsules. In the first, metal NPs serve as

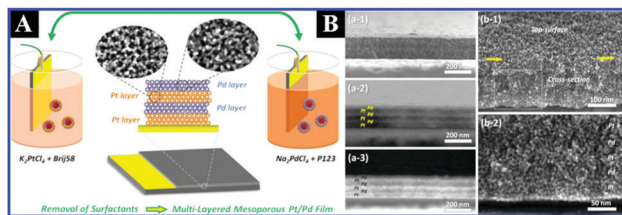


Fig. 18 (A) Procedure for fabricating multilayer mesoporous Pt/Pd films by electrochemical deposition. (B) Images of a six-layer mesoporous Pt/Pd LbL-assembled multilayer film: (a-1) low-magnification SEM image; (a-2) electron back-scattered diffraction (EBSD) image; (a-3) dark-field transmission electron microscopy image; (b-1) high-magnification SEM image; (b-2) enlarged SEM image of the square box in (b-1). (Reprinted with permission from ref. 320, Copyright 2012 American Chemical Society.)

polycations or polyanions during the film deposition, whereas in the second, metal ions are incorporated into PE films and subsequently reduced to form NPs. For example, Kidambi *et al.* presented a synthetic procedure to fabricate PE–Pd systems by alternating immersion of an alumina substrate in PdCl_4^{2-} and PEI solution followed by reduction of Pd(II) , as displayed in Fig. 19a.^{321,322} As well, the authors demonstrated another analogous system in which PAA and the PEI–Pd(II) complex were used as building blocks followed by reduction treatment giving rise to 3D hierarchical polymer–metal capsules (Fig. 19b). Moreover, the Pd NPs encapsulated in both $[\text{PAA/PEI-Pd(0)}]_n$ and reduced $[\text{PdCl}_4^{2-}/\text{PEI}]_n$ films exhibit different selective catalysis toward hydrogenation of allyl alcohol on account of varied rate of transport to the catalytic sites on the NPs. In another work, Liu *et al.* demonstrated the formation of Pd NPs on glass carbon by electrochemical reduction of films prepared by alternating adsorption of PdCl_4^{2-} and an electroactive polycation.³²³

7. Applications of LbL assembled nanoarchitectures with different dimensionality

LbL assembly of various types of nanosized materials is gathering new perspectives in a myriad of research fields. In this section, extensive applications of the LbL assembled multilayer assemblies, especially the GR-based LbL multilayer systems, in the fields of energy and catalysis are specifically illustrated.

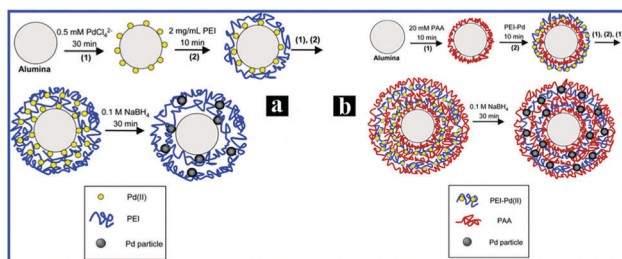


Fig. 19 (a) Formation of Pd NPs in $[\text{PdCl}_4^{2-}/\text{PEI}]_n$ films, (b) formation of Pd NPs in $[\text{PAA/PEI-Pd(0)}]_n$ films. (Reprinted with permission from ref. 321, Copyright 2005 American Chemical Society.)

7.1 Transparent conducting films (TCFs)

Up to now, the most intriguing progress in the development of TCFs predominantly focuses on GR-based TCFs owing to the extraordinary properties of GR.³²⁴ The highly aromatic nature of GR with extremely low electrical resistivity makes it a promising candidate as a new generation of transparent electrodes.³²⁵ The integration of GR nanosheets with conducting polymers³²⁶ or CNTs³²⁷ has been regarded as an effective way to increase the conductivity of GR-based multilayer thin films.³²⁸ For example, the LbL-assembled MWNT/GR multilayer film (Fig. 20) is featured by the formation of an interconnected network of conductive MWNTs integrating the GR nanosheets, which exhibits a low sheet resistance ($8 \text{ k}\Omega \text{ sq}^{-1}$) with a high transmittance (81%) after thermal treatment.²⁶⁸ Thermal treatment is pivotal to decrease sheet resistance owing to the removal of various oxygen-containing functional groups on GO nanosheets. It is worth noting that the performance of LbL assembled SPG as TCFs is comparable to those of other films made by solution-based methods including vacuum assisted flocculation,^{329,330} dip-coating³³¹ and LB assembly,³³² with resistance on the order of several $\text{k}\Omega$. Moreover, with a view to fabricating TCF with better performance, it is advisable not to integrate the insulating composition as partners of SPG within the LbL assembled system and chemical modifications of SPG should be avoided. Alternatively, thus far, many other GR-based multilayer films prepared by the LbL assembly approach have also been exploited as TCFs, such as GR/layered double hydroxide nanosheets,³³³ GR multilayers LbL assembled from PDDA and GO, as well as PAA/or PSS and CTAB–GO.³³⁴

7.2 Field effect transistors (FETs)

The high transportation of carriers in GR nanosheets makes it an attractive candidate for FET applications.³³⁵ Nonetheless, SPG

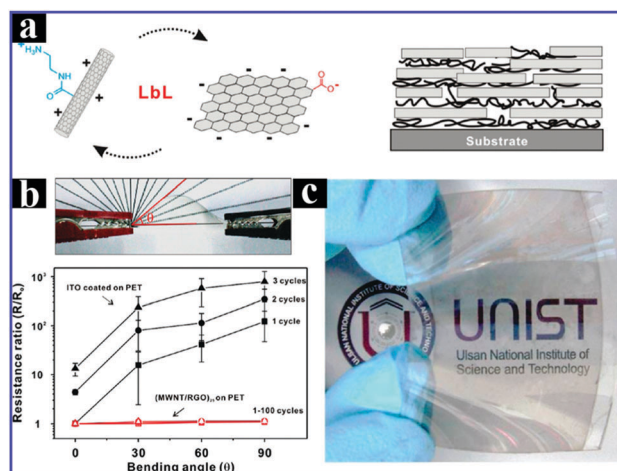


Fig. 20 (a) Schematic illustration of the fabrication of MWNT/GR LbL composite multilayer thin films, (b) variation of surface resistance of $(\text{MWNT/GR})_{25}$ coated on PET and ITO-coated PET substrates under different bending angles, and (c) photograph of the $(\text{MWNT/RGO})_{25}$ hybrid multilayer thin film on a PET substrate after mild thermal treatment. (Reprinted with permission from ref. 268, Copyright 2010 American Chemical Society.)

nanosheets could be contaminated by some impurities, defects, and dopants during the synthesis process, which would greatly diminish their FET performances. In addition, the unfavorable uniformity in SPG retards the electron mobility in SPG based FETs because of scattering occurring at the junctions of overlapping nanosheets. To surmount these obstacles of SPG for FET applications, multilayer thin films of GR nanoribbons were LbL assembled under ambient conditions by Zhu and co-workers.³³⁶ The GR nanoribbon thin film based FET showed p-type behavior which is remarkably different from that of ambipolar GR and SPG based FETs. In another work (Fig. 21), Li *et al.* fabricated multilayer thin films consisting of GO nanosheets and H₃PW₁₂O₄₀ (PW) using PAH as a linker *via* an efficient LbL assembly approach, followed by a photoreduction treatment for converting GO to GR.³³⁷ It was revealed that FET performances of the GR/PW multilayer thin films could be easily tuned by the number of layers deposited in the LbL assembly buildup.

7.3 Lithium ion batteries

GR is a promising material for lithium ion storage, which possesses a large amount of low energy sites owing to the host of lithium ions in both sides (C₃Li).³³⁸ The lithium ion storage capacity of GR could be further improved by the covalent Li₂ sites (C₂Li)³³⁹ and the low energy edge sites (C_{1.5}Li).³⁴⁰ Inspired by these discoveries, the SPG with large amounts of defects imparted by the oxidation–reduction process has been extensively investigated for lithium ion storage, which shows much improved lithium storage capacity.^{341,342} Generally speaking, it is desirable to keep as few-layer SPG as possible to provide a tunable stacking of SPG layers with a favorable interlayer spacing for lithium ion storage inside a lithium ion battery anode.²³⁸ Cassagneau and co-workers reported the assembly of

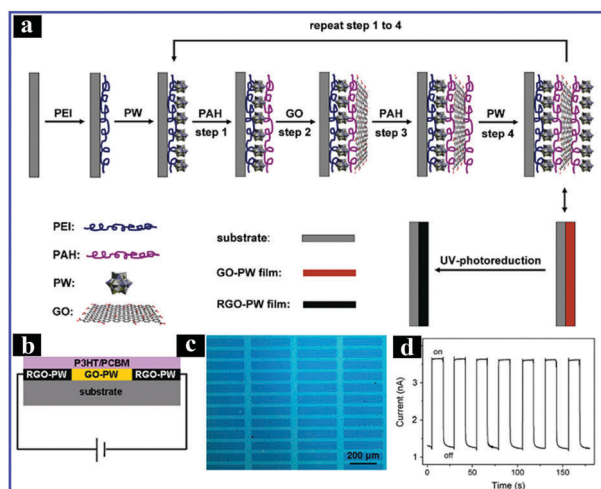


Fig. 21 (a) Schematic illustration of the LbL assembly of GR/PW multilayer thin films. (b) Cross-sectional schematic image of the photodetector. (c) Optical microscope image of the reduced pattern on (PAH/GO/PAH/PW)₆ multilayer films on a silicon substrate. (d) Photocurrent response of the photodetector based on the conductive patterns in (c) versus time under chopped irradiation at a bias voltage of 10 V. (Reprinted with permission from ref. 337, Copyright 2011 American Chemical Society.)

a rechargeable lithium-ion battery with polyethylene oxide, PDDA, and GO nanosheets as building blocks.³⁴³ The thus-obtained LbL assembled multilayer thin film demonstrates significantly high capacity (1232 mA h g⁻¹).^{344–347} Besides, SPG has also been integrated with other components which possess larger theoretical specific capacities as a conductive supporting material to retard the large volume variation during the charge–discharge process.^{348,349} The close interfacial interaction between SPG and other components is essential for superior performances.^{350,351} For instance, as shown in Fig. 22, free-standing LbL assembled GR/MnO₂ nanotube (NT) multilayer thin films were fabricated by an ultrafiltration technique and applied as the anode for lithium ion batteries, in which the ultrathin GR layer provides conductive routes promoting the conversion reaction of MnO₂ and, meanwhile, provides buffer layers to retain electrical contact with MnO₂ NT during the insertion/extraction of lithium.²⁸¹ The GR/MnO₂ NT films demonstrated fascinating cycle and rate capabilities with a reversible specific capacity.

7.4 Supercapacitors

Supercapacitors now play an important role in the progress of hybrid and electric vehicles, consumer electronics, and military and space applications. Materials possessing high specific surface area (SSA) such as CNTs, nanostructured metal oxides, and conducting polymers are ideal candidates for supercapacitor applications.^{352,353} Given that GR is featured with high theoretical SSA (2630 m² g⁻¹) which is larger than that of CNTs (1600 m² g⁻¹), investigations on GR based supercapacitors have therefore been extensively pursued.³⁵⁴ The integration of SPG with metal oxides in a LbL stacking manner is beneficial for generating a synergistic effect through the formation of an intimate interface for charge transport. For example, supercapacitors constructed from the LbL assembled

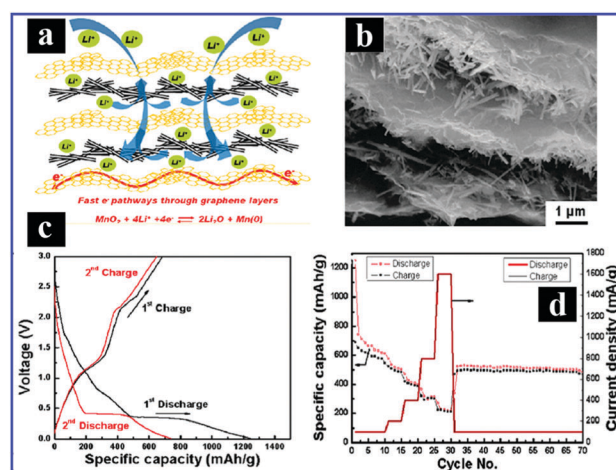


Fig. 22 (a) Schematic illustration of the LbL stacked GR/MnO₂ nanotube composites, (b) cross-sectional SEM image of GR/MnO₂ nanotube composites, (c) galvanostatic charge and discharge curves of the LbL GR/MnO₂ nanotube film, and (d) capacity of the GR/MnO₂ nanotube film at various current rates with the variation of cycle number. (Reprinted with permission from ref. 281, Copyright 2011 American Chemical Society.)

nanostructure of PSS-GR/manganese dioxide (MnO_2) nano-sheets exhibited promising specific capacitances.^{355–357} Specifically, as shown in Fig. 23(a–d), multilayer films with different alternating deposition layers were fabricated by using PSS-GR, MnO_2 , and PDDA as building blocks. It was found that the deposition layer remarkably influences the electrochemical performances of supercapacitors; the specific capacitance of the optimal ITO/(PDDA/PSS-GR/PDDA/PDDA/ MnO_2)₁₀ electrode reached 263 F g^{-1} at a discharge current density of 0.283 A g^{-1} and, moreover, it demonstrated good stability and high Coulombic efficiency. In another work, an impressive specific capacity was obtained over Co-Al-layered double hydroxide (LDH)/GO structures prepared by the LbL assembly strategy, owing to the ordered stacking of GO nanosheets and Co-Al-LDH for the efficient transportation of charge. Furthermore, LbL assembled GR composites can also reduce the restacking of GR and tune the pore size of the inter-plate for penetration of the electrolyte, which should also contribute to the improvement of supercapacitor performances. Despite the advancements made in the previous studies, there is a growing demand for developing hybrid supercapacitor systems to overcome the energy density limitations of the current generation of carbon-based supercapacitors. Most recently, as displayed in Fig. 23e, 3D high-performance hybrid supercapacitors and microsupercapacitors based on GR and MnO_2 which are rationally designed *via* the LbL deposition technique were demonstrated.³⁵⁸ The electrode can operate at high voltages with an ultrahigh volumetric capacitance of over 1100 F cm^{-3} corresponding to a

specific capacitance of the constituent MnO_2 of 1145 F g^{-1} which is close to the theoretical value of 1380 F g^{-1} . More significantly, the energy density of the full device is superior to commercially available supercapacitors.

7.5 Solar cells

The rapid developments of GR-based transparent composites promote their applications in solar cells.^{359,360} The wide absorption range of GR is beneficial for improving the power conversion efficiency of solar cells and, moreover, the work function of GR (4.5 eV) could be tuned by changing surface states or the number of bilayers assembled for efficient charge carrier injection.^{361–363} Hence, when applied as a photocathode, the unique properties of GR could enable it to replace the conventional Pt photocathode in DSSCs acting as a transparent Pt-free cathode.³⁶⁴ For example, Gong and co-workers³⁶⁵ assembled the GR/Pt multilayer thin films to reduce the Pt amount in the counter electrode in DSSCs and their results showed that the composite electrode showed comparable photovoltaic performances to the conventional sputtered Pt electrode. More specifically, the GR/Pt multilayer thin films were prepared by sintering the $(\text{PDDA/GR/PDDA}/\text{H}_2\text{PtCl}_6)_n$ multilayer thin film LbL-assembled on the FTO substrate, in which the GR layer intercalated between the FTO and Pt contributes to high photon-to-electron conversion efficiency (PCE, 6%). The advantage of multilayer structure for QD solar cells was demonstrated by Guo *et al.* using GR/CdS QD multilayer thin films (Fig. 24),²⁷⁸ for which PCE was significantly improved from 5% to 16% by tuning the number of bilayers of hybrid films from 2 to 8, owing to the synergistic effect of light absorption and charge transport over composite multilayers. Furthermore, the investigation on the electron transfer in $\text{Ti}_{0.91}\text{O}_2/\text{GR}$ multilayer thin films also revealed the highly efficient separation of photo-excited electrons and holes, which was apparently reflected by the substantial enhancement in the photocurrent.¹⁸¹ Consequently, the ability to independently control the property of each component layer in LbL assembly construction affords a controllable way to reduce the recombination of carriers and improve the PCE of solar cells.

7.6 Sensors

Molecular sensing of useful or toxic substances has been extensively investigated and the result has revealed that well-designed host structures are essential for high sensitivities and selectivities. In addition to organic supramolecular hosts,³⁶⁶ structure-controlled inorganic nanomaterials have become increasingly important in this field.³⁶⁷ Particularly, GR-based LbL assembled multilayers have gained increasing interest in electrochemical, electronic, and optical sensing applications due to the high electron transfer rate and carrier mobility of GR.³⁶⁸ Specifically, GR containing a large amount of modifiable oxygen-containing functional groups and highly reactive edging sites have been determined to be an attractive candidate to concentrate analytes. As shown in Fig. 25(a–c), the layered structures are formed by *in situ* reduction of GO in the presence of nonvolatile ionic liquids (G-IL) and subsequent electrostatic

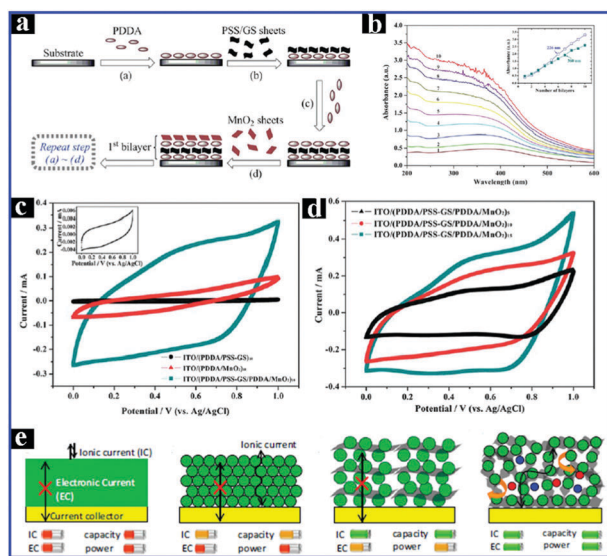


Fig. 23 (a) A schematic view for constructing multilayer films on a substrate. (b) UV-vis absorption spectra of multilayer films of $(\text{PDDA}/\text{PSS-GR}/\text{PDDA}/\text{MnO}_2)_n$ ($n = 1-10$) on a quartz glass substrate. The inset is a plot of absorbance at 226 nm and 360 nm *versus* number of bilayers. (c) CV curves of ITO/(PDDA/PSS-GR/PDDA/ MnO_2)₁₀, ITO/(PDDA/ MnO_2)₁₀, and ITO/(PDDA/PSS-GR)₁₀ electrodes at a scan rate of 40 mV s^{-1} . (d) CV curves of ITO/(PDDA/PSS-GR/PDDA/ MnO_2)_n ($n = 5, 10, 15$) electrodes at a scan rate of 40 mV s^{-1} . (e) Rational design of high-energy-high-power hybrid supercapacitor electrodes. (Reprinted with permission from ref. 355, Copyright 2011 Royal Society of Chemistry.)

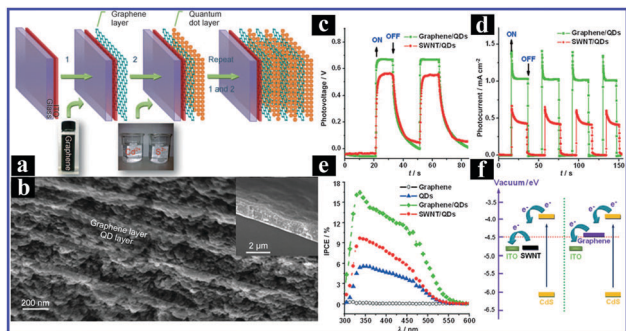


Fig. 24 (a) Schematic illustration of the preparation of LbL assembled GR/CdS QD hybrid films on ITO glass, (b) cross-sectional SEM image of GR/CdS QD multilayers, and (c–f) PEC performances of GR/CdS QD multilayer films. (Reprinted with permission from ref. 278, Copyright 2010 John Wiley & Sons, Inc.)

LbL assembly of (G–IL/PSS)_n multilayer thin films.³⁶⁹ This work demonstrated the use of layered (G–IL/PSS)_n composites on a quartz crystal microbalance (QCM) for selective gas sensing and it was found that the nanospace formed between sp²-hybridized carbon nanosheets of GR has a higher affinity for toxic aromatic hydrocarbons than for their aliphatic carbons, thus giving rise to highly selective gas sensing activity. Alternatively, LbL assembled GR multilayers have been used as sensors for detecting hydrogen peroxide (H₂O₂).^{370,371} Apart from gas and H₂O₂ sensors, glucose sensors have also been reported based on modified GR multilayers which exhibit satisfactory detection limit and sensitivity.³⁷² For example, as illustrated in Fig. 25d, the flowchart demonstrates the capability of GR as a spacer to form electrochemically active multilayered nanostructures by the LbL assembly strategy, in which methylene green (MG) and positively charged methylimidazolium functionalized multi-walled carbon nanotubes (MWNTs) were used as an example of electroactive species and electrochemically useful components for the assembly, respectively. Electrochemical studies indicated that the thus-assembled nanostructures possess excellent electrocatalytic activity toward the oxidation of nicotinamide adenine dinucleotide (NADH) which suggests their great potential for the development of molecular biosensors or biofuel cells. Virtually, LbL assembled GR-based multilayer films have been extensively utilized as versatile biosensors for detecting various biomolecules such as DNA and protein markers.^{373–377}

7.7 Proton exchange membrane fuel cells (PEMFCs)

Fuel cells are regarded as the most efficient and less polluting power-generating technology, thus making them a potential and viable candidate to moderate the fast increase in power requirements and to minimize the impact of the increased power consumption on the environment. Among them, proton exchange membrane fuel cells (PEMFCs) are considered to be the most promising power sources. The challenge in PEMFCs arises predominantly from the need for an inexpensive, more active and durable proton exchange membrane (PEM). For example, with regard to the development of one typical fuel

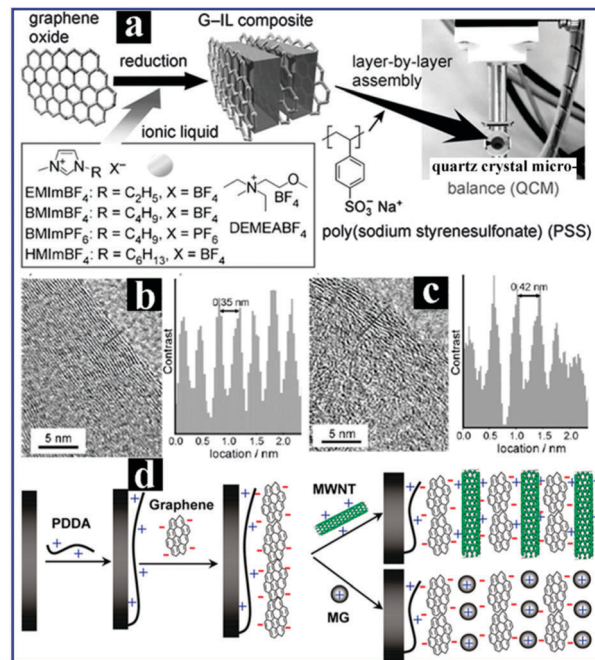


Fig. 25 (a) Schematic illustration of the preparation of (G–IL) composites and their LbL assembly on a quartz crystal microbalance (QCM). High-resolution TEM images of GR reduced in (b) water and (c) 1-ethyl-3-methylimidazolium tetrafluoroborate (EMImBF₄) IL with the corresponding average layer spacing. (d) Schematic illustration of the strategies for the controllable formation of electrochemically functional nanostructures on electrodes with GR as the spacer. (Reprinted with permission from ref. 369 and 372, Copyright 2010 John Wiley & Sons, Inc.)

cell such as the direct methanol fuel cell, PEM films with high methanol permeation could not only reduce the cell voltage at the cathode stemming from a mixed potential, but also decrease cell efficiency and poison cathode catalysts.³⁷⁸ Although increasing the thickness of the PEM membrane helps in reducing the methanol crossover, a thick membrane could lead to the swelling of the membrane.³⁷⁹ Till now, various approaches have been developed to modify the Nafion-based PEMs to suppress the methanol permeation.³⁸⁰ Among them, the LbL technique has facilitated extensive applications of PEMFC multilayers since thermal and chemical stability of the Nafion membranes could be well-preserved within the assembled PE films which constitute a component of PEM. For example, Jiang and co-workers prepared an effective methanol-blocking multilayer on a Nafion membrane through LbL assembly of oppositely charged PEs (*i.e.*, PDDA, PSS, and PAZO), thus reducing the methanol permeation.³⁸¹ Moreover, some metal NPs (*e.g.*, Pd,³⁸² Au³⁸³ and Pt³⁸⁴), oxide NPs (*e.g.*, SiO₂,³⁸⁵ TiO₂,³⁸⁶ and ZrO₂³⁸⁷), and CNTs (*e.g.*, MWCNTs^{388,389}) have also been employed as methanol-blocking agents for the Nafion membrane *via* LbL assembly approaches, thus producing promising PEMFCs.

GR nanosheets, as another promising alternative catalyst support for fuel cells, have recently been extensively explored based on LbL assembly buildup on account of their intrinsic structural advantages and performances.^{390,391} Notably, Lin's group presented a simple and environmentally friendly approach

to prepare soluble GR nanosheets by polyelectrolyte (*i.e.*, PDDA)-mediated reduction of GO in which PDDA simultaneously serves as a reducing agent and stabilizer.³⁹² Moreover, it was found that the PDDA moieties anchored on the substrate of GR nanosheets facilitate the *in situ* growth of highly dispersed Pt NPs based on the electrostatic interaction between PDDA and PtCl_6^{2-} to form Pt/GR nanocomposites with excellent catalytic activity toward formic acid oxidation. This work connotes a potential idea for fabricating LbL assembled Pt/GR multilayer thin films by alternating deposition of GR-PDDA and Pt NPs or PtCl_6^{2-} precursor on a glass carbon electrode for oxygen reduction reaction or oxygen evolution reactions associated with PEMFCs. More recently, as shown in Fig. 26, Alamgir's group harnessed surface limited redox replacement to provide precise LbL growth of Pt monolayers on GR nanosheets, by which fully wetted 4–5 monolayer Pt films can be grown on the GR substrate.³⁹³ Furthermore, the authors found that incorporating the GR layer at the Pt–Au interface modifies the growth mechanism, charge transfers, equilibrium interatomic distances, and associated strain of the synthesized Pt monolayers. Cyclic voltammetry (CV) and the oxygen reduction reaction results show that the inserted GR monolayer in the multilayer films results in increased activity for the Pt due to a GR-induced compressive strain, as well as a higher resistance against loss of the catalytically active Pt surface.

7.8 Catalysis

Synthesizing metal/semiconductor hybrid nanocomposites for multifunctional catalytic applications, including photocatalysis, thermal catalysis, and electrocatalysis, has been attracting enormous research attention. Generally, the strategies for distribution of metal NPs on semiconductors are mainly centered on conventional methods including photoreduction, deposition-precipitation, and dipping-calcination.³⁹⁴ Despite the advantages afforded by these synthetic approaches, rational fabrication of well-defined metal/semiconductor hybrid nanocomposites in conjunction with monodisperse deposition of metal NPs and tunable deposition amount of metal components on the semiconductor is still far from satisfactory. Towards this end, the LbL assembly technique demonstrates significant advantages over conventional methods. For example, hierarchically ordered M/TiO₂ nanotube array (M/TNTs, M = Au, Ag, Pt) heterostructures were prepared *via* LbL assembly, which involves alternating deposition of tailor-made negatively charged metal NPs on the positively charged PE-modified (*e.g.*, PAH) TNT substrate.^{394,395} Strikingly, the thus-assembled M/TNT hybrid nanostructures exhibited significantly enhanced photocatalytic performances toward liquid-phase degradation of organic dye pollutants under UV light irradiation ($\lambda = 365 \pm 15$ nm) in comparison with blank TNTs, in which metal NPs were determined to play a pivotal role as “electron traps” for separation of photogenerated electron–hole charge carriers. Moreover, it was found that the M/TNT nanostructures also demonstrated efficient thermal catalytic activities toward reduction of nitrophenol to nitroaniline under ambient conditions. The promising catalytic performances of M/TNT nanocomposites were predominantly attributed to the monodisperse distribution of metal NPs on the TNTs. Consequently, surface

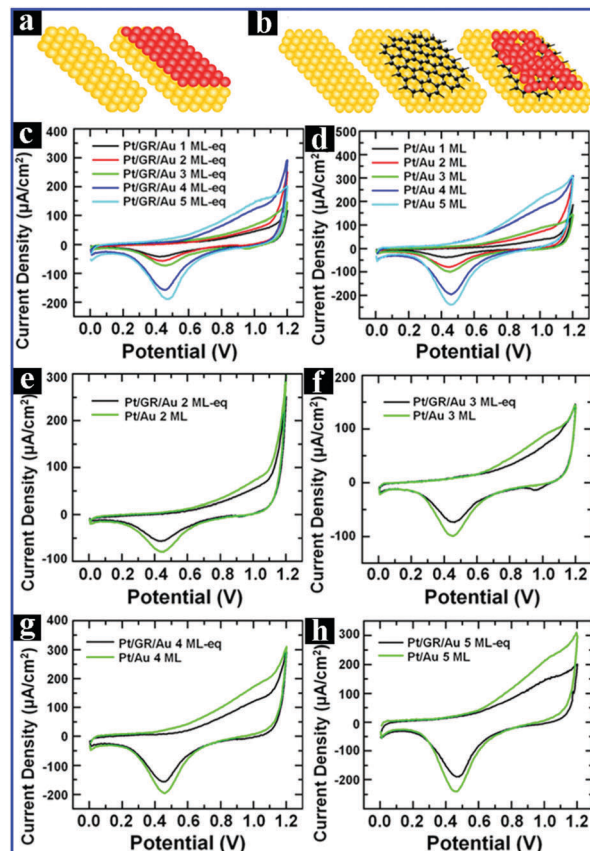


Fig. 26 (a) Pt/Au samples, where Pt is grown directly on a bare Au substrate by SLRR. (b) Pt/GR/Au samples, where GR is first transferred on top of the Au substrate before Pt deposition by SLRR. Cyclic voltammograms for (c) Pt/Au and (d) Pt/GR/Au with varied ML, (e–h) 2, 3, 4, and 5 ML samples, respectively, comparing samples with graphene to those without. CVs were performed in N₂-saturated 0.1 M H₂SO₄. Voltages are referenced to a Ag/AgCl electrode. (Reprinted with permission from ref. 393, Copyright 2015 American Chemical Society.)

modification of 1D semiconductors through the LbL assembly strategy can be utilized as an effective method to achieve uniform deposition of metal NPs for versatile catalytic applications.^{396–398}

When metal NPs become atomically small (< 2 nm) and are composed of a precise number of metal atoms passivated with a stabilizing ligand, it was referred to as metal clusters which are distinct from bulk metal NPs such as unique atom packing, quantum confinement effect, and discrete molecule-like band structure. More recently, Au NPs and gold (Au_x) clusters were judiciously used as ingredients for LbL assembly buildup on the TNT framework, for which Au NPs and Au_x clusters were successively deposited on TNT based on pronounced electrostatic interaction leading to a well-defined Au_x/Au/TNTA ternary heterostructure.³⁹⁹ More significantly, as shown in Fig. 27, the superior photocatalytic performances of the Au_x/Au/TNTA heterostructure over Au/TNT and Au_x/TNT binary counterparts toward reduction of aromatic nitro compounds under ambient conditions reveal the synergistic interaction of Au NPs and Au_x clusters, *i.e.*, electron relay and plasmonic sensitization of Au

NPs for Au_x clusters, thereby bridging the gap between these two different sized metal nanostructures.

Apart from the metal/semiconductor nanocomposites, GR/semiconductor nanocomposites prepared by the LbL assembly approach have recently been achieved for photocatalytic applications. As reported by our group, visible-light-responsive CdS QDs and PAH-modified GR were selected as building blocks for constructing CdS QDs/GR multilayer thin films, in which negatively charged CdS QDs and positively charged GR were alternately stacked, as shown in Fig. 28.²⁷⁹ The as-prepared CdS QDs/GR multilayer thin films show promising photocatalytic performances toward anaerobic reduction of a series of aromatic nitro compounds to corresponding amino compounds under visible light irradiation ($\lambda > 420$ nm). More significantly, photocatalytic and PEC performances of the CdS QDs/GR multilayer thin films can be tuned by assembly cycles. This work suggests the great potential photocatalytic applications of LbL assembled GR/semiconductor multilayer thin films. Alternatively, Bi₂WO₆ nanoplate and polytungstogermanate multilayer films fabricated by the LbL technique were also demonstrated to exhibit significantly enhanced visible-light-responsive photocatalytic performances in comparison with the randomly distributed powder counterparts.^{211,400}

Harvesting energy from green resources and developing suitable storage systems are the top priorities in current research on energy systems. In this regard, besides the photocatalytic activities, electrocatalytic performances of LbL assembled multilayer thin films were also extensively evaluated such as methanol oxidation and selective hydrogenation of a series of unsaturated

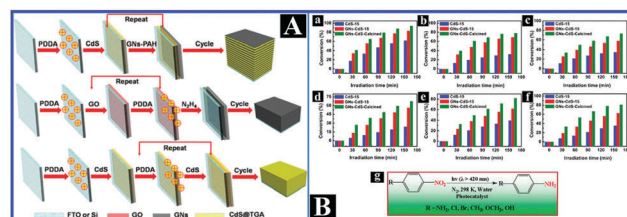


Fig. 28 (A) Schematic illustration of LbL self-assembly of GNs–CdS QDs, pure GNs, and pure CdS QD multilayer films. (B) Photocatalytic reduction of substituted aromatic nitro compounds over CdS QD film (15 layers), of GNs–CdS QD composite film (15 layers), and calcined GNs–CdS QD composite film (15 layers) under visible light irradiation ($\lambda > 420$ nm), with the addition of ammonium formate as a quencher for photogenerated holes and with N₂ purging under ambient conditions. (a) 4-Nitroaniline, (b) 1-chloro-4-nitrobenzene, (c) 1-bromo-4-nitrobenzene, (d) 4-nitrotoluene, (e) 4-nitroanisole, and (f) 4-nitrophenol. (g) Photocatalytic reduction model under the experimental conditions. (Reprinted with permission from ref. 279, Copyright 2014 American Chemical Society.)

alcohols. As shown in Fig. 29, Kim *et al.* developed a simple method of integrating electroactive Au NPs with the GO nanosheet substrate by LbL assembly for creation of 3D electrocatalytic thin films which are highly active toward methanol oxidation. Specifically, this approach involves the alternating assembly of positively charged Au NPs with GO nanosheets on the basis of electrostatic interactions, in which GO nanosheets acting as structural components of the multilayer thin film are beneficial for the utilization and dispersion of Au NPs by virtue of their high catalytic surface area and excellent conduction of GR nanosheets, thus avoiding irreversible aggregation of Au NPs

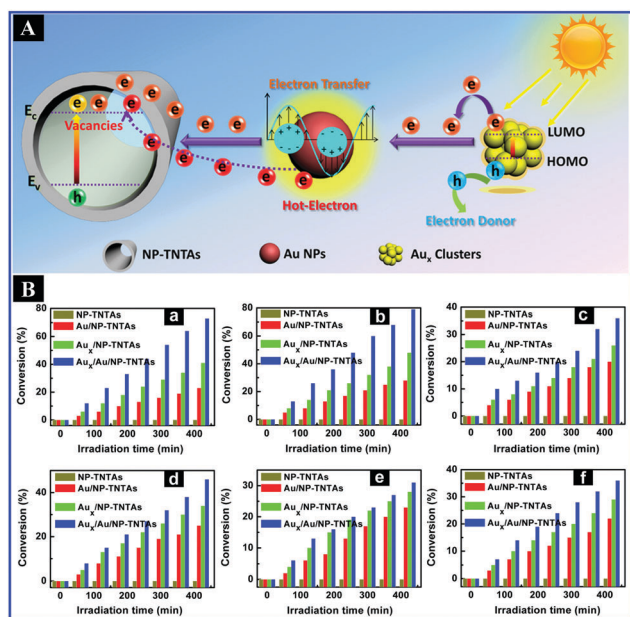


Fig. 27 (A) Schematic illustration depicting the photocatalytic mechanism over the Au_x/Au/NP-TNTA ternary heterostructure. (B) Photocatalytic performances of (a) 4-NA, (b) 2-NA, (c) 3-NA, (d) 4-NP, (e) 2-NP, and (f) 3-NP over blank NP-TNTA, Au/NP-TNTA, Au_x/NP-TNTA, and Au_x/Au/NP-TNTA nanostructures under visible light irradiation ($\lambda > 420$ nm) with the addition of ammonium formate as a quencher for photogenerated holes and with N₂ purging under ambient conditions. (Reprinted with permission from ref. 399, Copyright 2015 American Chemical Society.)

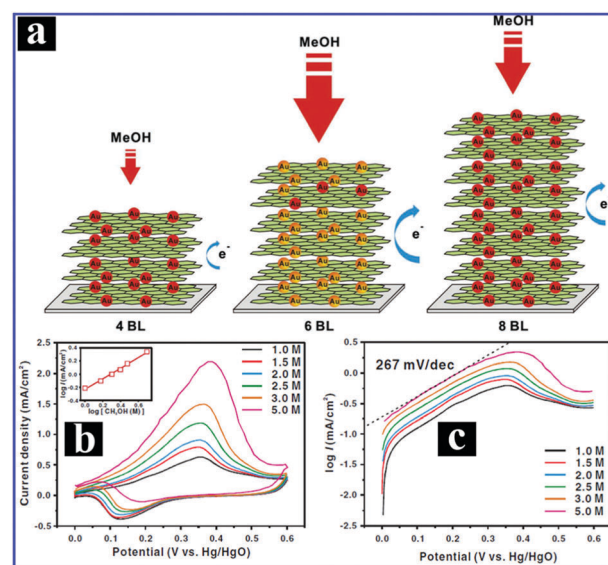


Fig. 29 (a) Schematic illustration of the mechanism for electrocatalytic activity of (Au/GR)_n multilayer thin films toward methanol oxidation with the variation of bilayer numbers. (b) Cyclic voltammograms of the (Au/GR)₆ thin film thermally treated at 150 °C in 0.10 M KOH with different concentrations of CH₃OH. (c) The Tafel plots with a representative linear fit. All measurements were performed in a saturated N₂ at a scan rate of 20 mV s⁻¹. (Reprinted with permission from ref. 301, Copyright 2012 John Wiley & Sons, Inc.)

during electrocatalytic cycles and loss of the nanoscale catalytic effect. In addition, the authors demonstrated that electrocatalytic activities of these multilayer thin films can be tuned by the number of bilayers and thermal treatment afforded by the advantageous features of LbL assembly. The general concept presented by the authors offers new categories of electroactive catalysts for direct methanol fuel cells in view of the versatility of LbL assembly.

8. Conclusions and future perspectives

LbL assembly represents a simple, robust, efficient, and highly versatile method, which allows for the integration of a large variety of materials (*e.g.*, polymers, biomolecules, clays, metal oxides, colloidal NPs, and even biologically active compounds) into various multilayer systems with tunable structures, compositions, properties, and controllable innovative functions. As such, it is not surprise at all to see the promising potential applications of LbL assembled multilayer assemblies in a myriad of fields including but not limited to drug delivery, energy storage and conversion, catalysis, and bioelectronics.

In this review, we have concisely introduced the development history and basic principles of the LbL assembly technique and summarized the influences of various parameters on the LbL assembly buildup (*e.g.*, pH, temperature, ionic strength, solvent, and properties of PEs) in combination with the different intermolecular interactions responsible for the LbL assembly process such as electrostatic, charge-transfer, host-guest, biospecific, hydrogen bonding, covalent bonding, and coordination chemistry interactions. In addition, predominant attention was paid to elucidate the principle on how to achieve the rational construction of a great set of multilayer assemblies with well-defined architectures and tailored thickness, structures, and compositions *via* the LbL assembly technique by judiciously choosing building blocks of different dimensionality (*e.g.*, 0D, 1D, 2D, and 3D). Furthermore, extensive applications of multilayer assemblies including transparent conducting films, field effect transistors, lithium ion batteries, supercapacitors, solar cells, sensors, proton exchange membrane fuel cells, and catalysis have been demonstrated and new assembling concepts and methodologies have been proposed.

Despite the considerable advancements that have been made during the past two decades, it is advisable for research communities to rationally evaluate the advantages and disadvantages of LbL assembly technology, especially for the latter, with a view to improving its future burgeoning developments. It should be particularly emphasized that disadvantages of LbL assembly are principally centered on the limitations of respective molecular interactions dominating the LbL assembly process. For example, electrostatic interaction is only applicable to the fabrication of charged and water-soluble multilayer materials sensitive to external stimuli; hydrogen bonding interaction generally produces less stable multilayer assemblies; charge-transfer interaction is only limited to nonionic molecules; host-guest interaction is merely confined to a perfect

recognition mode; coordination chemistry interaction is generally restricted by materials selections; covalent bonding interaction is limited to some particular molecules. All these disadvantages remarkably influence the construction of stable and robust multilayer assemblies. Despite the disadvantages associated with the LbL assembly technique in the current stage, many stimulating challenges and opportunities still await us to explore the significant potential of LbL assembly techniques in the near future, as specifically elucidated in the following.

Firstly, thus far, the majority of the reported studies were mainly focused on the fabrication of LbL multilayer assemblies through conventional electrostatic interactions, and LbL assembly of multilayer systems *via* other intermolecular interactions or integrated interactions is still far from satisfactory. In this regard, it is envisaged that prominent LbL assembly techniques based on multiple intermolecular interactions would provide new alternative avenues for precisely controlling the growth of multilayer films and hence promote the generation of much more well-defined nanoarchitectures with new innovative functionalities.

Secondly, judicious combination of the LbL assembly technique with various other bottom-up or top-down strategies (*e.g.*, photolithography and printing techniques) would enrich the technical routes for LbL assembly buildup, which would without doubt be beneficial for creating a diverse set of novel nanoarchitectures with high performances and low cost for extensive practical applications.

Thirdly, note that the GR-driven “gold-rush” wave in recent years in many disciplines and potential applications unleashes the fascinating properties of GR, which can be further harnessed as an excellent nanobuilding block for LbL assembly of 2D or 3D multilayer films or nanostructures by taking full advantage of its intrinsic structure and surface charge merits. Alternatively, apart from GR, various exfoliated atomically thick inorganic nanosheets such as monolayer oxide nanosheets and transition metal dichalcogenide nanosheets have sparked ever increasing interest over the past few years owing to their unique and novel electronic structures as well as distinctive physicochemical properties, which can be further used as efficacious constructing components for LbL assembly of a large variety of multi-dimensional nanoarchitectures.

Fourth, there are two main themes that can be identified for current developments in LbL assembly technologies. One involves moving away from the random diffusion-driven kinetics for layer deposition and the other is the advancement from manual assembly toward automated systems. Thus, judicious choice of newly developed assembly technologies will significantly enable the engineering of diverse multilayer thin films and hierarchical nanostructures with tailor-made physicochemical properties.

Finally, LbL assembly technology has the advantage of unlimited applicability to a wide range of materials, which makes the LbL assembly technique accommodate most of the pivotal applications of future technology. The remaining challenges for the LbL methods in practical utilization would be to satisfy commercially based merits and industrial scalability. These final issues should be easily addressed by virtue of the intrinsic simplicity of LbL procedures.

In summary, although remarkable developments have been achieved in the previous studies, undoubtedly, there is still much space for us to fully take advantage of the LbL assembly technique for constructing varied multilayer systems with superior performances which would possess great potential for practical applications. It is hoped that this review could afford enriched information on the prominent LbL assembly technology for rational design of various multilayered nanoarchitectures for versatile applications.

Abbreviation

PE	Polyelectrolyte
PAA	Polyacrylic acid
PAH	Poly(allylamine hydrochloride)
PDDA	Poly(diallyldimethylammonium chloride)
PSS	Poly(sodium 4-styrene sulfonate)
TALH	Titanium(IV) bis(ammonium lactato)dihydroxide
PANI	Polyaniline
PVA	Poly(vinyl alcohol)
PDMAEA	Poly(2- <i>N,N'</i> -(dimethyl amino ethyl acrylate))
PET	Poly(ethylene terephthalate)
PEC	Photoelectrochemical
IPCE	Incident photon-to-electron conversion efficiency
PCE	Photon-to-electron conversion efficiency
PS	Polystyrene
MS	Mesoporous silicas
SPG	Solution processed graphene
PEMFCs	Proton exchange membrane fuel cells
PAZO	Poly(1-(4-(3-carboxy-4-hydroxyphenylazo)benzene sulfonamido)-1,2-ethanediyl, sodium salt)
PEMFCs	Proton exchange membrane fuel cells
PSQ	Poly(methylsilsequioxane)
PVPON	Poly(vinylpyrrolidone)
β -CD	β -Cyclodextrin
AD	Adamantane
PCTDA	3,4,9,10-Perylenetetracarboxyldianhydride
EBSD	Electron back-scattered diffraction
EMImBF ₄	1-Ethyl-3-methylimidazolium tetrafluoroborate
MWCNT	Multi-walled carbon nanotube
PEM	Proton exchange membrane
TCFs	Transparent conducting films
FETs	Field effect transistors
SSA	Specific surface area
NPs	Nanoparticles
CaCO ₃	Calcium carbonate
PLB	Poly-L-lysine

Acknowledgements

This work was supported by the Nanyang Technological University startup grant: M4080977.120, Singapore Ministry of Education Academic Research Fund (AcRF) Tier 1: M4011021.120

A*Star SERC grant: M4070178.120, National Research Foundation Corp Lab grant: M4011021.120, Singapore-Berkeley Research Initiative for Sustainable Energy (SinBeRise), and the National Research Foundation (NRF), Prime Minister's Office, Singapore under its Campus for Research Excellence and Technological Enterprise (CREATE) program. Prof. Yi-Jun Xu acknowledges the support by the NSFC (21173045, 20903023), the Award Program for Minjiang Scholar Professorship, the NSF of Fujian Province for Distinguished Young Investigator Grant (2012J06003), Program for Returned High-Level Overseas Chinese Scholars of Fujian Province, and Key Project of National Natural Science Foundation of China (U1463204).

References

- 1 K. B. Blodgett, *J. Am. Chem. Soc.*, 1935, **57**, 1007–1022.
- 2 I. Langmuir and V. J. Schaefer, *J. Am. Chem. Soc.*, 1937, **59**, 2075–2076.
- 3 D. R. Talham, *Chem. Rev.*, 2004, **104**, 5479–5502.
- 4 K. Ariga, Y. Yamauchi, T. Mori and J. P. Hill, *Adv. Mater.*, 2013, **25**, 6477–6512.
- 5 S. Acharya, J. P. Hill and K. Ariga, *Adv. Mater.*, 2009, **21**, 2959–2981.
- 6 R. G. Nuzzo and D. L. Allara, *J. Am. Chem. Soc.*, 1983, **105**, 4481–4483.
- 7 C. D. Bain, J. Ewall and G. M. Whitesides, *J. Am. Chem. Soc.*, 1989, **111**, 7155–7164.
- 8 K. L. Prime and G. M. Whitesides, *Science*, 1991, **252**, 1164–1167.
- 9 A. Ulman, *Chem. Rev.*, 1996, **96**, 1533–1554.
- 10 Z. Matharu, A. J. Bandodkar, V. Gupta and B. D. Malhotra, *Chem. Soc. Rev.*, 2012, **41**, 1363–1402.
- 11 J. Borge and J. F. Mano, *Chem. Rev.*, 2014, **114**, 8883–8942.
- 12 S. T. Milner, *Science*, 1991, **251**, 905–914.
- 13 S. Edmondson, V. L. Osborne and W. T. S. Huck, *Chem. Soc. Rev.*, 2004, **33**, 14–22.
- 14 R. Barbey, L. Lavanant, D. Paripovic, N. Schüwer, C. Sugnaux, S. Tugulu and H.-A. Klok, *Chem. Rev.*, 2009, **109**, 5437–5527.
- 15 M. N. R. Ashfold, F. Claeysens, G. M. Fuge and S. J. Henley, *Chem. Soc. Rev.*, 2004, **33**, 23–31.
- 16 M. A. Malik, M. Afzaal and P. O'Brien, *Chem. Rev.*, 2010, **110**, 4417–4446.
- 17 G. Ozaydin-Ince, A. M. Coclite and K. K. Gleason, *Rep. Prog. Phys.*, 2012, **75**, 016501.
- 18 J. Hong, J. Y. Han, H. Yoon, P. Joo, T. Lee, E. Seo, K. Char and B.-S. Kim, *Nanoscale*, 2011, **3**, 4515–4531.
- 19 Y. Li, X. Wang and J. Sun, *Chem. Soc. Rev.*, 2012, **41**, 5998–6009.
- 20 W. Tong, X. Song and C. Gao, *Chem. Soc. Rev.*, 2012, **41**, 6103–6124.
- 21 Y. Xiang, S. Lu and S. P. Jiang, *Chem. Soc. Rev.*, 2012, **41**, 7291–7321.
- 22 Z. Tang, Y. Wang, P. Podsiadlo and N. A. Kotov, *Adv. Mater.*, 2006, **18**, 3203–3224.

- 23 R. K. Iler, *J. Colloid Interface Sci.*, 1966, **21**, 569–594.
- 24 J. J. Kirkland, *Anal. Chem.*, 1965, **37**, 1458–1461.
- 25 G. Decher and J.-D. Hong, *Makromol. Chem., Macromol. Symp.*, 1991, **46**, 321–327.
- 26 P. Berndt, K. Kurihara and T. Kunitake, *Langmuir*, 1992, **8**, 2486–2490.
- 27 Y. Lvov, K. Ariga, I. Ichinose and T. Kunitake, *J. Am. Chem. Soc.*, 1995, **117**, 6117–6123.
- 28 Y. Lvov, K. Ariga and T. Kunitake, *Chem. Lett.*, 1994, 2323–2326.
- 29 K. Ariga, Y. Yamauchi, G. Rydzek, Q. Ji, Y. Yonamine, K. C.-W. Wu and J. P. Hill, *Chem. Lett.*, 2014, **43**, 36–68.
- 30 G. Decher, *Science*, 1997, **277**, 1232–1237.
- 31 N. A. Kotov, I. Dekany and J. H. Fendler, *J. Phys. Chem.*, 1995, **99**, 13065–13069.
- 32 W. B. Stockton and M. F. Rubner, *Macromolecules*, 1997, **30**, 2717–2725.
- 33 L. Wang, Z. Wang, X. Zhang, J. Shen, L. Chi and H. Fuchs, *Macromol. Rapid Commun.*, 1997, **18**, 509–514.
- 34 H. Xiong, M. Cheng, Z. Zhou, X. Zhang and J. Shen, *Adv. Mater.*, 1998, **10**, 529–532.
- 35 Y. Shimazaki, M. Mitsuishi, S. Ito and M. Yamamoto, *Langmuir*, 1997, **13**, 1385–1387.
- 36 N. A. Kotov, *Nanostruct. Mater.*, 1999, **12**, 789–796.
- 37 D. Cochlin and A. Laschewsky, *Macromol. Chem. Phys.*, 1999, **200**, 609–615.
- 38 W. Muller, H. Ringsdorf, E. Rump, G. Wildburg, X. Zhang, L. Angermaier, W. Knoll, M. Liley and J. Spinke, *Science*, 1993, **262**, 1706–1708.
- 39 J. Choi and M. F. Rubner, *Macromolecules*, 2005, **38**, 116–124.
- 40 K. Itano, J. Y. Choi and M. F. Rubner, *Macromolecules*, 2005, **38**, 3450–3460.
- 41 P. Bieker and M. Schönhoff, *Macromolecules*, 2010, **43**, 5052–5059.
- 42 D. Yoo, S. S. Shiratori and M. F. Rubner, *Macromolecules*, 1998, **31**, 4309–4318.
- 43 S. S. Shiratori and M. F. Rubner, *Macromolecules*, 2000, **33**, 4213–4219.
- 44 S. E. Burke and C. J. Barrett, *Biomacromolecules*, 2003, **4**, 1773–1783.
- 45 Y. Lvov, G. Decher and H. Möhwald, *Langmuir*, 1993, **9**, 481–486.
- 46 K. Büscher, K. Graf, H. Ahrens and C. A. Helm, *Langmuir*, 2002, **18**, 3585–3591.
- 47 M. Salomäki, I. A. Vinokurov and J. Kankare, *Langmuir*, 2005, **21**, 11232–11240.
- 48 H. L. Tan, M. J. McMurdo, G. Pan and P. G. Van Patten, *Langmuir*, 2003, **19**, 9311–9314.
- 49 R. R. Costa, C. A. Custódio, F. J. Arias, J. C. Rodríguez-Cabello and J. F. Mano, *Nanomedicine*, 2013, **9**, 895–902.
- 50 R. R. Costa, E. Castro, F. J. Arias, J. C. Rodríguez-Cabello and J. F. Mano, *Biomacromolecules*, 2013, **14**, 2403–2410.
- 51 S. T. Dubas and J. B. Schlenoff, *Macromolecules*, 2001, **34**, 3736–3740.
- 52 K. Büscher, K. Graf, H. Ahrens and C. A. Helm, *Langmuir*, 2002, **18**, 3585–3591.
- 53 S. T. Dubas, T. R. Farhat and J. B. Schlenoff, *J. Am. Chem. Soc.*, 2001, **123**, 5368–5369.
- 54 M. Salomäki, T. Laiho and J. Kankare, *Macromolecules*, 2004, **37**, 9585–9590.
- 55 M. Salomäki, P. Tervasmäki, S. Areva and J. Kankare, *Langmuir*, 2004, **20**, 3679–3683.
- 56 M. Salomäki and J. Kankare, *Macromolecules*, 2008, **41**, 4423–4428.
- 57 E. Poptoshev, B. Schoeler and F. Caruso, *Langmuir*, 2004, **20**, 829–834.
- 58 M. Koetse, A. Laschewsky, A. M. Jonas and W. Wagenknecht, *Langmuir*, 2002, **18**, 1655–1660.
- 59 J. Choi and M. F. Rubner, *Macromolecules*, 2005, **38**, 116–124.
- 60 O. Soltwedel, P. Nestler, H.-G. Neumann, M. Paßvogel, R. Köhler and C. A. Helm, *Macromolecules*, 2012, **45**, 7995–8004.
- 61 P. Kujawa, P. Moraille, J. Sanchez, A. Badia and F. M. Winnik, *J. Am. Chem. Soc.*, 2005, **127**, 9224–9234.
- 62 Y. Jang, J. Seo, B. Akgun, S. Satija and K. Char, *Macromolecules*, 2013, **46**, 4580–4588.
- 63 P. Nestler, M. Paßvogel and C. A. Helm, *Macromolecules*, 2013, **46**, 5622–5629.
- 64 G. Liu, J. Zhao, Q. Sun and G. Zhang, *J. Phys. Chem. B*, 2008, **112**, 3333–3338.
- 65 G. Liu, S. Zou, L. Fu and G. Zhang, *J. Phys. Chem. B*, 2008, **112**, 4167–4171.
- 66 B. Wu, C. Li, H. Yang, G. Liu and G. Zhang, *J. Phys. Chem. B*, 2012, **116**, 3106–3114.
- 67 S. Yang, Y. Zhang, L. Wang, S. Hong, J. Xu, Y. Chen and C. Li, *Langmuir*, 2006, **22**, 338–343.
- 68 S. A. Sukhishvili and S. Granick, *J. Am. Chem. Soc.*, 2000, **122**, 9550–9551.
- 69 S. A. Sukhishvili and S. Granick, *Macromolecules*, 2002, **35**, 301–310.
- 70 Y. Zhang, Y. Guan, S. Yang, J. Xu and C. C. Han, *Adv. Mater.*, 2003, **15**, 832–835.
- 71 V. Kozlovskaya, E. Kharlampieva, M. L. Mansfield and S. A. Sukhishvili, *Chem. Mater.*, 2006, **18**, 328–336.
- 72 A. N. Zelikin, Q. Li and F. Caruso, *Angew. Chem., Int. Ed.*, 2006, **45**, 7743–7745.
- 73 C. J. Ochs, G. K. Such, Y. Yan, M. P. van Koevorden and F. Caruso, *ACS Nano*, 2010, **4**, 1653–1663.
- 74 F. Huo, H. Xu, L. Zhang, Y. Fu, Z. Wang and X. Zhang, *Chem. Commun.*, 2003, 874–875.
- 75 Y. Shimazaki, M. Mitsuishi, S. Ito and M. Yamamoto, *Langmuir*, 1997, **13**, 1385–1387.
- 76 Y. Shimazaki, M. Mitsuishi, S. Ito and M. Yamamoto, *Macromolecules*, 1999, **32**, 8220–8223.
- 77 Y. Shimazaki, S. Ito and N. Tsutsumi, *Langmuir*, 2000, **16**, 9478–9482.
- 78 Y. Shimazaki, R. Nakamura, S. Ito and M. Yamamoto, *Langmuir*, 2001, **17**, 953–956.
- 79 Y. Zhang and W. Cao, *Langmuir*, 2001, **17**, 5021–5024.

- 80 X. Wang, K. Naka, H. Itoh, T. Uemura and Y. Chujo, *Macromolecules*, 2003, **36**, 533–535.
- 81 J. Zhang, Y. Liu, G. Wu, M. Schonhoff and X. Zhang, *Langmuir*, 2011, **27**, 10370–10375.
- 82 Y. Zhang and W. Cao, *New J. Chem.*, 2001, **25**, 483–486.
- 83 A. Van der Heyden, M. Wilczewski, P. Labbe and R. Auzely, *Chem. Commun.*, 2006, 3220–3222.
- 84 O. Crespo-Biel, B. Dordi, D. N. Reinhoudt and J. Huskens, *J. Am. Chem. Soc.*, 2005, **127**, 7594–7600.
- 85 C. Li, G.-F. Luo, H.-Y. Wang, J. Zhang, Y.-H. Gong, S. X. Cheng, R.-X. Zhuo and X.-Z. Zhang, *J. Phys. Chem. C*, 2011, **115**, 17651–17659.
- 86 J. D. Hong, K. Lowack, J. Schmitt and G. Decher, *Prog. Colloid Polym. Sci.*, 1993, **93**, 93–98.
- 87 N. M. Green, *Adv. Protein Chem.*, 1975, **29**, 85–133.
- 88 T. Cassier, K. Lowack and G. Decher, *Supramol. Sci.*, 1998, **5**, 309–315.
- 89 X. Cui, R. Pei, Z. Wang, F. Yang, Y. Ma, S. Dong and X. Yang, *Biosens. Bioelectron.*, 2003, **18**, 59–67.
- 90 S. Takahashi, K. Sato and J. Anzai, *Anal. Bioanal. Chem.*, 2012, **402**, 1749–1758.
- 91 Y. W. Chu, B. Y. Wang, H.-S. Lin, T.-Y. Lin, Y.-J. Hung, D. A. Engebretson, W. Lee and J. R. Carey, *Chem. Commun.*, 2013, **49**, 2397–2399.
- 92 Y. Liu, M. L. Bruening, D. E. Bergbreiter and R. M. Crooks, *Angew. Chem., Int. Ed. Engl.*, 1997, **36**, 2114–2116.
- 93 G. K. Such, J. F. Quinn, A. Quinn, E. Tjipto and F. Caruso, *J. Am. Chem. Soc.*, 2006, **128**, 9318–9319.
- 94 G. K. Such, E. Tjipto, A. Postma, A. P. R. Johnston and F. Caruso, *Nano Lett.*, 2007, **7**, 1706–1710.
- 95 Y. Tian, Q. He, C. Tao and J. Li, *Langmuir*, 2006, **22**, 360–362.
- 96 A. K. Cheetham, C. N. R. Rao and R. K. Feller, *Chem. Commun.*, 2006, 4780–4795.
- 97 A. U. Czaja, N. Trukhan and U. Muller, *Chem. Soc. Rev.*, 2009, **38**, 1284–1293.
- 98 J.-R. Li, J. Sculley and H.-C. Zhou, *Chem. Rev.*, 2012, **112**, 869–932.
- 99 A. Betard and R. A. Fischer, *Chem. Rev.*, 2012, **112**, 1055–1083.
- 100 L. E. Kreno, K. Leong, O. K. Farha, M. Allendorf, R. P. Van Duyne and J. T. Hupp, *Chem. Rev.*, 2012, **112**, 1105–1125.
- 101 M. A. Rahim, H. Ejima, K. L. Cho, K. Kempe, M. Müllner, J. P. Best and F. Caruso, *Chem. Mater.*, 2014, **26**, 1645–1653.
- 102 P. A. Chiarelli, M. S. Johal, J. L. Casson, J. B. Roberts, J. M. Robinson and H.-L. Wang, *Adv. Mater.*, 2001, **13**, 1167–1171.
- 103 P. A. Chiarelli, M. S. Johal, D. J. Holmes, J. L. Casson, J. M. Robinson and H.-L. Wang, *Langmuir*, 2002, **18**, 168–173.
- 104 M. Michel, A. Izquierdo, G. Decher, J.-C. Voegel, P. Schaaf and V. Ball, *Langmuir*, 2005, **21**, 7854–7859.
- 105 M. Kolasinska, R. Krastev, T. Gutberlet and P. Warszynski, *Langmuir*, 2009, **25**, 1224–1232.
- 106 P. Schaaf, J.-C. Voegel, L. JERRY and F. Boulmedais, *Adv. Mater.*, 2012, **24**, 1001–1016.
- 107 P. Sher, C. A. Custódio and J. F. Mano, *Small*, 2010, **6**, 2644–2648.
- 108 J. Cho, K. Char, J. D. Hong and K. B. Lee, *Adv. Mater.*, 2001, **13**, 1076–1078.
- 109 J. B. Schlenoff, S. T. Dubas and T. Farhat, *Langmuir*, 2000, **16**, 9968–9969.
- 110 K. C. Krogman, J. L. Lowery, N. S. Zacharia, G. C. Rutledge and P. T. Hammond, *Nat. Mater.*, 2009, **8**, 512–518.
- 111 S. Y. Kim, J. Hong, R. Kaviani, S. W. Lee, M. N. Hyder, S.-H. Yang and P. T. Hammond, *Energy Environ. Sci.*, 2013, **6**, 888–897.
- 112 P. Calvert, *Chem. Mater.*, 2001, **13**, 3299–3305.
- 113 J. Hiller, J. D. Mendelsohn and M. F. Rubner, *Nat. Mater.*, 2002, **1**, 59–63.
- 114 H.-J. Kim, K. Lee, S. Kumar and J. Kim, *Langmuir*, 2005, **21**, 8532–8538.
- 115 Y. Fu, S.-J. Li, J. Xu, M. Yang, J.-D. Zhang, Y.-H. Jiao, J.-C. Zhang, K. Zhang and Y.-G. Jia, *Langmuir*, 2011, **27**, 672–677.
- 116 R. Chen and S. F. Bent, *Adv. Mater.*, 2006, **18**, 1086–1090.
- 117 R. Chen and S. F. Bent, *Chem. Mater.*, 2006, **18**, 3733–3741.
- 118 X. Jiang, H. Huang, F. B. Prinz and S. F. Bent, *Chem. Mater.*, 2008, **20**, 3897–3905.
- 119 H.-B.-R. Lee and S. F. Bent, *Chem. Mater.*, 2012, **24**, 279–286.
- 120 C. N. McMahon, L. Alemany, R. L. Callender, S. G. Bott and A. R. Barron, *Chem. Mater.*, 1999, **11**, 3181–3188.
- 121 Y. Du and S. M. George, *J. Phys. Chem. C*, 2007, **111**, 8509–8517.
- 122 A. A. Dameron, D. Seghete, B. B. Burton, S. D. Davidson, A. S. Cavanagh, J. A. Bertrand and S. M. George, *Chem. Mater.*, 2008, **20**, 3315–3326.
- 123 H. Zhou and S. F. Bent, *J. Phys. Chem. C*, 2013, **117**, 19967–19973.
- 124 B. H. Lee, M. K. Ryu, S.-Y. Choi, K.-H. Lee, S. Im and M. M. Sung, *J. Am. Chem. Soc.*, 2007, **129**, 16034–16041.
- 125 J. Liu, B. Yoon, E. Kuhlmann, M. Tian, J. Zhu, S. M. George, Y.-C. Lee and R. Yang, *Nano Lett.*, 2013, **13**, 5594–5599.
- 126 B. H. Lee, B. Yoon, V. R. Anderson and S. M. George, *J. Phys. Chem. C*, 2012, **116**, 3250–3257.
- 127 T. Yoshimura, S. Tatsuura and W. Sotoyama, *Appl. Phys. Lett.*, 1991, **59**, 482–484.
- 128 J. Sun, M. Gao and J. Feldmann, *J. Nanosci. Nanotechnol.*, 2001, **1**, 133–136.
- 129 X. Hong, J. Li, M. Wang, J. Xu, W. Guo, J. Li, Y. Bai and T. Li, *Chem. Mater.*, 2004, **16**, 4022–4027.
- 130 P. R. Van Tassel, *Curr. Opin. Colloid Interface Sci.*, 2012, **17**, 106–113.
- 131 B. Mu, P. Liu, P. Du, Y. Dong and C. Lu, *J. Polym. Sci., Part A: Polym. Chem.*, 2011, **49**, 1969–1976.
- 132 Y. Wang, Y. Liu, Y. Cheng, E. Kim, G. W. Rubloff, W. E. Bentley and G. F. Payne, *Adv. Mater.*, 2011, **23**, 5817–5821.
- 133 N. Raman, M.-R. Lee, S. P. Palecek and D. M. Lynn, *J. Controlled Release*, 2014, **191**, 54–62.
- 134 J. J. Richardson, M. Bjornmalm and F. Caruso, *Science*, 2015, **348**, 2491–2502.

- 135 C. M. Niemeyer, *Angew. Chem., Int. Ed.*, 2001, **40**, 4128–4158.
- 136 C. A. Mirkin, *Inorg. Chem.*, 2000, **39**, 2258–2272.
- 137 W. Shenton, S. A. Davis and S. Mann, *Adv. Mater.*, 1999, **11**, 449–452.
- 138 K. S. Mayya, D. I. Gittins and F. Caruso, *Chem. Mater.*, 2001, **13**, 3833–3836.
- 139 N. Nath and A. Chikoti, *J. Am. Chem. Soc.*, 2001, **123**, 8197–8202.
- 140 D. I. Gittins and F. Caruso, *J. Phys. Chem. B*, 2001, **105**, 6846–6852.
- 141 K. S. Mayya, B. Schoeler and F. Caruso, *Adv. Funct. Mater.*, 2003, **13**, 183–188.
- 142 N. Du, H. Zhang and D. Yang, *Nanoscale*, 2012, **4**, 5517–5526.
- 143 Z. J. Liang, A. S. Sussha, A. M. Yu and F. Caruso, *Adv. Mater.*, 2003, **15**, 1849–1853.
- 144 A. Yu, G. Q. Max Lu, J. Drennan and I. R. Gentle, *Adv. Funct. Mater.*, 2007, **17**, 2600–2605.
- 145 K. Muller, J. F. Quinn, A. P. R. Johnston, M. Becker, A. Greiner and F. Caruso, *Chem. Mater.*, 2006, **18**, 2397–2403.
- 146 Y. Guo, J. Hu, H. Liang, L. Wan and C. Bai, *Adv. Funct. Mater.*, 2005, **15**, 196–202.
- 147 Y. Tian, Q. He, C. Tao, Y. Cui and J. Li, *Biomacromolecules*, 2006, **7**, 2539–2542.
- 148 S. Hou, J. Wang and C. R. Martin, *Nano Lett.*, 2005, **5**, 231–234.
- 149 Y. J. Wang, Y. Tang, A. G. Dong, X. D. Wang, N. Ren, W. Shan and Z. Gao, *Adv. Mater.*, 2002, **14**, 994–997.
- 150 N. Du, H. Zhang, B. Chen, X. Ma, Z. Liu, J. Wu and D. Yang, *Adv. Mater.*, 2007, **19**, 1641–1645.
- 151 C. Zhai, N. Du, H. Zhang, J. Yu, P. Wu, C. Xiao and D. Yang, *Nanoscale*, 2011, **3**, 1798–1801.
- 152 N. Du, H. Zhang, P. Wu, J. Yu and D. Yang, *J. Phys. Chem. C*, 2009, **113**, 17387–17391.
- 153 P. Wu, H. Zhang, N. Du, L. Ruan and D. Yang, *J. Phys. Chem. C*, 2009, **113**, 8147–8151.
- 154 B. Chen, H. Zhang, N. Du, D. Li, X. Ma and D. Yang, *Mater. Res. Bull.*, 2009, **44**, 889–892.
- 155 N. Du, H. Zhang, X. Ma and D. Yang, *Chem. Commun.*, 2008, 6182–6184.
- 156 N. Du, H. Zhang, J. Yu, P. Wu, C. Zhai, Y. Xu, J. Wang and D. Yang, *Chem. Mater.*, 2009, **21**, 5264–5271.
- 157 Y. J. Wang, Y. Tang, X. D. Wang, W. L. Yang and Z. Gao, *Chem. Lett.*, 2000, **29**, 1344–1345.
- 158 S. Mayya, D. I. Gittins and F. Caruso, *Nano Lett.*, 2001, **1**, 727–730.
- 159 Z. Liu, X. Zhang, S. Nishimoto, M. Jing, D. A. Tryk, T. Murakami and A. Fujishima, *Langmuir*, 2007, **23**, 10916–10919.
- 160 K. J. Koski and Y. Cui, *ACS Nano*, 2013, **7**, 3739–3743.
- 161 M. Chhowalla, H. S. Shin, G. Eda, L.-J. Li, K. P. Loh and H. Zhang, *Nat. Chem.*, 2013, **5**, 263–275.
- 162 Q. H. Wang, K. Kalantar-Zadeh, A. Kis, J. N. Coleman and M. S. Strano, *Nat. Nanotechnol.*, 2012, **7**, 699–712.
- 163 G. Pacchioni, *Chem. – Eur. J.*, 2012, **18**, 10144–10158.
- 164 Y. Okamoto, S. Ida, J. Hyodo, H. Hagiwara and T. Ishihara, *J. Am. Chem. Soc.*, 2011, **133**, 18034–18037.
- 165 Y. Sun, H. Cheng, S. Gao, Z. Sun, Q. Liu, Q. Liu, F. Lei, T. Yao, J. He, S. Wei and Y. Xie, *Angew. Chem.*, 2012, **124**, 8857–8861.
- 166 S. Ida, Y. Okamoto, M. Matsuka, H. Hagiwara and T. Ishihara, *J. Am. Chem. Soc.*, 2012, **134**, 15773–15782.
- 167 S. Liang, L. Wen, S. Lin, J. Bi, P. Feng, X. Fu and L. Wu, *Angew. Chem.*, 2014, **126**, 2995–2999.
- 168 M. Mattesini, J. S. de Almeida, L. Dubrovinsky, N. Dubrovinskaia, B. Johansson and R. Ahuja, *Phys. Rev. B: Condens. Matter Mater. Phys.*, 2004, **70**, 212101.
- 169 T. Kasuga, M. Hiramatsu, A. Hoson, T. Sekino and K. Niihara, *Langmuir*, 1998, **14**, 3160–3163.
- 170 M. Zukalova, M. Kalbač, L. Kavan, I. Exnar and M. Gratzel, *Chem. Mater.*, 2005, **17**, 1248–1255.
- 171 L. Y. Page and P. Strobel, *J. Solid State Chem.*, 1982, **44**, 273–281.
- 172 T. Sasaki, M. Watanabe, Y. Michiue, Y. Komatsu, F. Izumi and S. Takenouchi, *Chem. Mater.*, 1995, **7**, 1001–1007.
- 173 T. Sasaki, M. Watanabe, H. Hashizume, H. Yamada and H. Nakazawa, *J. Am. Chem. Soc.*, 1996, **118**, 8329–8335.
- 174 T. Sasaki and M. Watanabe, *J. Am. Chem. Soc.*, 1998, **120**, 4682–4689.
- 175 T. Sasaki, M. Watanabe, H. Hashizume, H. Yamada and H. Nakazawa, *Chem. Commun.*, 1996, 229–230.
- 176 L. Wang and T. Sasaki, *Chem. Rev.*, 2014, **114**, 9455–9486.
- 177 R. Ma and T. Sasaki, *Adv. Mater.*, 2010, **22**, 5082–5104.
- 178 T. Sasaki, Y. Ebina, T. Tanaka, M. Harada, M. Watanabe and G. Decher, *Chem. Mater.*, 2001, **13**, 4661–4667.
- 179 Z. S. Wang, T. Sasaki, M. Muramatsu, Y. Ebina, K. Takada, L. Z. Wang and M. Watanabe, *Chem. Mater.*, 2003, **15**, 807–812.
- 180 N. Sakai, T. Sasaki, K. Matsubara and T. Tatsuma, *J. Mater. Chem.*, 2010, **20**, 4371–4378.
- 181 K. K. Manga, Y. Zhou, Y. Yan and K. P. Loh, *Adv. Funct. Mater.*, 2009, **19**, 3638–3643.
- 182 P. Sun, R. Ma, M. Osada, T. Sasaki, J. Wei, K. Wang, D. Wu, Y. Cheng and H. Zhu, *Carbon*, 2012, **50**, 4518–4523.
- 183 M. Osada, T. Sasaki, K. Ono, Y. Kotani, S. Ueda and K. Kobayashi, *ACS Nano*, 2011, **5**, 6871–6879.
- 184 N. Sakai, K. Fukuda, Y. Omomo, Y. Ebina, K. Takada and T. Sasaki, *J. Phys. Chem. C*, 2008, **112**, 5197–5202.
- 185 R. Ma, Z. Liu, L. Li, N. Iyi and T. Sasaki, *J. Mater. Chem.*, 2006, **16**, 3809–3813.
- 186 T. Kameyama, K.-I. Okazaki, K. Takagi and T. Torimoto, *Electrochemistry*, 2011, **79**, 776–778.
- 187 T. Sasaki, Y. Ebina, K. Fukuda, T. Tanaka, M. Harada and M. Watanabe, *Chem. Mater.*, 2002, **14**, 3524–3530.
- 188 B. Seger, J. McCray, A. Mukherji, X. Zong, Z. Xing and L. Z. Wang, *Angew. Chem., Int. Ed.*, 2013, **52**, 6400–6403.
- 189 S. W. Keller, H. N. Kim and T. E. Mallouk, *J. Am. Chem. Soc.*, 1994, **116**, 8817–8818.
- 190 Z. S. Wang, Y. Ebina, K. Takada, M. Watanabe and T. Sasaki, *Langmuir*, 2003, **19**, 9534–9537.

- 191 R. E. Schaak and T. E. Mallouk, *Chem. Mater.*, 2002, **14**, 1455–1471.
- 192 T. C. Ozawa, K. Fukuda, K. Akatsuka, Y. Ebina, T. Sasaki, K. Kurashima and K. Kosuda, *J. Phys. Chem. C*, 2008, **112**, 17115–17120.
- 193 Y. Ebina, T. Sasaki and M. Watanabe, *Solid State Ionics*, 2002, **151**, 177–182.
- 194 T. C. Ozawa, K. Fukuda, K. Akatsuka, Y. Ebina, K. Kurashima and T. Sasaki, *J. Phys. Chem. C*, 2009, **113**, 8735–8742.
- 195 T. C. Ozawa, K. Fukuda, K. Akatsuka, Y. Ebina and T. Sasaki, *Chem. Mater.*, 2007, **19**, 6575–6580.
- 196 T. C. Ozawa, K. Fukuda, K. Akatsuka, Y. Ebina, T. Sasaki, K. Kurashima and K. Kosuda, *J. Phys. Chem. C*, 2008, **112**, 1312–1315.
- 197 J. Y. Kim, I. Chung, J. H. Choy and G. S. Park, *Chem. Mater.*, 2001, **13**, 2759–2761.
- 198 L. S. Zhang, W. Z. Wang, L. Zhou and H. L. Xu, *Small*, 2007, **3**, 1618–1625.
- 199 S. Ida, C. Ogata, U. Unal, K. Izawa, T. Inoue, O. Altuntasoglu and Y. Matsumoto, *J. Am. Chem. Soc.*, 2007, **129**, 8956–8957.
- 200 V. Chevallier, G. Nihoul and V. Madigou, *J. Solid State Chem.*, 2008, **181**, 439–449.
- 201 K. Toda, N. Ohtake, M. Kawakami, S. Tokuoka, K. Uematsu and M. Sato, *Jpn. J. Appl. Phys.*, 2002, **41**, 7021–7024.
- 202 K. Toda, S. Tokuoka, N. Ohtake, K. Uematsu and M. Sato, *Electroceramics in Japan VI*, 2003, vol. 248, pp. 27–30.
- 203 K. Toda, H. Sato, A. Sugawara, S. Tokuoka, K. Uematsu, M. Sato, A. A. Bokov and Z. G. Ye, *Electroceramics in Japan VII*, 2004, vol. 269, pp. 165–168.
- 204 K. Toda, H. Sato, A. Sugawara, S. Tokuoka, K. Uematsu and M. Sato, *Electroceramics in Japan VIII*, 2005, vol. 301, pp. 227–230.
- 205 K. Toda, A. Sugawara, K. Uematsu and M. Sato, *Jpn. J. Appl. Phys.*, 2005, **44**, 6973–6976.
- 206 K. Toda, A. Sugawara, K. Uematsu, M. Sato and M. Osada, *Electroceramics in Japan IX*, 2006, vol. 320, pp. 7–10.
- 207 M. Osada, K. Akatsuka, Y. Ebina, H. Funakubo, K. Ono, K. Takada and T. Sasaki, *ACS Nano*, 2010, **4**, 5225–5232.
- 208 B. W. Li, M. Osada, T. C. Ozawa, R. Ma, K. Akatsuka, Y. Ebina, H. Funakubo, S. Ueda, K. Kobayashi and T. Sasaki, *Jpn. J. Appl. Phys.*, 2009, **48**, 09KA15-1-5.
- 209 B. W. Li, M. Osada, T. C. Ozawa, K. Akatsuka, Y. Ebina, R. Ma, K. Ono, H. Funakubo and T. Sasaki, *Jpn. J. Appl. Phys.*, 2010, **49**, 09MA01-4.
- 210 B.-W. Li, M. Osada, Y. Ebina, K. Akatsuka, K. Fukuda and T. Sasaki, *ACS Nano*, 2014, **8**, 5449–5461.
- 211 S. Zhang, J. Shen, H. Fu, W. Dong, Z. Zheng and L. Shi, *J. Solid State Chem.*, 2007, **180**, 1456–1463.
- 212 L. F. Nazar, S. W. Liblong and X. T. Yin, *J. Am. Chem. Soc.*, 1991, **113**, 5889–5890.
- 213 R. E. Schaak and T. E. Mallouk, *Chem. Mater.*, 2000, **12**, 3427–3434.
- 214 Q. M. Gao, O. Giraldo, W. Tong and S. L. Suib, *Chem. Mater.*, 2001, **13**, 778–786.
- 215 Y. Omomo, T. Sasaki, L. Wang and M. Watanabe, *J. Am. Chem. Soc.*, 2003, **125**, 3568–3575.
- 216 Z. Y. Zeng, Z. Y. Yin, X. Huang, H. Li, Q. Y. He, G. Lu, F. Boey and H. Zhang, *Angew. Chem., Int. Ed.*, 2011, **50**, 11093–11097.
- 217 Y. Sun, S. Gao, F. Lei and Y. Xie, *Chem. Soc. Rev.*, 2015, **44**, 623–636.
- 218 Y. Lin, T. V. Williams and J. W. Connell, *J. Phys. Chem. Lett.*, 2010, **1**, 277–283.
- 219 Y. H. Hu, X. F. Li, L. Andrew, M. Cai, D. S. Geng, M. N. Banis, R. Y. Li and X. L. Sun, *ECS J. Solid State Sci. Technol.*, 2013, **2**, 3034–3039.
- 220 A. K. Geim and K. S. Novoselov, *Nat. Mater.*, 2007, **6**, 183–191.
- 221 Y. Zhang, Z.-R. Tang, X. Fu and Y.-J. Xu, *ACS Nano*, 2010, **4**, 7303–7314.
- 222 Y. Zhang, Z.-R. Tang, X. Fu and Y.-J. Xu, *ACS Nano*, 2011, **5**, 7426–7435.
- 223 N. Zhang, R. Ciriminna, M. Pagliaro and Y.-J. Xu, *Chem. Soc. Rev.*, 2014, **43**, 5276–5287.
- 224 M.-Q. Yang, N. Zhang, M. Pagliaro and Y.-J. Xu, *Chem. Soc. Rev.*, 2014, **43**, 8240–8254.
- 225 Y. Zhang, N. Zhang, Z.-R. Tang and Y.-J. Xu, *ACS Nano*, 2012, **6**, 9777–9789.
- 226 N. Zhang, M.-Q. Yang, Z.-R. Tang and Y.-J. Xu, *ACS Nano*, 2014, **8**, 623–633.
- 227 C. Han, Z. Chen, N. Zhang, J. C. Colmenares and Y.-J. Xu, *Adv. Funct. Mater.*, 2015, **25**, 221–229.
- 228 M.-Q. Yang and Y.-J. Xu, *Phys. Chem. Chem. Phys.*, 2013, **15**, 19102–19118.
- 229 S. Liu, Z. Chen, N. Zhang, Z.-R. Tang and Y.-J. Xu, *J. Phys. Chem. C*, 2013, **117**, 8251–8261.
- 230 S. Liu, M.-Q. Yang and Y.-J. Xu, *J. Mater. Chem. A*, 2014, **2**, 430–440.
- 231 N. Zhang, M.-Q. Yang, S. Liu, Y. Sun and Y.-J. Xu, *Chem. Rev.*, 2015, **115**, 10307–10377.
- 232 C. Han, M.-Q. Yang, N. Zhang and Y.-J. Xu, *J. Mater. Chem. A*, 2014, **2**, 19156–19166.
- 233 L. Yuan, M.-Q. Yang and Y.-J. Xu, *J. Mater. Chem. A*, 2014, **2**, 14401–14412.
- 234 B. Weng, M.-Q. Yang, N. Zhang and Y.-J. Xu, *J. Mater. Chem. A*, 2014, **2**, 9380–9389.
- 235 S. Liu, M.-Q. Yang, Z.-R. Tang and Y.-J. Xu, *Nanoscale*, 2014, **6**, 7193–7198.
- 236 L. Yuan, M.-Q. Yang and Y.-J. Xu, *Nanoscale*, 2014, **6**, 6335–6345.
- 237 M. Park, Y. Kim, Y. Ko, S. Cheong, S. W. Ryu and J. Cho, *J. Am. Chem. Soc.*, 2014, **136**, 17213–17223.
- 238 M. Yang, Y. Hou and N. A. Kotov, *Nano Today*, 2012, **7**, 430–447.
- 239 X. S. Li, W. W. Cai, J. H. An, S. Kim, J. Nah, D. X. Yang, R. Piner, A. Velamakanni, I. Jung, E. Tutuc, S. K. Banerjee, L. Colombo and R. S. Ruoff, *Science*, 2009, **324**, 1312–1314.
- 240 Y. M. Lin, C. Dimitrakopoulos, K. A. Jenkins, D. B. Farmer, H. Y. Chiu, A. Grill and P. Avouris, *Science*, 2010, **327**, 662.

- 241 D. Li, M. B. Mueller, S. Gilje, R. B. Kaner and G. G. Wallace, *Nat. Nanotechnol.*, 2008, **3**, 101–105.
- 242 Y. Hernandez, V. Nicolosi, M. Lotya, F. M. Blighe, Z. Sun, S. De, I. T. McGovern, B. Holland, M. Byrne, Y. K. Gunko, J. J. Boland, P. Niraj, G. Duesberg, S. Krishnamurthy, R. Goodhue, J. Hutchison, V. Scardaci, A. C. Ferrari and J. N. Coleman, *Nat. Nanotechnol.*, 2008, **3**, 563–568.
- 243 J. Zhang, F.-X. Xiao, G. Xiao and B. Liu, *Nanoscale*, 2014, **6**, 11293–11302.
- 244 Z. Ren, J. Zhang, F.-X. Xiao and G. Xiao, *J. Mater. Chem. A*, 2014, **2**, 5330–5339.
- 245 A. Lerf, H. Y. He, M. Forster and J. Klinowski, *J. Phys. Chem. B*, 1998, **102**, 4477–4482.
- 246 N. A. Kotov, I. Dekany and J. H. Fendler, *Adv. Mater.*, 1996, **8**, 637–641.
- 247 J. Shen, Y. Hu, C. Li, C. Qin, M. Shi and M. Ye, *Langmuir*, 2009, **25**, 6122–6128.
- 248 W. X. Zhao, Q. Zhang, Y. Hao, Y. Li, Y. Fang and D. Chen, *Macromolecules*, 2010, **43**, 9411–9416.
- 249 J. Liu, L. Tao, W. Yang, D. Li, C. Boyer, R. Wuhrer, F. Braet and T. P. Davis, *Langmuir*, 2010, **26**, 10068–10075.
- 250 J. Hong, Y. S. Kang and S. W. Kang, *Ind. Eng. Chem. Res.*, 2011, **50**, 3095–3099.
- 251 K. Arigo, J. P. Hill and Q. Ji, *Phys. Chem. Chem. Phys.*, 2007, **9**, 2319–2340.
- 252 K. Jasuja and V. Berry, *ACS Nano*, 2009, **3**, 2358–2366.
- 253 I. V. Lightcap, T. H. Kosel and P. V. Kamat, *Nano Lett.*, 2010, **10**, 577–583.
- 254 F. Bei, X. Hou, S. L. Y. Chang, G. P. Simon and D. Li, *Chem. – Eur. J.*, 2011, **17**, 5958–5964.
- 255 X. Chen, G. Wu, J. Chen, X. Chen, Z. Xie and X. Wang, *J. Am. Chem. Soc.*, 2011, **133**, 3693–3695.
- 256 U. Lange, T. Hirsch, V. M. Mirsky and O. S. Wolfbeis, *Electrochim. Acta*, 2011, **56**, 3707–3712.
- 257 C. Zhu, S. Guo, Y. Zhai and S. Dong, *Langmuir*, 2010, **26**, 7614–7618.
- 258 B.-S. Kong, J. Geng and H.-T. Jung, *Chem. Commun.*, 2009, 2174–2176.
- 259 S.-T. Han, Y. Zhou, C. Wang, L. He, W. Zhang and V. A. L. Roy, *Adv. Mater.*, 2013, **25**, 872–877.
- 260 Y. Zhou, J. Yang, X. Cheng, N. Zhao, H. Sun and D. Li, *RSC Adv.*, 2013, **3**, 3391–3398.
- 261 Q. Xi, X. Chen, D. G. Evans and W. Yang, *Langmuir*, 2012, **28**, 9885–9892.
- 262 T.-R. Kuo, D.-Y. Wang, Y.-C. Chiu, Y.-C. Yeh, W.-T. Chen, C.-H. Chen, C.-W. Chen, H.-C. Chang, C.-C. Hu and C.-C. Chen, *Anal. Chim. Acta*, 2014, **809**, 97–103.
- 263 C. Liu, K. Wang, S. Luo, Y. Tang and L. Chen, *Small*, 2011, **7**, 1203–1206.
- 264 V. C. Tung, L. M. Chen, M. J. Allen, J. K. Wassei, K. Nelson, R. B. Kaner and Y. Yang, *Nano Lett.*, 2009, **9**, 1949–1955.
- 265 S. Stankovich, D. A. Dikin, G. H. B. Dommett, K. M. Kohlhaas, E. J. Zimney, E. A. Stach, R. D. Piner, S. T. Nguyen and R. S. Ruoff, *Nature*, 2006, **442**, 282–286.
- 266 D. Yu and L. Dai, *J. Phys. Chem. Lett.*, 2010, **1**, 467–470.
- 267 Y. K. Kim and D. H. Min, *Langmuir*, 2009, **25**, 11302–11306.
- 268 T.-K. Hong, D. W. Lee, H. J. Choi, H. S. Shin and B.-S. Kim, *ACS Nano*, 2010, **4**, 3861–3868.
- 269 D. W. Lee, T.-K. Hong, D. Kang, J. Lee, M. Heo, J. Y. Kim, B.-S. Kim and H. S. Shin, *J. Mater. Chem.*, 2011, **21**, 3438–3442.
- 270 H. Hwang, P. Joo, M. S. Kang, G. Ahn, J. T. Han, B.-S. Kim and J. H. Cho, *ACS Nano*, 2012, **6**, 2432–2440.
- 271 M. E. Calvo, S. Colodrero, T. C. Rojas and H. Miguez, *Adv. Funct. Mater.*, 2008, **18**, 2708–2715.
- 272 A. Szeghalmi, M. Helgert, R. Brunner, F. Heyroth, U. Gosele and M. Knez, *Appl. Opt.*, 2009, **48**, 1727–1732.
- 273 E. R. Kleinfeld and G. S. Ferguson, *Science*, 1994, **265**, 370–373.
- 274 L. Z. Wang, T. Sasaki, Y. Ebina, K. Kurashima and M. Watanabe, *Chem. Mater.*, 2002, **14**, 4827–4832.
- 275 T. Tanaka, Y. Ebina, K. Takada, K. Kurashima and T. Sasaki, *Chem. Mater.*, 2003, **15**, 3564–3568.
- 276 N. Yang, Y. Zhang, J. E. Halpert, J. Zhai, D. Wang and L. Jiang, *Small*, 2012, **8**, 1762–1770.
- 277 H.-B. Yao, L.-H. Wu, C.-H. Cui, H.-Y. Fang and S.-H. Yu, *J. Mater. Chem.*, 2010, **20**, 5190–5195.
- 278 C. X. Guo, H. B. Yang, Z. M. Sheng, Z. S. Lu, Q. L. Song and C. M. Li, *Angew. Chem., Int. Ed.*, 2010, **49**, 3014–3017.
- 279 F.-X. Xiao, J. Miao and B. Liu, *J. Am. Chem. Soc.*, 2014, **136**, 1559–1569.
- 280 Z. Liang, K. L. Dzienis, J. Xu and Q. Wang, *Adv. Funct. Mater.*, 2006, **16**, 542–548.
- 281 A. Yu, H. W. Park, A. Davies, D. C. Higgins, Z. Chen and X. Xiao, *J. Phys. Chem. Lett.*, 2011, **2**, 1855–1860.
- 282 J. F. Quinn, A. P. R. Johnston, G. K. Such, A. N. Zelikin and F. Caruso, *Chem. Soc. Rev.*, 2007, **36**, 707–718.
- 283 F. Caruso, *Chem. – Eur. J.*, 2000, **6**, 413–419.
- 284 Y. Wang, A. S. Angelatos and F. Caruso, *Chem. Mater.*, 2008, **20**, 848–858.
- 285 F. Caruso, R. A. Caruso and H. Möhwald, *Science*, 1998, **282**, 1111–1114.
- 286 R. A. Caruso, A. Sussha and F. Caruso, *Chem. Mater.*, 2001, **13**, 400–409.
- 287 F. Caruso, X. Shi, R. A. Caruso and A. Sussha, *Adv. Mater.*, 2001, **13**, 740–744.
- 288 P. Kittitheeranun, W. Sajomsang, S. Phanpee, A. Treetong, T. Wutikhun, K. Suktham, S. Puttipipatkachorn and U. Rungsardthong Ruktanonchai, *Int. J. Pharm.*, 2015, **492**, 92–102.
- 289 G. B. Sukhorukov, D. V. Volodkin, A. M. Gunther, A. I. Petrov, D. B. Shenoy and H. Mohwald, *J. Mater. Chem.*, 2004, **14**, 2073–2081.
- 290 Y. Wang and F. Caruso, *Chem. Mater.*, 2005, **17**, 953–961.
- 291 M. Hartmann, *Chem. Mater.*, 2005, **17**, 4577–4593.
- 292 A. S. Angelatos, A. P. R. Johnston, Y. Wang and F. Caruso, *Langmuir*, 2007, **23**, 4554–4562.
- 293 D. V. Volodkin, A. I. Petrov, M. Prevot and G. B. Sukhorukov, *Langmuir*, 2004, **20**, 3398–3406.
- 294 A. G. Dong, Y. J. Wang, Y. Tang, N. Ren, Y. H. Zhang and Z. Gao, *Chem. Mater.*, 2002, **14**, 3217–3219.

- 295 A. G. Dong, Y. J. Wang, D. J. Wang, W. L. Yang, Y. H. Zhang, N. Ren, Z. Gao and Y. Tang, *Microporous Mesoporous Mater.*, 2003, **64**, 69–81.
- 296 N. Ren, Y. H. Yang, Y. H. Zhang, Q. R. Wang and Y. Tang, *J. Catal.*, 2007, **246**, 215–222.
- 297 P. Yang, A. H. Rizvi, B. Messer, B. F. Chmelka, G. M. Whitesides and G. D. Stucky, *Adv. Mater.*, 2001, **13**, 427–431.
- 298 D. Wang, R. A. Caruso and F. Caruso, *Chem. Mater.*, 2001, **13**, 364–371.
- 299 D. Wang and F. Caruso, *Chem. Commun.*, 2001, 489–490.
- 300 Y. Wang and F. Caruso, *Adv. Funct. Mater.*, 2004, **14**, 1012–1018.
- 301 Y. Choi, M. Gu, J. Park, H.-K. Song and B.-S. Kim, *Adv. Energy Mater.*, 2012, **2**, 1510–1518.
- 302 C. Xue, M. Gao, Y. Xue, L. Zhu, L. Dai, A. Urbas and Q. Li, *J. Phys. Chem. C*, 2014, **118**, 15332–15338.
- 303 J. Hong, K. Char and B.-S. Kim, *J. Phys. Chem. Lett.*, 2010, **1**, 3442–3445.
- 304 E. Donath, G. B. Sukhorukov, F. Caruso, S. A. Davis and H. Möhwald, *Angew. Chem., Int. Ed.*, 1998, **37**, 2201–2205.
- 305 A. P. R. Johnston, E. S. Read and F. Caruso, *Nano Lett.*, 2005, **5**, 953–956.
- 306 A. P. R. Johnston and F. Caruso, *Angew. Chem., Int. Ed.*, 2007, **46**, 2677–2680.
- 307 A. Yu, Y. Wang, B. Barlow and F. Caruso, *Adv. Mater.*, 2005, **17**, 1737–1741.
- 308 Y. Itoh, M. Matsusaki, T. Kida and M. Akashi, *Biomacromolecules*, 2006, **7**, 2715–2718.
- 309 D. B. Shenoy, A. A. Antipov, G. B. Sukhorukov and H. Möhwald, *Biomacromolecules*, 2003, **4**, 265–272.
- 310 D. G. Shchukin, A. A. Patel, G. B. Sukhorukov and Y. M. Lvov, *J. Am. Chem. Soc.*, 2004, **126**, 3374–3375.
- 311 N. G. Balabushevich, O. P. Tiourina, D. V. Volodkin, N. I. Larionova and G. B. Sukhorukov, *Biomacromolecules*, 2003, **4**, 1191–1197.
- 312 A. N. Zelikin, J. F. Quinn and F. Caruso, *Biomacromolecules*, 2006, **7**, 27–30.
- 313 A. S. Angelatos, B. Radt and F. Caruso, *J. Phys. Chem. B*, 2005, **109**, 3071–3076.
- 314 S. Ogawa, E. A. Decker and D. J. McClements, *J. Agric. Food Chem.*, 2004, **52**, 3595–3600.
- 315 Y. S. Gu, A. E. Decker and D. J. McClements, *Langmuir*, 2005, **21**, 5752–5760.
- 316 E. Tjijto, K. D. Cadwell, J. F. Quinn, A. P. R. Johnston, N. L. Abbott and F. Caruso, *Nano Lett.*, 2006, **6**, 2243–2248.
- 317 J. K. Ferri, W. Dong and R. Miller, *J. Phys. Chem. B*, 2005, **109**, 14764–14768.
- 318 D. G. Shchukin, K. Köhler, H. Möhwald and G. B. Sukhorukov, *Angew. Chem., Int. Ed.*, 2005, **44**, 3310–3314.
- 319 Y. Wang, A. Yu and F. Caruso, *Angew. Chem., Int. Ed.*, 2005, **44**, 2888–2892.
- 320 H. Wang, S. Ishihara, K. Ariga and Y. Yamauchi, *J. Am. Chem. Soc.*, 2012, **134**, 10819–10821.
- 321 S. Kidambi and M. L. Bruening, *Chem. Mater.*, 2005, **17**, 301–307.
- 322 S. Kidambi, J. Dai, J. Li and M. L. Bruening, *J. Am. Chem. Soc.*, 2004, **126**, 2658–2659.
- 323 J. Liu, L. Cheng, Y. Song, B. Liu and S. Dong, *Langmuir*, 2001, **17**, 6747–6750.
- 324 R. R. Nair, P. Blake, A. N. Grigorenko, K. S. Novoselov, T. J. Booth, T. Stauber, N. M. R. Peres and A. K. Geim, *Science*, 2008, **320**, 1308.
- 325 D. S. Hecht and R. B. Kaner, *MRS Bull.*, 2011, **36**, 749–755.
- 326 H. X. Chang, G. F. Wang, A. Yang, X. M. Tao, X. Q. Liu, Y. D. Shen and Z. J. Zheng, *Adv. Funct. Mater.*, 2010, **20**, 2893–2902.
- 327 P. J. King, U. Khan, M. Lotya, S. De and J. N. Coleman, *ACS Nano*, 2010, **4**, 4238–4246.
- 328 H. A. Becerril, J. Mao, Z. Liu, R. M. Stoltenberg, Z. Bao and Y. Chen, *ACS Nano*, 2008, **2**, 463–470.
- 329 G. Eda, G. Fanchini and M. Chhowalla, *Nat. Nanotechnol.*, 2008, **3**, 270–274.
- 330 J. H. Lee, D. W. Shin, V. G. Makotchenko, A. S. Nazarov, V. E. Fedorov, Y. H. Kim, J. Y. Choi, J. M. Kim and J. B. Yoo, *Adv. Mater.*, 2009, **21**, 4383–4387.
- 331 Y. W. Zhu, W. W. Cai, R. D. Piner, A. Velamakanni and R. S. Ruoff, *Appl. Phys. Lett.*, 2009, **95**, 103104.
- 332 X. L. Li, G. Y. Zhang, X. D. Bai, X. M. Sun, X. R. Wang, E. Wang and H. J. Dai, *Nat. Nanotechnol.*, 2008, **3**, 538–542.
- 333 D. Chen, X. Wang, T. Liu, X. Wang and J. Li, *ACS Appl. Mater. Interfaces*, 2010, **2**, 2005–2011.
- 334 Q. Tang, Z. Tang, J. Wu, J. Lin and I. Oh, *J. Mater. Chem.*, 2011, **21**, 5378–5385.
- 335 K. S. Novoselov, A. K. Geim, S. V. Morozov, D. Jiang, Y. Zhang, S. V. Dubonos, I. V. Grigorieva and A. A. Firsov, *Science*, 2004, **306**, 666–669.
- 336 Y. Zhu and J. M. Tour, *Nano Lett.*, 2010, **10**, 4356–4362.
- 337 H. Li, S. Pang, S. Wu, X. Feng, K. Muellen and C. Bubeck, *J. Am. Chem. Soc.*, 2011, **133**, 9423–9429.
- 338 J. R. Dahn, T. Zheng, Y. H. Liu and J. S. Xue, *Science*, 1995, **270**, 590–593.
- 339 K. Sato, M. Noguchi, A. Demachi, N. Oki and M. Endo, *Science*, 1994, **264**, 556–558.
- 340 A. Gerouki, M. A. Goldner, R. B. Goldner, T. E. Haas, T. Y. Liu and S. Slaven, *J. Electrochem. Soc.*, 1996, **143**, 262–263.
- 341 X. Zhao, C. M. Hayner, M. C. Kung and H. H. Kung, *ACS Nano*, 2011, **5**, 8739–8749.
- 342 S. Y. Yin, Y. Y. Zhang, J. H. Kong, C. J. Zou, C. M. Li, X. H. Lu, J. Ma, F. Y. C. Boey and X. D. Chen, *ACS Nano*, 2011, **5**, 3831–3838.
- 343 T. Cassagneau and J. H. Fendler, *Adv. Mater.*, 1998, **10**, 877–881.
- 344 Z. S. Wu, W. C. Ren, L. Xu, F. Li and H. M. Cheng, *ACS Nano*, 2011, **5**, 5463–5471.
- 345 A. L. M. Reddy, A. Srivastava, S. R. Gowda, H. Gullapalli, M. Dubey and P. M. Ajayan, *ACS Nano*, 2010, **4**, 6337–6342.
- 346 D. Y. Pan, S. Wang, B. Zhao, M. H. Wu, H. J. Zhang, Y. Wang and Z. Jiao, *Chem. Mater.*, 2009, **21**, 3136–3142.
- 347 E. Yoo, J. Kim, E. Hosono, H. Zhou, T. Kudo and I. Honma, *Nano Lett.*, 2008, **8**, 2277–2282.
- 348 S. M. Paek, E. Yoo and I. Honma, *Nano Lett.*, 2009, **9**, 72–75.

- 349 D. H. Wang, D. W. Choi, J. Li, Z. G. Yang, Z. M. Nie, R. Kou, D. H. Hu, C. M. Wang, L. V. Saraf, J. G. Zhang, I. A. Aksay and J. Liu, *ACS Nano*, 2009, **3**, 907–914.
- 350 H. L. Wang, L. F. Cui, Y. A. Yang, H. S. Casalongue, J. T. Robinson, Y. Y. Liang, Y. Cui and H. J. Dai, *J. Am. Chem. Soc.*, 2010, **132**, 13978–13980.
- 351 S. B. Yang, X. L. Feng, L. Wang, K. Tang, J. Maier and K. Mullen, *Angew. Chem., Int. Ed.*, 2010, **49**, 4795–4799.
- 352 P. Simon and Y. Gogotsi, *Nat. Mater.*, 2008, **7**, 845–854.
- 353 G. A. Snook, P. Kao and A. S. Best, *J. Power Sources*, 2011, **196**, 1–12.
- 354 L. L. Zhang, R. Zhou and X. S. Zhao, *J. Mater. Chem.*, 2010, **20**, 5983–5992.
- 355 Z. Li, J. Wang, X. Liu, S. Liu, J. Ou and S. Yang, *J. Mater. Chem.*, 2011, **21**, 3397–3403.
- 356 J. Yan, Z. J. Fan, T. Wei, W. Z. Qian, M. L. Zhang and F. Wei, *Carbon*, 2010, **48**, 3825–3833.
- 357 J. T. Zhang, J. W. Jiang and X. S. Zhao, *J. Phys. Chem. C*, 2011, **115**, 6448–6454.
- 358 M. F. Ei-Kady, M. Ihns, M. Li, J. Y. Hwang, M. F. Mousavi, L. Chaney, A. T. Lech and R. B. Kaner, *Proc. Natl. Acad. Sci. U. S. A.*, 2015, **112**, 4233–4238.
- 359 H. Park, P. R. Brown, V. Buloyic and J. Kong, *Nano Lett.*, 2012, **12**, 133–140.
- 360 X. Wang, L. J. Zhi and K. Mullen, *Nano Lett.*, 2008, **8**, 323–327.
- 361 J. W. G. Wildoer, L. C. Venema, A. G. Rinzler, R. E. Smalley and C. Dekker, *Nature*, 1998, **391**, 59–62.
- 362 X. C. Dong, D. L. Fu, W. J. Fang, Y. M. Shi, P. Chen and L. J. Li, *Small*, 2009, **5**, 1422–1426.
- 363 Y. M. Shi, K. K. Kim, A. Reina, M. Hofmann, L. J. Li and J. Kong, *ACS Nano*, 2010, **4**, 2689–2694.
- 364 L. Kavan, J. H. Yum and M. Gratzel, *ACS Nano*, 2011, **5**, 165–172.
- 365 F. Gong, H. Wang and Z.-S. Wang, *Phys. Chem. Chem. Phys.*, 2011, **13**, 17676–17682.
- 366 K. Ariga, J. P. Hill, M. V. Lee, A. Vinu, R. Charvet and S. Acharya, *Sci. Technol. Adv. Mater.*, 2008, **9**, 014109.
- 367 K. Ariga, A. Vinu, J. P. Hill and T. Mori, *Coord. Chem. Rev.*, 2007, **251**, 2562–2591.
- 368 Y. X. Liu, X. C. Dong and P. Chen, *Chem. Soc. Rev.*, 2012, **41**, 2283–2307.
- 369 Q. Ji, I. Honma, S.-M. Paek, M. Akada, J. P. Hill, A. Vinu and K. Ariga, *Angew. Chem., Int. Ed.*, 2010, **49**, 9737–9739.
- 370 Y. Mao, Y. Bao, W. Wang, Z. Li, F. Li and L. Niu, *Talanta*, 2011, **85**, 2106–2112.
- 371 Y. Cui, B. Zhang, B. Liu, H. Chen, G. Chen and D. Tang, *Microchim. Acta*, 2011, **174**, 137–144.
- 372 X. Wang, J. Wang, H. Cheng, P. Yu, J. Ye and L. Mao, *Langmuir*, 2011, **27**, 11180–11186.
- 373 N. Mohanty and V. Berry, *Nano Lett.*, 2008, **8**, 4469–4476.
- 374 Y. Ohno, K. Maehashi and K. Matsumoto, *J. Am. Chem. Soc.*, 2010, **132**, 18012–18013.
- 375 X. C. Dong, Y. M. Shi, W. Huang, P. Chen and L. J. Li, *Adv. Mater.*, 2010, **22**, 1649–1653.
- 376 M. Zhou, Y. M. Zhai and S. J. Dong, *Anal. Chem.*, 2009, **81**, 5603–5613.
- 377 B. Zhang and T. Cui, *Appl. Phys. Lett.*, 2011, **98**, 073116.
- 378 Y. Xiang, M. Yang, Z. B. Guo and Z. Cui, *J. Membr. Sci.*, 2009, **337**, 318–323.
- 379 J. G. Liu, T. S. Zhao, Z. X. Liang and R. Chen, *J. Power Sources*, 2006, **153**, 61–67.
- 380 C. H. Rhee, H. K. Kim, H. Chang and J. S. Lee, *Chem. Mater.*, 2005, **17**, 1691–1697.
- 381 S. P. Jiang, Z. C. Liu and Z. Q. Tian, *Adv. Mater.*, 2006, **18**, 1068–1072.
- 382 H. L. Tang, M. Pan, S. P. Jiang, Z. H. Wan and R. Z. Yuan, *Colloids Surf., A*, 2005, **262**, 65–70.
- 383 S. C. Mu, H. L. Tang, Z. H. Wan, M. Pan and R. Z. Yuan, *Electrochem. Commun.*, 2005, **7**, 1143–1147.
- 384 S. P. Jiang, L. Li, Z. C. Liu, M. Pan and H. L. Tang, *Electrochem. Solid-State Lett.*, 2005, **8**, 574–576.
- 385 H. Tang, Z. Wan, M. Pan and S. P. Jiang, *Electrochem. Commun.*, 2007, **9**, 2003–2008.
- 386 B. R. Matos, E. I. Santiago, J. F. Q. Rey, A. S. Ferlauto, E. Traversa, M. Linardi and F. C. Fonseca, *J. Power Sources*, 2011, **196**, 1061–1068.
- 387 K. Li, G. B. Ye, J. J. Pan, H. N. Zhang and M. Pan, *J. Membr. Sci.*, 2010, **347**, 26–31.
- 388 S. Wang, S. P. Jiang and X. Wang, *Nanotechnology*, 2008, **19**, 265601.
- 389 D. L. Wang, S. F. Lu and S. P. Jiang, *Chem. Commun.*, 2010, **46**, 2058–2060.
- 390 S. Zhang, Y. Shao, G. Yin and Y. Lin, *J. Mater. Chem. A*, 2013, **1**, 4631–4641.
- 391 S. Guo, S. J. Dong and E. W. Wang, *ACS Nano*, 2010, **4**, 547–555.
- 392 S. Zhang, Y. Shao, H. Liao, M. H. Engelhard, G. Yin and Y. Lin, *ACS Nano*, 2011, **5**, 1785–1791.
- 393 A. Abdelhafiz, A. Vitale, C. Joiner, E. Vogel and F. A. Alamgir, *ACS Appl. Mater. Interfaces*, 2015, **7**, 6180–6188.
- 394 F. Xiao, *Chem. Commun.*, 2012, **48**, 6538–6540.
- 395 F. Xiao, *J. Phys. Chem. C*, 2012, **116**, 16487–16498.
- 396 F.-X. Xiao, J. Miao, H.-Y. Wang and B. Liu, *J. Mater. Chem. A*, 2013, **1**, 12229–12238.
- 397 F.-X. Xiao, J. Miao and B. Liu, *Mater. Horiz.*, 2014, **1**, 259–263.
- 398 N.-N. Chai, H.-X. Wang, C.-X. Hu, Q. Wang and H.-L. Zhang, *J. Mater. Chem. A*, 2015, **3**, 16613–16620.
- 399 F.-X. Xiao, Z. Zeng and B. Liu, *J. Am. Chem. Soc.*, 2015, **137**, 10735–10744.
- 400 S. Gao, D. Pan and R. Cao, *J. Colloid Interface Sci.*, 2011, **358**, 593–597.